The University of Chicago

Topology and Entanglement in Fermionic Systems

A Dissertation Submitted to
The Faculty of The Division of The Physical Sciences
in Candidacy for The Degree of
Doctor of Philosophy

Department of Physics

By

Hassan Shapourian

Chicago, Illinois

June, 2019

Copyright © 2019 by Hassan Shapourian
All Rights Reserved.

To my parents and to my love, Maryam.

Table of Contents

List of Figures

List of Tables

Acknowledgements

First and foremost, I would like to thank my advisor Shinsei Ryu, for his guidance and patience. This dissertation would have not been possible without his continual support and his invaluable scientific and technical insights. I admire his incredibly broad knowledge and genuine interest in physics. It was a great pleasure to work with Shinsei and learn from him. I particularly appreciate his modesty and hands-on research style which make him very approachable. I distinctly remember how welcoming he was to me in the early days of my graduate school when I was trying to navigate my research interests and asked him all sorts of detailed questions. Shinsei's academic and life advice will always remain with me.

I would like to express my gratitude to the past and present fellow graduate students in our group Po-Yao Chang, Xiao Chen, Chang-Tse Hsieh, Apoorv Tiwari, Bode Sule, Xueda Wen, Jonah Kudler-Flam, Ian MacCormack, and Mao-Tian Tan for their help, cooperative attitude, and overall for making my PhD years more enjoyable. I also wish to thank my officemates Alex Bogatskii, Umang Mehta, Kyle Kawagoe, Carolyn Zhang, and Havey Hsiao for several fun and science conservations. I am extremely thankful to postdoctoral researchers Pouyan Ghaemi, Ken Shiozaki, Norm Tubman, Yuxuan Wang, Peng Ye, and Gil Cho at UIUC, and Paolo Glorioso, Laimei Nie, and Matthew Lapa at U.Chicago for sharing their knowledge and perspective on various physics topics. My special thanks go to Ken Shiozaki for his encouraging mentorship and productive collaborations. It was a great experience working with him. Some of the work presented here is the result of our joint collaborations. I wish to thank my late friend, mentor, and collaborator Darius Sadri. I benefited tremendously from his inspiring words about life and physics. I miss him so much.

I am extremely thankful to Taylor Hughes and Bryan Clark for giving me the opportunity to work with them and their support and advice at various stages. I greatly appreciate numerous personal and professional interactions with Taylor and Bryan. It is my honor to thank all my mentors and teachers, especially Eduardo Fradkin, Tony Leggett, Andrei Bernevig, Piers Coleman, Chetan Nayak, and David Huse.

It is my pleasure to acknowledge my collaborators for their insightful discussions and fruitful collaborations. Many thanks go to Seongshik Oh and his group for involving me in their projects and sharing with me their exciting results about thin-film topological insulators over the past three years. During my Ph.D., I spent a semester as a graduate fellow at Kavli Institute for Theoretical Physics at UC Santa Barbara which was very enjoyable. I appreciate this enlightening experience as well as many inspiring conversations with Leon Balents, Matthew Fisher, and Cenke Xu. It was a great opportunity to work with Leon and his students Kasra Hejazi and Chunxiao Liu. I am also grateful to Pasquale Calabrese and Erik Tonni for giving me the opportunity to visit their group at SISSA (Trieste). I enjoyed my time in Italy. I also thank Paola Ruggiero for helpful conversations and our recent collaboration.

I wish to thank my dissertation committee members Emil Martinec, Dam T. Son, and Jon Simon for their time and inputs.

I am grateful to the physics department at the University of Illinois Urbana-Champaign and the University of Chicago for their support and for the opportunities I have had here as a student, a researcher, and a teacher. I would like to thank our graduate director Lance Cooper (UIUC) and David Reid (U.Chicago) who are incredibly helpful. My degree transfer process from UIUC to U.Chicago went very smoothly thanks to their cooperation. Appreciation is due to our graduate affairs administrator Amy Schulz for being thoughtful and considerate.

Graduate school is by itself challenging and being away from your home country adds even more to it. I thank the Iranian students' community in Princeton, Urbana, and Chicago for organizing various cultural events and friendly gatherings. In particular, I would like to express my gratitude to Mohammad Rahimi, Majid Shafiee-Jood, Mani Rouhi Rad, Shayan Hemmatian, Hessam Akhlaghpour, Ali Javadi, Moein Malekakhlagh, Mohammad Hosein Bateni, Sasan Amini, Mohammad Tehrani, and Arta Jamshidi.

I am deeply indebted to my wonderful wife, Maryam, for her limitless encouragement, companionship, patience, and love. Since the beginning of our marriage, we have walked side by side through a lot of ups and downs and it has been your energetic presence which is always heart-

warming and a source of happiness. There is this saying that "Happy is the man who finds a true friend, and far happier is he who finds that true friend in his wife." I am truly blessed to be married to my best friend. I never forget numerous refreshing conversations with you over long hikes and road trips during the past five years, which helped me free my mind from daily challenges and prepare for more productive research. Collaborating with such smart scientist as you on physics projects has made research even more fun. I hope to continue our collaborations in the future. Maryam, thank you for all your sacrifices and for believing in me at every step of the way in academic and real life. I am utterly grateful for having you in my life and look forward to experiencing together new chapters of our lives.

Finally, I would like to thank my parents for their love, support, and for putting up with the physical separation. I would never have come this far if it was not for their encouragement, selflessness, generosity, and open-mindedness. Words cannot express my gratitude towards them. I am also grateful to my parents-in-law, Ardeshir and Mahnaz, for their love, care, and support. I wish to thank my brother, Hadi, for always being there for me, his kindness, and support. I vividly remember our childhood adventures and joyful memories of exploring nature. I am grateful to my sister, Hoorieh, for making my life more cheerful.

Abstract

This dissertation brings together ideas from quantum information theory and condensed matter physics to study many-particle systems of fermions. We revisit the structure of the Hilbert space and operator algebras in Fermi systems which provides a natural platform to discuss the notion of entanglement and local operations. We generalize the partial transpose, which is a well-known operation to diagnose entanglement in density matrices of qubits and bosonic systems, to fermionic systems. Our idea was inspired by the observation that time-reversal acts as transposition on density matrices; hence, we looked for a way to apply partial time-reversal to density matrices of fermions. We present a comprehensive set of benchmarks on our proposed definition of fermionic partial transpose and explain the fundamental differences between the bosonic and fermionic partial transpose. We use this new framework and the associated entanglement measure, logarithmic negativity, to study the entanglement content of free fermions with an arbitrary shape of Femi surface in all dimensions as well as topological insulators and superconductors. In particular, we show how thermal fluctuations destroy the quantum coherence of the ground state as temperature is increased.

Furthermore, we report the discovery of a surprising connection between topological invariants and the partial transpose in time-reversal symmetric topological insulators and superconductors. In short, we find that partition functions on non-orientable spacetime manifolds such as the Klein bottle or real-projective plane can be obtained by combining untransposed and partially transposed density matrix. This relation turns out to be general and can be used to study various other topological phases protected by anti-unitary symmetries. Similar to the partition functions, the quantities we introduce are complex numbers and their complex phase is a topological invariant. These topological invariants can be regarded as order parameters of topological phases in the sense that they admit discrete values and can only change by jumping from one value to another as we transition from one topological phase to another.

Notation, Symbols, and Acronyms

AZ	Altland Zirnbaur (symmetry classes of fermions)
BCS	Bardeen-Cooper-Schrieffer
BdG	Bogoliubov-de-Gennes
CFT	Conformal field theory
GHZ	Greenberger–Horne–Zeilinger
LOCC	Local operations and classical communications
PHS	Particle-hole symmetry
PPT	Positive partial transpose
(R)EE	(Rényi) entanglement entropy
RN	Rényi negativity
SPT	Symmetry protected topological
SSH	Su-Schrieffer-Heeger
TI	Topological insulator
TQFT	Topological quantum field theory
TRS	Time-reversal symmetry
TSC	Topological superconductor
$f_j, f_j^\dagger$	Complex fermion operators
a_j, b_j, c_j	Majorana fermion operators
$(-1)^F$	Fermion-number parity operator
ρ^{T_A}	Partially transposed density matrix
$\mathscr{E}$	Logarithmic negativity
$Z(X, \cdots)$	Partition function on spacetime manifold X (ellipses refer to other details)
$\hat{T}, \hat{C}, \hat{S}$	Time-reversal, particle-hole, chiral symmetry operators

Chapter 1

Introduction

" There is no law except the law that there is no law."

— John Wheeler

ENTANGLEMENT has been perceived as one of the intriguing manifestations of quantum phenomena, since the birth of quantum mechanics. Being intrinsic and fundamental, quantum entanglement is a frontier in various research areas ranging from many-body physics to spacetime physics and quantum information. There have been numerous attempts in developing theoretical tools to quantify the quantum entanglement (see for example the review articles [7, 34]). Throughout this dissertation, our interest in entanglement is twofold: First, the notion of entanglement and the corresponding entanglement measures in generic fermionic systems and second, using those entanglement measures to characterize topological phases of fermions.

1.1 Entanglement

A fundamental question is how the entanglement between two parts of a quantum system can be quantified in terms of some computable measures. In general, a quantum system can be in a pure state or a mixed state. Pure states are described by wave functions, for example, the zero temperature ground state wave function of a Hamiltonian. Bipartite entanglement of pure states

is often quantified in terms of the von Neumann and the Rényi entanglement entropies (See for example Refs. [7, 34, 65, 217]). The scaling of these measures have been found very useful in distinguishing and characterizing various phases of matter, such as gapless phases and quantum critical points described by conformal field theories (CFTs) [32, 33, 98], and gapped phases such as topologically ordered phases [127, 134].

On the other hand, mixed states are described by density matrices, for example, finite temperature states of a Hamiltonian or states of a subsystem of a global system obtained by partial tracing. A decent candidate to quantify the quantum entanglement within mixed states is known as the (logarithmic) negativity of a partially transposed density matrix [67, 100, 109, 110, 159, 162, 218]. Several methods have been developed to efficiently compute the entanglement negativity in different setups ranging from Harmonic oscillator chains [8, 9, 11, 43, 73, 141] and quantum spin chains [19–21, 142, 176, 181, 233, 234] to CFTs [5, 35, 36, 177] and massive quantum field theories [26]. The entanglement negativity of topologically ordered phases in (2+1) dimensions were also studied [42, 132, 230, 231]. The applicability of the negativity in characterizing finite-temperature systems [37, 68, 158, 192] and out-of-equilibrium scenarios [53, 68, 99, 229] was also investigated. In addition to these literatures, there are other useful numerical frameworks to evaluate the entanglement negativity such as tree tensor network [39], Monte Carlo implementation of partial transpose [4, 51], and rational interpolations [153].

We emphasize that the systems studied in all these works above are made out of distinguishable objects (qubits, spins, etc.) or bosons where local operators acting on different parts of the system commute. As it turned out, defining an analogue of entanglement negativity (and logarithmic negativity) for fermionic systems, and in particular partial transpose of fermionic density matrices, is not simply a straightforward extension of what is known for bosonic systems, because of the Fermi statistics.

One possible approach to define partial transpose for fermionic systems would be to use a particular basis such as the occupation number basis, and simply adopt the definition of the bosonic partial transpose – we simply ignore any fermion sign which may arise when we re-

arrange fermionic operators. In some cases, this procedure is equivalent to use a Jordan-Wigner transformation (and alike) to map fermionic systems to bosonic counterparts and then take the bosonic partial transpose. This was the working definition of partial transpose for fermionic systems in early works [44, 54–56, 69, 70, 97].

It was however noted that if this definition of partial transpose is used to define entanglement negativity for fermioic systems, it fails to capture important fermionic quantum correlations. For example, with this definition of entanglement negativity, there is no entanglement in the topological phase of the Kitaev Majorana chain [191]. [1]

In this dissertation, we introduce a partial transpose operation that can be applied to fermionic systems, in short, fermionic partial transpose. One of our motivations here, besides quantifying entanglement, is to construct topological invariants that can diagnose and characterize fermionic symmetry-protected topological phases of matter protected by anti-unitary symmetries of various kinds. Examples of symmetry-protected topological phases include time-reversal symmetric topological insulators in (2+1) dimensions (e.g., quantum spin Hall insulators), and time-reversal symmetric topological superconductors in (1+1)-dimensions (e.g., the Kitaev chain with time-reversal symmetry). As we will see, we use the fermionic partial transpose to define a fermionic analog of (logarithmic) entanglement negativity, which we call the fermionic entanglement negativity or simply (and loosely) the entanglement negativity when there is no confusion.

The fact that the bosonic partial transpose fails to capture quantum correlations in fermionic systems and that the fermionic partial transpose needs to be used instead suggests that quantum entanglement in fermionic systems, is fundamentally different from bosonic one.

1.2 Topological insulators and superconductors

The discovery of topological phases has added a new level of complexity to our understanding of quantum phases of matter. Topological materials are locally featureless in the bulk and cannot

[1] There are more issues than we just pointed out here for "borrowing" the bosonic definition of partial transpose to discuss fermionic systems. See also Sec. 3.1.

be distinguished from ordinary (topologically trivial) insulators or superconductors; however, they are characterized by exotic boundary modes such as Majorana zero modes and Dirac surface states (see Fig. 1.1), which have potential applications in spintronics and quantum computation.

Technically, topological phases of matter are gapped quantum phases which cannot be adiabatically connected to a trivial state, i.e., tensor product state. Topological phases can be realized in the presence of various symmetries, such as time-reversal, charge conjugation, and/or space group symmetry. More specifically, there exists a group of gapped quantum phases, which can be adiabatically connected to a trivial state in the absence of symmetries, while cannot be turned into a trivial phase once a certain set of symmetries are enforced. Such gapped quantum phases are called symmetry-protected topological (SPT) phases. Topological insulators and superconductors are celebrated examples of SPT phases of fermions [25, 50, 76, 80, 81, 89, 92, 103, 118, 126, 145, 170, 178, 182, 222, 240]. Other examples of bosonic SPT phases have been also widely discussed [45, 46, 80, 117, 133, 139, 165, 184, 202, 219]. On the other hand, topologically ordered phases [59, 125, 128, 129, 135, 146, 166, 211, 225, 227, 239] are phases of matter which are topologically distinct from a trivial state even in the absence of symmetries. Topologically ordered phases can also be enriched by the presence of symmetries. They can exhibit a particular pattern of symmetry fractionalization, which can be used to distinguish and characterize different topologically ordered phases with symmetries. Topologically ordered phases of this kind are called symmetry-enriched [16, 72, 107, 140, 143, 209, 212, 213, 226]. Our main focus in this work is topological insulators and superconductors, although some of our discussion should be readily applicable to symmetry-enriched topological phases as well.

Topological insulators and superconductors often have a simple description in terms of a ground state of a free fermion Hamiltonian, i.e., a quadratic Bloch-BdG Hamiltonian of the form

$$\hat{H} = \sum_{\mathsf{r},\mathsf{r}'} \hat{\psi}_i^\dagger(\mathsf{r}) H^{ij}(\mathsf{r},\mathsf{r}') \hat{\psi}_j(\mathsf{r}'), \tag{1.1}$$

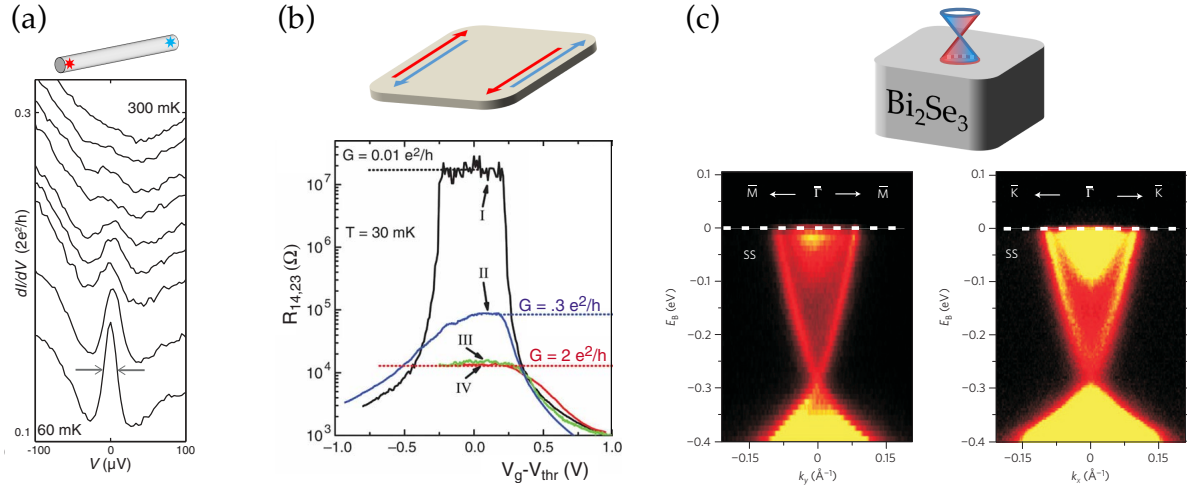

Figure 1.1: Materials realization of topological insulators and superconductors. (a) 1d p-wave topological superconductor with Majorana end-modes realized in InSb nanowire on a s-wave superconductor (niobium titanium nitride). The signature of Majorana zero-modes shows up as a zero-bias peak in differential conductance. (b) 2d quantum spin Hall effect with helical edge modes in CdHgTe quantum well. The signature of helical edge modes (cases III and IV) can be seen from a two-point resistance plateau at twice the resistance quantum e^2/h. (c) 3d topological insulator with 2d Dirac-like surface states in Bi_2Se_3 crystal. The Dirac-like dispersion of in-gap states is evident from the angle-resolved photoemission spectroscopy (ARPES) plot. The graphs are adapted from [130, 150, 242].

class\dim.	T	C	S	0	1	2	3	4	5	6	7
A	0	0	0	$\mathbb{Z}$	0	$\mathbb{Z}$	0	$\mathbb{Z}$	0	$\mathbb{Z}$	0
AIII	0	0	1	0	$\mathbb{Z}$	0	$\mathbb{Z}$	0	$\mathbb{Z}$	0	$\mathbb{Z}$
AI	+	0	0	$\mathbb{Z}$	0	0	0	$2\mathbb{Z}$	0	$\mathbb{Z}_2$	$\mathbb{Z}_2$
BDI	+	+	1	$\mathbb{Z}_2$	$\mathbb{Z}$	0	0	0	$2\mathbb{Z}$	0	$\mathbb{Z}_2$
D	0	+	0	$\mathbb{Z}_2$	$\mathbb{Z}_2$	$\mathbb{Z}$	0	0	0	$2\mathbb{Z}$	0
DIII	−	+	1	0	$\mathbb{Z}_2$	$\mathbb{Z}_2$	$\mathbb{Z}$	0	0	0	$2\mathbb{Z}$
AII	−	0	0	$2\mathbb{Z}$	0	$\mathbb{Z}_2$	$\mathbb{Z}_2$	$\mathbb{Z}$	0	0	0
CII	−	−	1	0	$2\mathbb{Z}$	0	$\mathbb{Z}_2$	$\mathbb{Z}_2$	$\mathbb{Z}$	0	0
C	0	−	0	0	0	$2\mathbb{Z}$	0	$\mathbb{Z}_2$	$\mathbb{Z}_2$	$\mathbb{Z}$	0
CI	+	−	1	0	0	0	$2\mathbb{Z}$	0	$\mathbb{Z}_2$	$\mathbb{Z}_2$	$\mathbb{Z}$

Table 1.1: Periodic table of topological insulators and superconductors; the left-most column (A, AIII, …, CI) denotes the ten symmetry classes of fermionic Hamiltonians, which are characterized by the presence/absence of time-reversal (T), particle-hole (C), and chiral (S) symmetry of different types denoted by ± 1.

where $\hat{\psi}_i(\mathsf{r})$ is a multi-component fermion annihilation operator, and index r labels a site on a d-dimensional lattice. Quadratic Bogoliubov-de-Gennes (BdG) Hamiltonians defined on a lattice can be treated similarly. The single-particle Hamiltonians $H^{ij}(\mathsf{r},\mathsf{r}')$ belong to one of the ten Altland-Zirnbauer (AZ) symmetry classes and are, in general, subject to a set of symmetry constraints [2] as follows

$$\hat{C}\hat{\psi}_j^\dagger\hat{C}^{-1} = \hat{\psi}_k[\mathscr{U}_C]_{kj}, \quad \hat{C}i\hat{C}^{-1} = i, \tag{1.2}$$

$$\hat{T}\hat{\psi}_j^\dagger\hat{T}^{-1} = \hat{\psi}_k^\dagger[\mathscr{U}_T]_{kj}, \quad \hat{T}i\hat{T}^{-1} = -i, \tag{1.3}$$

$$\hat{S}\hat{\psi}_j^\dagger\hat{S}^{-1} = \hat{\psi}_k[\mathscr{U}_S]_{kj}, \quad \hat{S}i\hat{S}^{-1} = -i, \tag{1.4}$$

where $\hat{T}$, $\hat{C}$, and $\hat{S}$ are the time-reversal symmetry (TRS), particle-hole symmetry (PHS), and chiral symmetry operators, respectively. The Hermite conjugate of the above equations leads to the transformation rule for the fermion annihilation operators, $\hat{\psi}_j$. Note that the last two symmetry operators involve complex conjugation and hence are anti-unitary. Here, $\mathscr{U}_C, \mathscr{U}_T$ and $\mathscr{U}_S$ are unitary matrices and satisfy

$$\mathscr{U}_\alpha\mathscr{U}_\alpha^* = \pm 1 \tag{1.5}$$

for $\alpha = C, T$ and $\mathscr{U}_S^2 = 1$. The $\pm$ signs correspond to symmetry operator which squares to $+1$, and to the fermion number parity $(-1)^F$, respectively. With this setup, we then ask, whether two gapped quadratic Hamiltonians, which belong to the same symmetry class, can be continuously transformed into each other without closing the gap. That is, gapped Hamiltonians of a given symmetry class can be categorized into different topological equivalence classes. The result of this classification is summarized by the *Periodic Table* of topological insulators (TIs) and topological superconductors (TSCs) [126, 168, 178, 182, 183]; see Table 1.1. Systematic derivations of this classification table can be found in Refs. [126, 182]. A few comments on notable features of the

[2] A Hamiltonian belongs to a certain symmetry class if it satisfies the condition $\hat{O}\hat{H}\hat{O}^{-1} = \hat{H}$ where $\hat{O}$ is the symmetry operator (i.e., $\hat{T}, \hat{C}$, or $\hat{S}$) of that symmetry class.

table are in order. The symbols "$\mathbb{Z}$", "$\mathbb{Z}_2$", "$2\mathbb{Z}$", and "0", indicate whether or not topological phases exist for a given symmetry class in a given dimension, and if they exist, what kind of topological invariant characterizes the topological phases. For instance, "$\mathbb{Z}$" indicates that the topological phase is characterized by an integer topological invariant, and "0" simply means there is no topological phase. In other words, all states in such symmetry class and dimension are adiabatically connected.

The classification table exhibits a periodicity of 2 and 8 as a function of spatial dimension, for the complex (first two rows) and real (the last eight rows) symmetry classes, respectively. In fact, the table is only shown up to $d = 7$ for this reason. In addition, notice that the classifications for symmetry classes in consecutive rows are related by a dimensional shift.

As mentioned, an observable consequence of having a topologically non-trivial state is the existence of gapless boundary modes. A simple way to explain this is by noting that topologically non-trivial and trivial states in a phase diagram are always separated by a quantum phase transition, if the symmetry conditions are strictly enforced. This, in turn, implies that if a TI or TSC is in spatial proximity to a trivial phase, there should be a gapless state localized at the boundary between the two phases. This gapless (i.e., critical) state can be thought of as a phase transition occurring locally in space, where the parameters of the Hamiltonian change as a function of the direction transverse to the boundary. Such gapless boundary modes are *protected* in the sense that they are stable against perturbations as long as the bulk gap is not destroyed and the symmetries are preserved. In particular, gapless boundary modes are completely robust against disorder and evade Anderson localization. The presence of such gapless boundary states is the most salient feature of TIs and TSCs, and in fact, can be considered as a definition of TIs and TSCs. This close connection between non-trivial bulk topological properties and gapless boundary modes is known as the *bulk-boundary correspondence*.

Non-interacting topological phases are rather well-understood and various types of materials ranging from binary compounds and alloys to complex oxides host topological electronic structures [92, 170]. More interestingly, there exist strongly correlated materials where the topological

Symmetry group	Dimension 1	2	3
AIII	$\mathbb{Z}_4$	0	$\mathbb{Z}_8$
AI	$\mathbb{Z}_2$	0	0
BDI	$\mathbb{Z}_8$	0	0
D	$\mathbb{Z}_2$	$\mathbb{Z}$	0
DIII	$\mathbb{Z}_2$	$\mathbb{Z}_2$	$\mathbb{Z}_{16}$
AII	0	$\mathbb{Z}_2$	$\mathbb{Z}_2$

Table 1.2: Classification of interacting topological insulators and superconductors.

phase emerges as a result of strong electron-electron interaction and spin-orbit coupling. Some examples are heavy transition metal compounds such as iridates $(Na,Li)_2IrO_3$, $Sr[Ir/Ti]O_3$, and $R_2Ir_2O_7$, and the Kondo insulator SmB_6 (See the review papers [64, 238] and references therein). The discovery of emergent topological phases begs the question that whether non-interacting topological classification is valid in the presence of interactions.

It turned out that the non-interacting classification is rather fragile, and can be dramatically altered once interaction effects are taken into account [75, 76]. Since this remarkable finding, there have been several works which discuss the breakdown of the non-interacting classification in the presence of interactions [74, 88, 103, 113, 144, 148, 167, 179, 223, 224, 244, 245]. In most cases we study in this dissertation, the non-interacting classification is reduced as a result of interactions. A summary of interacting classification is shown in Table 1.2. For instance, let us consider time-reversal symmetric TSC of class BDI in one dimension. The non-interacting classification is $\mathbb{Z}$ whereas the interaction reduces $\mathbb{Z}$ to $\mathbb{Z}_8$ (i.e. $\mathbb{Z}$ mod 8). This surprising result implies that 8 copies of a p-wave topological superconductor is adiabatically connected to a trivial superconductor as long as we allow for TRS symmetric interactions.

A practical approach to classify topological materials is through understanding which bulk characteristics in topological media lead to exotic boundary modes. These bulk characteristics are typically topological invariants, which means they are quantized numbers and do not change under smooth deformations unless the system undergoes a phase transition. The bulk topological characteristics will in turn help to predict materials with novel properties and to synthesize ma-

terials with specific functionalities. There are various topological invariants for non-interacting TIs and TSCs using single-particle states (e.g., eigenstates of the Hamiltonian (1.1)). For example, the $\mathbb{Z}_2$-valued topological invariants have been introduced for TIs both in two and three spatial dimensions [82, 115, 147, 174, 175]. For TSCs protected by TRS, the integer-valued topological invariants ("the winding number") have been introduced [182]. However, the discovered breakdown of non-interacting classification clearly indicates that the situation at the interacting level is more intricate, and a general framework to distinguish interacting TIs and TSCs is lacking. This should be contrasted from the quantized Hall conductance, which can be formulated within many-body physics without referring to single-particle wave functions (as it is ultimately related to the response function).

One of our goals in this dissertation is to introduce *many-body* topological invariants for TIs and TSCs protected by an orientation-reversing symmetry, such as TRS. Our topological invariants do not rely on single-particle descriptions, and have the same status as the many-body Chern number [152].

The basic strategy behind our construction of many-body topological invariants can be best illustrated by drawing an analogy with the many-body Chern-number. The many-body Chern number is formulated as a response of the many-body ground state wave functions to the twisted boundary conditions by $U(1)$ phase. Here, the $U(1)$ phase is associated with the symmetry of the system (i.e., the particle number conservation). Similarly, for phases of matter with more generic symmetry, one can consider twisting the boundary condition using the symmetry of the system. For SPT phases protected by orientation reversing symmetry, the symmetry-twisted boundary conditions naturally give rise to non-orientable spacetime manifolds [49, 79, 80, 103, 104, 116–119, 240]. From the topological quantum field theory description of TSCs [118, 240], one expects that the complex phase of the partition function, when the system is put on an appropriate non-orientable manifold, is quantized and serves as a topological invariant. In this work, we design many-body topological invariants, such that they return the quantized phase of the partition function.

Let us briefly sketch the connection between the fermionic partial transpose and many-body topological invariants. For the case of bosonic SPT phases, it was noted that to effectively realize non-orientable spacetime in the canonical (operator) formalism, one can make use of partial transpose [164, 193]. Now, we expect that the same strategy should work to detect fermionic SPT phases and construct many-body topological invariants for them. As we will explain in detail, the low-energy effective theory of fermionic SPT phases is described by topological quantum field theories (TQFTs). Such TQFTs may involve path integrals on non-orientable spacetime. If there is a sensible definition of partial transpose for fermionic systems, the many-body topological invariant constructed from it should agree with the expected result from TQFTs on non-orientable manifolds. This comparison with TQFTs further guided us to look for a proper definition of fermionic partial transpose. [3]

1.3 Dissertation overview

This dissertation attempts to answer two main questions:

- How do we quantify the entanglement between two parts of a many-body fermionic system?
- How do we diagnose non-trivial topology within a given quantum state of TIs or TSCs?

Chapters 3 and 4 provide some answers to the first question, and Chapter 5 focuses on the second question.

We begin our discussion by several preliminary remarks regarding the structure of the Hilbert space and the algebra of operators in fermionic systems in Chapter 2. This provides a natural language to explain the notion of entanglement in mixed states, separability, and partial transpose in fermionic systems and serves as a basic material for the subsequent chapters. In Chapter 3, we

[3] For field theory experts, to define the kinds of TQFTs relevant to fermionic SPT phases protected by TRS, one needs to specify an appropriate Pin structure (or proper generalization thereof). The fermionic partial transpose should implement something equivalent in the canonical formalism.

discuss the fermionic entanglement negativity from a perspective more inclined to quantum information theory. In particular, we present a systematic investigation of properties of fermionic entanglement negativity among which are the monotonicity under local quantum operations and classical communications, additivity and invariance under a local unitary. We show the success of the fermionic partial transpose in capturing the entanglement within one-dimensional TIs and TSCs. We further conjecture that the entanglement negativity of inseparable states which mix local fermion-number parity is always non-vanishing. The next two chapters are devoted to applications of the fermionic partial transpose. In Chapter 4, we study the entanglement in systems with a Fermi surface. Such system in one dimension describes the critical theory at the transition point between topological and trivial phases. We show that how the leading order term of entanglement negativity or Rényi entropies can be derived analytically by relating the entanglement calculations to partition functions on certain spacetime manifolds. We also compute the entanglement negativity for finite-temperature states and discuss the signatures of short-range quantum coherence in a many-body system because of thermal fluctuations. Chapter 5 is devoted to the second application of the partial transpose which is distinguishing different topological phases protected by anti-unitary symmetries. We introduce several quantities in terms of trace of density matrix and its partial transpose which effectively simulate the partition function on non-orientable spacetime manifolds. These quantities are generally complex numbers, and the complex phase is a topological invariant. Finally, we wrap up our discussion with several remarks and possible interesting directions for future research in Chapter 6.

Chapter 2

Hilbert space of fermionic systems

"Never underestimate the joy people derive from hearing something they already know."

— Enrico Fermi

FERMI statistics is an intrinsic property of fermions and distinguishes them from bosons. This property may affect the usual properties of multi-particle Hilbert spaces such as tensor product structure, operator algebras, and the notion of entanglement in fermionic systems. Here, we review the structure of the Hilbert space of local fermionic modes and define the algebras of physical operators, which include density matrix operators and any physical manipulation of Fermi systems. Next, we present the definitions of entangled and separable (i.e., unentangled) states. The goal of this chapter is to provide essential background materials and to set the stage for the subsequent chapters.

Let $\mathscr{H}$ be the Hilbert space of a quantum system. The algebra $\mathscr{G}$ of linear bounded operators on the Hilbert space is generally characterized by C^* algebras. Physical operators refer to a subset of linear operators whose algebra is denoted by $\mathbf{L}(\mathscr{H})$. If the Hilbert space admits superselection

Part of the material presented in this chapter was previously published in: H. Shapourian, K. Shiozaki, S. Ryu, Phys. Rev. B 95, 165101 (2017) and H. Shapourian and S. Ryu, Phys. Rev. A 99, 022310 (2019). Some text has been modified. Copyright by the American Physical Society (APS); reuse permitted according to APS copyright policies.

sectors, i.e., $\mathscr{H} = \oplus_j \mathscr{H}_j$, then the algebra of physical operators can be represented as $\oplus_j \mathbf{L}(\mathscr{H}_j)$, since physical operators do not mix the superselection sectors.

Definition 2.1. (Local fermionic modes). The Hilbert space is a Fock space associated with a system of N fermionic degrees of freedom ("sites") $j = 1, \cdots, N$. The Fock space is spanned by 2^N basis vectors $|n_1, \cdots, n_N\rangle$ where $n_j = 0, 1$ is the occupation number of jth site. Any linear operator can be defined in terms of creation and annihilation (complex fermion) operators $f_j^\dagger$ and f_j which act on the basis vectors as

$$f_j |n_1, \cdots, n_{j-1}, 1, n_{j+1}, \cdots, n_N\rangle = (-1)^{\sum_{i=1}^{j-1} n_i} |n_1, \cdots, n_{j-1}, 0, n_{j+1}, \cdots, n_N\rangle, \tag{2.1}$$

$$f_j |n_1, \cdots, n_{j-1}, 0, n_{j+1}, \cdots, n_N\rangle = 0, \tag{2.2}$$

and $f_j^\dagger$ is the Hermitian conjugate. Hence, the creation and annihilation operators obey the anticommutation relations

$$f_j f_k^\dagger + f_k^\dagger f_j = \delta_{jk}, \tag{2.3}$$

$$f_j f_k + f_k f_j = f_j^\dagger f_k^\dagger + f_k^\dagger f_j^\dagger = 0 \tag{2.4}$$

which generate the algebra $\mathscr{G}$.

In order to algebraically handle generic many-particle operators, a representation of operators in terms of Majorana operators comes handy. Here is a good place to introduce them.

Definition 2.2. (Majorana fermion operators). For a fermionic Fock space $\mathscr{H}$ generated by N local fermionic modes f_j, we define Majorana (real) fermion operators by

$$c_{2j-1} = f_j^\dagger + f_j, \quad c_{2j} = -i(f_j^\dagger - f_j), \quad j = 1, \ldots, N. \tag{2.5}$$

These operators satisfy the commutation relation

$$c_j c_k + c_k c_j = 2\delta_{jk}. \tag{2.6}$$

The operator algebra generated by the Majorana operators acting on the Hilbert space of $2N$ Majorana sites is called the Clifford algebra and any operator $X \in \mathcal{G}$ acting on this space can be expanded in terms of c_j, $j = 1, \cdots, 2N$,

$$X = \sum_{k=1}^{2N} \sum_{p_1 < p_2 \cdots < p_k} X_{p_1 \cdots p_k} c_{p_1} \cdots c_{p_k}, \tag{2.7}$$

where $X_{p_1 \cdots p_k}$ are complex numbers and fully anti-symmetric under permutations of $\{1, \ldots, k\}$.

We introduce the fermion-number parity for a basis vector by $(\sum_j n_j)$ mod 2. The fermion-number parity can also be measured by applying the operator

$$(-1)^F := (-1)^{\sum_j n_j}, \tag{2.8}$$

which assigns a $\mathbb{Z}_2$ index to each basis vector. Throughout this dissertation, we assume a global fermion-number parity symmetry as a fundamental symmetry in fermionic systems. This is so, simply because Hamiltonians of our interest are always bosonic operators, and commute with the fermion number parity operator [235]. As a result, the Hilbert space splits into two sectors $\mathcal{H} = \mathcal{H}_0 \oplus \mathcal{H}_1$, corresponding to the states with even (odd) number of fermions, respectively, where we can write $(-1)^F |\phi\rangle = \pm |\phi\rangle$ for $|\phi\rangle \in \mathcal{H}_0$ ($|\phi\rangle \in \mathcal{H}_1$). In other words, the Hilbert space is $\mathbb{Z}_2$ graded [76].

Similarly, the operator algebra is $\mathbb{Z}_2$ graded as well, $\mathcal{G} = \mathcal{G}_0 \oplus \mathcal{G}_1$. Namely, an operator X is fermion-number parity even (odd) if it preserves (changes) the number of fermions modulo 2,

$$(-1)^F X (-1)^F = (-1)^r X, \quad \text{for } X \in \mathcal{G}_r \ (r = 0, 1). \tag{2.9}$$

This simply means that the algebra of operators $\mathscr{G}_0$ ($\mathscr{G}_1$) is spanned by products of even (odd) number of f_j and $f_j^\dagger$.

Definition 2.3. (Physical operators). The physical operators are those operators which preserve the fermion-number parity symmetry [13, 23, 28, 247] and act on each fermion-number parity sector separately, i.e.,

$$\mathscr{G}_0 = \mathbf{L}(\mathscr{H}_0) \oplus \mathbf{L}(\mathscr{H}_1). \tag{2.10}$$

It is evident that no physical operator can change the occupation number locally on a single site as it changes the fermion-number parity. When an operator X corresponds to a physical operator, $X \in \mathscr{G}_0$, the expansion only contains even number of Majorana operators, i.e., k is even in Eq. (2.7). The Hamiltonian is an example of a physical operator. Another important class of physical operators is density matrix operators.

Definition 2.4. (Density matrix). The state of a system is described by a density matrix ρ defined on the Hilbert space $\mathscr{H}$ and satisfies the following three conditions:

1. It is Hermitian $\rho^\dagger = \rho$.
2. ρ is positive semi-definite.
3. $\mathrm{Tr}\,\rho = 1$.

A system is said to be in a pure state, if $\rho^2 = \rho$, otherwise, it is in a mixed state. Physically, mixed states represent finite-temperature states of systems, or reduced density matrices obtained from a given pure state by taking the partial trace. We denote the set of state density matrices by $\mathscr{S}(\mathscr{H}) = \mathscr{S}(\mathscr{H}_0) \oplus \mathscr{S}(\mathscr{H}_1)$.

Definition 2.5. (Bipartite systems). In order to define a bipartite entanglement, we divide the system of N fermion sites into subsystems A and B with m_A and m_B sites, respectively, where

$m_A + m_B = N$. The Hilbert space is then factorized as a tensor product,

$$\mathscr{H} = \mathscr{H}_A \otimes \mathscr{H}_B. \tag{2.11}$$

For instance, a generic density matrix $\rho \in \mathscr{S}(\mathscr{H}^A \otimes \mathscr{H}^B)$ can be expanded as

$$\rho = \sum_{k_1,k_2}^{k_1+k_2=\text{even}} \rho_{p_1\cdots p_{k_1},q_1\cdots q_{k_2}} a_{p_1}\cdots a_{p_{k_1}} b_{q_1}\cdots b_{q_{k_2}}, \tag{2.12}$$

where $\{a_j\}$ and $\{b_j\}$ are Majorana operators acting on $\mathscr{H}^A$ and $\mathscr{H}^B$, respectively, and the even fermion-number parity condition is shown by the constraint $k_1 + k_2 = \text{even}$.

Definition 2.6. (Product state). Any pure state $|\Psi\rangle$ in $\mathscr{H}^A \otimes \mathscr{H}^B$ obtained from tensor product of two local states $|\Phi_\alpha\rangle \in \mathscr{H}_\alpha$ as

$$|\Psi\rangle = |\Phi_A\rangle \otimes |\Phi_B\rangle, \tag{2.13}$$

is a product state and is not entangled.

According to the above definition, it is easy to define an entangled pure state: A superposition state $|\Psi\rangle = \sum_i \alpha_i |\Phi_A^{(i)}\rangle \otimes |\Phi_B^{(i)}\rangle$, where $|\Phi_{A/B}^{(i)}\rangle$ is a set of local orthogonal states, is entangled when $\alpha_i \neq 0$ for more than one i. The amount of entanglement in a given state can be quantified by the entropy of information within either subsystem A or B, in the form of the von Neumann entropy or the Rényi entropies.

Definition 2.7. (von Neumann entanglement entropy).

$$S(\rho_A) = -\text{Tr}(\rho_A \ln \rho_A) = -\sum_i |\alpha_i|^2 \ln |\alpha_i|^2. \tag{2.14}$$

Definition 2.8. (Rényi entropies).

$$\mathscr{R}_n(\rho_A) = \frac{1}{1-n} \ln \mathrm{Tr}(\rho_A^n) = \frac{1}{1-n} \ln \sum_i |\alpha_i|^{2n}. \tag{2.15}$$

Here, $\rho_A = \mathrm{Tr}_B(|\Psi\rangle \langle\Psi|) = \sum_i |\alpha_i|^2 |\Phi_A^{(i)}\rangle \langle\Phi_A^{(i)}|$ is the reduced density matrix associated with $\mathscr{H}_A$. Notice that $S(\rho_A) = S(\rho_B)$ and $\mathscr{R}_n(\rho_A) = \mathscr{R}_n(\rho_B)$ and clearly, $S, \mathscr{R}_n \geq 0$ where the equality holds for a product state. For analytical calculations, S is usually obtained from $\mathscr{R}_n$ via $S = \lim_{n\to 1} \mathscr{R}_n$.

In order to define entanglement in mixed states where $\rho^2 \neq \rho$, the first step is to define subalgebras of *local* operators acting on each Hilbert subspace. However, these subalgebras, denoted by $\mathscr{G}(\mathscr{H}^i)$, $i = A, B$, contain both fermion-number parity even and odd terms and do not commute with each other in general. Hence, in order to decompose the algebra of operators, we define the $\mathbb{Z}_2$ graded tensor product as

$$XY = X \otimes_{\mathrm{gr}} Y, \quad YX = (-1)^{xy} X \otimes_{\mathrm{gr}} Y, \tag{2.16}$$

where $X \equiv X \otimes_{\mathrm{gr}} \mathbb{I}_B$ and $Y \equiv \mathbb{I}_A \otimes_{\mathrm{gr}} Y$ are local operators in $\mathscr{G}$ and $X \in \mathscr{G}_x(\mathscr{H}^A)$ and $Y \in \mathscr{G}_y(\mathscr{H}^B)$ are two elements of the subalgebras $x, y = 0$ or 1 corresponding to even or odd sectors. So, the algebra of linear operators admits the following decomposition

$$\mathscr{G} = \mathscr{G}(\mathscr{H}^A) \otimes_{\mathrm{gr}} \mathscr{G}(\mathscr{H}^B). \tag{2.17}$$

Similar to the full Hilbert space, we may define local physical operators acting on each Hilbert subspace as a set of operators which preserve the fermion-number parity within that subspace. We should note that the space of physical operators on the full Hilbert space is larger than the space spanned by the tensor product of local physical operators on Hilbert subspaces, $\mathscr{G}_0(\mathscr{H}^A) \otimes$

$\mathcal{G}_0(\mathcal{H}^B) \subseteq \mathcal{G}_0$. In fact, we have

$$\mathcal{G}_0 = (\mathcal{G}_0(\mathcal{H}^A) \otimes \mathcal{G}_0(\mathcal{H}^B)) \cup (\mathcal{G}_1(\mathcal{H}^A) \otimes_{\mathrm{gr}} \mathcal{G}_1(\mathcal{H}^B)), \tag{2.18}$$

where we write the usual tensor product for the product of local physical observables as they always commute. In the case of density matrices $\mathcal{S}(\mathcal{H})$, this means that $\mathcal{S}(\mathcal{H}^A) \otimes \mathcal{S}(\mathcal{H}^B) \subseteq \mathcal{S}(\mathcal{H})$, where $\mathcal{S}(\mathcal{H}^A)$ and $\mathcal{S}(\mathcal{H}^B)$ refer to the set of local density matrices. As we see below, this is essential for the existence of the space of entangled states.

Again, we use the unentangled states as a hint to define entangled states. Similar to the definition 2.6 of the pure product state, any element $\rho = \rho_A \otimes \rho_B$ in the set $\mathcal{S}(\mathcal{H}^A) \otimes \mathcal{S}(\mathcal{H}^B)$, is also called a product state and unentangled. In contrast with pure states, there exists a set containing superposition of mixed product states which are not entangled. They are called separable states and denoted by $\mathcal{S}_{\mathrm{sep}}$.

Definition 2.9. (Separable states). A convex combination of product states in the form

$$\rho_{\mathrm{sep}} = \sum_i w_i \, \rho_{A,i} \otimes \rho_{B,i}, \tag{2.19}$$

is called separable where w_i are real positive coefficients satisfying $\sum_i w_i = 1$, and $\rho_{\alpha,i} \in \mathcal{S}(\mathcal{H}^\alpha)$, $\alpha = A, B$. The above condition is also equivalent to the separability criterion defined with reference to the bipartitioned operator algebra [23].

In Eq. (2.19), the probability distribution w_i can be classically produced by a random number generator, and in this sense, $\mathcal{S}_{\mathrm{sep}}$ is not quantum entangled but merely classically correlated [100, 159]. By definition $\mathcal{S}_{\mathrm{sep}}$ forms a convex set [109, 110]. Hence, we expect that the complement of this set contains entangled or inseparable states. However, deciding whether a density matrix admits a decomposition in the form (2.19) or not is rather complicated. Indeed, it is characterized as an NP-hard problem [10, 90]. Despite this intrinsic difficulty, we may be able to characterize a

large subset of entangled density matrices associated with the ground state or thermal ensemble of local Hamiltonians in condensed matter physics.

The entanglement in mixed states could be quantified by the difference between the von Neumann or Rényi entropies of different partitions. A candidate quantity is the mutual information defined below.

Definition 2.10. (Mutual information).

$$I_{\mathrm{vN}}(\rho) = S_{\mathrm{vN}}(\rho_A) + S_{\mathrm{vN}}(\rho_B) - S_{\mathrm{vN}}(\rho), \tag{2.20}$$

$$I_n(\rho) = S_n(\rho_A) + S_n(\rho_B) - S_n(\rho), \tag{2.21}$$

where $\rho_A = \mathrm{Tr}_B \rho$ and $\rho_B = \mathrm{Tr}_A \rho$.

However, the mutual information is known to count classical correlations and is not an entanglement measure for generic mixed states. For instance, it may be non-zero for some separable states.

Another alternative is the positive partial transpose (PPT) [83, 100, 109, 110, 159, 197, 232] which is a test originally designed to diagnose separable states in bosonic systems based on the fact that density matrices are positive semi-definite operators. Before we get into the definition of partial transpose for fermions, let us briefly review the bosonic partial transpose.

Definition 2.11. (Bosonic partial transpose). The partial transpose of a density matrix $\rho = \sum_{ijkl} \rho_{ijkl} |e_A^{(i)}, e_B^{(j)}\rangle \langle e_A^{(k)}, e_B^{(l)}|$ written in a local orthonormal basis $\{|e_A^{(k)}\rangle, |e_B^{(j)}\rangle\}$ is defined by exchanging the indices of subsystem A (or B) as in

$$\rho^{T_A} = \sum_{ijkl} \rho_{ijkl} |e_A^{(k)}, e_B^{(j)}\rangle \langle e_A^{(i)}, e_B^{(l)}|, \tag{2.22}$$

where the partial transpose operation acts as

$$(|e_A^{(i)}, e_B^{(j)}\rangle \langle e_A^{(k)}, e_B^{(l)}|)^{T_A} = |e_A^{(k)}, e_B^{(j)}\rangle \langle e_A^{(i)}, e_B^{(l)}|. \tag{2.23}$$

Note that ρ^{T_A} is a Hermitian operator in bosonic theories and the PPT test follows by checking whether or not ρ^{T_A} contains any negative eigenvalue. A separable state passes the PPT test, i.e. all the eigenvalues of ρ^{T_A} are non-negative, whereas an inseparable (i.e., entangled) state yields negative eigenvalues after partial transpose. [2] Hence, the PPT criterion can be used to determine whether a given density matrix is separable or not. Similar to the entropic measures of pure-state entanglement in (2.14) and (2.15), the (logarithmic) entanglement negativity associated with the spectrum of the partially transposed density matrix is defined as a candidate to quantify mixed-state entanglement [67, 162, 218].

Definition 2.12. (Entanglement negativity). The negativity and the logarithmic negativity are defined by

$$\mathcal{N}(\rho) = \frac{\left\|\rho^{T_A}\right\| - 1}{2}, \tag{2.24}$$

$$\mathcal{E}(\rho) = \ln \left\|\rho^{T_A}\right\|, \tag{2.25}$$

where $||A|| = \mathrm{Tr}\sqrt{AA^\dagger}$ is the trace norm, i.e., sum of the singular values of A. When A is Hermitian, the singular values are simplified into the absolute value of the eigenvalues of A.

The above quantities essentially measure the *negativity* of the eigenvalues of ρ^{T_A}, this is where these quantities bear their names from. It is easy to see that $\mathcal{N}(\rho_{\text{sep}}) = \mathcal{E}(\rho_{\text{sep}}) = 0$.

Different approaches have been devised to efficiently compute the logarithmic negativity in various systems. Harmonic oscillator chains were studied using the covariance matrix technique [8, 9, 11, 43, 73, 141] and quantum spin chains were studied using the density matrix renormalization group [19–21, 176, 233] and exactly [181, 234]. The topologically ordered phases were also investigated for the (2+1) dimensional Chern-Simons theories [230, 231] and for the toric code where exact calculations are applicable [42, 132]. A particularly important progress was due to a systematic approach developed for CFTs [35, 36]. This approach was further expanded

[2] A technical point is that there exists a set of inseparable states which also pass the PPT test [102]. They are said to contain bound entanglement which cannot be used for quantum computing processes such as teleportation [101]. We never encounter this situation in fermionic density matrices. For more details on this issue, visit Chapter 3.

to study massive quantum field theories [26] as well as finite-temperature [37, 68, 192] and out-of-equilibrium situations [53, 68, 99, 229]. The entanglement spectrum of partial transpose in CFTs was also recently studied [177]. Among other useful numerical methods, tree tensor network [39], Monte Carlo simulations [4, 51], and rational interpolations [153] are notable.

One of the goals in this dissertation is to revisit the problem of finding the entanglement in fermionic mixed states. In the previous studies on fermionic systems, initial work by Eisler and Zimborás [69] and later works [44, 54–56, 70, 97], the definition of the fermionic partial transpose was based on the partial transpose of the corresponding bosonic density matrix. In other words, the action of the partial transpose on a fermionic density matrix is obtained from the action of the partial transpose on the bosonic density matrix through a Jordan-Wigner transformation. This method leads to a number of difficulties and inconsistencies as follows. It fails to capture important fermionic quantum correlations. For example, with this definition of entanglement negativity, there is no entanglement in the topological phase of the Kitaev Majorana chain [191]. It was also observed that, with the above definition, the partial transpose may turn Gaussian states (e.g., ground states or thermal states of non-interacting fermion systems) into non-Gaussian states. More specifically, the partially transposed density matrix would be a linear combination of two Gaussian operators, which in general do not commute with each other. Therefore, the spectrum of the partially transposed density matrix (and hence entanglement negativity) cannot be computed easily even for non-interacting fermionic systems. This may be regarded just as a technical difficulty, which is in contrast with (i) bosonic cases where the partial transpose of Gaussian states remains Gaussian [11, 186, 197] and (ii) the calculations of other entanglement measures (von-Neumann or Rényi entanglement entropies) for non-interacting fermion systems where the spectrum of Gaussian density matrices can be easily obtained from covariance matrices [160]. These issues motivate us to look for an alternative definition of the partial transpose for fermions. Partial transpose may seem to be a basis dependent algebraic manipulation and from this perspective there are several ways to implement such operation. However, it turned out this

perspective is not particularly helpful especially when it comes to generalizing partial transpose to fermions or anyons which obey non-trivial mutual statistics.

Here, we present a different definition of fermionic partial transpose, in contrast to the prior definition of partial transpose [69] for fermions, based on the partial time-reversal transformation which can be used as a means to detect time-reversal SPT phases of fermions or bosons [190, 194].

In the remainder of this chapter, we explicitly write the fermionic partial transpose in three representations: Occupation-number, Majorana fermion, and coherent state bases. The difference between bosonic partial transpose (that is a matrix partial transposition) and the fermionic one is most obvious in the occupation-number basis. Due to anti-commutation of local fermionic modes, let us fix our convention by defining the "normal-ordered" occupation-number basis as

$$|\{n_j\}_{j\in A},\{n_j\}_{j\in B}\rangle = (f_{j_1}^\dagger)^{n_{j_1}}\cdots(f_{j_{m_A}}^\dagger)^{n_{j_{m_A}}}\cdots(f_{j'_{m_B}}^\dagger)^{n_{j'_{m_B}}}|0\rangle \tag{2.26}$$

where n_j's are occupation numbers for the subsystems A and B, respectively, and $|0\rangle$ denotes the vacuum state where all n_j's are zero. Normal-ordering in this representation simply means that all fermionic degrees of freedom within each subsystem are clustered together. Such normal-ordering can always be achieved for any given set of local fermionic sites, after shuffling around the fermion operators and keeping track of minus signs due to the anti-commutation relation. For instance, consider four fermion sites living on a chain and label them from 1 to 4. Let us partition it such that sites 1 and 4 belong to the subsystem A and sites 2 and 3 belong to the subsystem B. To normal-order a state like $|1011\rangle = f_1^\dagger f_3^\dagger f_4^\dagger|0\rangle$ means to bring the fermion site 4 next to site 1 and write it in this form $|\{n_j\}_{j\in A},\{n_j\}_{j\in B}\rangle$, i.e., $|11,01\rangle = f_1^\dagger f_4^\dagger f_3^\dagger|0\rangle = -f_1^\dagger f_3^\dagger f_4^\dagger|0\rangle$ which differs from the original (spatial) ordering by a minus sign.

Hence, a normal-ordered density matrix ρ in this basis reads as

$$\sum_{n_j,\bar{n}_j}^{\sum_j n_j+\bar{n}_j=\text{even}} \rho(\{n_j\},\{\bar{n}_j\})|\{n_j\}_A,\{n_j\}_B\rangle\langle\{\bar{n}_j\}_A,\{\bar{n}_j\}_B| \tag{2.27}$$

where $\rho(\{n_j\},\{\bar{n}_j\}) = \langle \{n_j\}_A, \{n_j\}_B | \rho | \{\bar{n}_j\}_A, \{\bar{n}_j\}_B \rangle$ and the constraint $\sum_j n_j + \bar{n}_j =$ even implies $\rho \in \mathscr{S}(\mathscr{H}^A \otimes \mathscr{H}^B)$.

Definition 2.13. (Fermionic partial transpose). The partial transpose in the occupation number basis is given by

$$\Big(|\{n_j\}_A, \{n_j\}_B\rangle \langle \{m_j\}_A, \{m_j\}_B| \Big)^{T_A} = (-1)^{\phi(n,\bar{n})} U_A^\dagger |\{m_j\}_A, \{n_j\}_B\rangle \langle \{n_j\}_A, \{m_j\}_B| U_A, \tag{2.28}$$

where the phase factor is

$$\phi(\{n_j\},\{\bar{n}_j\}) = \frac{[(\tau_A + \bar{\tau}_A) \bmod 2]}{2} + (\tau_A + \bar{\tau}_A)(\tau_B + \bar{\tau}_B) \tag{2.29}$$

in which $\tau_{A(B)} = \sum_{j\in A(B)} n_j$ and $\bar{\tau}_{A(B)} = \sum_{j\in A(B)} m_j$, are the number of occupied states (i.e., the Hamming weight) in each subsystem. Note that U_A is a unitary transformation (partial particle-hole transformation) $U_A = \prod_{j\in A} c_{2j-1}$ acting on $\mathscr{H}^A$. As far as the entanglement negativity is concerned $U_A^\dagger \rho^{T_A} U_A$ and ρ^{T_A} have identical eigenvalues which lead to the same value for the entanglement negativity. It is now evident that the fermionic definition (2.28) is distinct from the bosonic partial transpose (2.23) (which is just exchanging the states of subsystem A adopted in Ref. [69]) due to presence of a phase factor.

Alternatively, the action of partial transpose on density matrices can be derived in another basis in terms of the Majorana fermion operators. The partial transpose in this basis provides a convenient way to algebraically prove various properties of the fermionic negativity later in this dissertation.

Let us start with reviewing how the transpose acts in this basis. A standard anti-automorphism $X \mapsto X^T$ of a Clifford algebra is defined by reversing the ordering of generators in the expansion (2.7) as in $(c_{p_1} c_{p_2} \dots c_{p_k})^T = c_{p_k} \cdots c_{p_2} c_{p_1}$. Given $X, Y \in \mathscr{G}$, this operation is involutive $(X^T)^T = X$, linear $(zX)^T = zX^T$ for a complex number z, and satisfy $(XY)^T = Y^T X^T$. This is what we call

the transpose operation. It is easy to show that for density matrices $\rho \in \mathscr{S}(\mathscr{H})$ the spectrum of ρ and ρ^T are identical [191].

Definition 2.14. (Fermionic partial transpose in Majorana basis). The fermionic partial transpose is defined only in the subalgebra of physical operators $\mathscr{G}_0$. The partial transpose of a density matrix (2.12) is given by [191, 195]

$$\rho^{T_A} := \sum_{k_1,k_2}^{k_1+k_2=\text{even}} X_{p_1\cdots p_{k_1},q_1\cdots q_{k_2}} i^{k_1} a_{p_1}\cdots a_{p_{k_1}} b_{q_1}\cdots b_{q_{k_2}}, \tag{2.30}$$

and similarly for ρ^{T_B}.

The partial transpose is consistent with the full transpose, since first, taking successive partial transpose with respect to the two subsystems is identical to taking the full transpose, [3]

$$(X^{T_A})^{T_B} = X^T, \tag{2.31}$$

and second, the identity operator is invariant under the partial transpose,

$$(\mathbb{I})^{T_A} = \mathbb{I}. \tag{2.32}$$

In addition, the definition (2.30) implies that

$$(X^{T_A})^{T_A} = (-1)^{F_A} X (-1)^{F_A}. \tag{2.33}$$

where $(-1)^{F_A}$ is the fermion-number parity operator (2.8) defined within the Hilbert subspace $F_A = \sum_{j\in A} f_j^\dagger f_j$. This property reflects the fact that the fermionic partial transpose is related to the action of time-reversal operator of spinless fermions in the Euclidean spacetime [190]. This

[3] This is a nice property of our definition of a partial transpose. Although it is natural to expect that such identity should hold, it is not necessary. In other words, a definition of partial transpose can still be considered consistent with the full transpose as long as it satisfies $(X^{T_A})^{T_B} = UX^TU^\dagger$ where U is a unitary operator.

also means that ρ^{T_A} for fermions is pseudo-Hermitian[4] and may contain complex eigenvalues. Nevertheless, the singular values can be used to calculate the norm in definition 2.12 for the entanglement negativity. In Chapter 3, we check that the fermionic entanglement negativity satisfies usual properties expected for an entanglement measure and provide several examples.

To motivate our definition of the fermionic partial transpose, it is useful to recapitulate the bosonic partial transpose in the coherent state representation. As was shown by Simon [197], the partial transpose has a geometric interpretation as partial time-reversal or mirror reflection in phase space. This idea can be readily illustrated in a single bosonic mode defined in terms of the operators $a = (q + ip)/\sqrt{2}$ and $a^\dagger = (q - ip)/\sqrt{2}$ where q and p are position and momentum operators, respectively, which obey the canonical commutation relation $[q, p] = i$ or equivalently $[a, a^\dagger] = 1$. The time-reversal transformation for a basis vector $|\alpha\rangle\langle\alpha^*|$ in the coherent state representation [236] is given by

$$|\alpha\rangle\langle\alpha^*| \to |\alpha^*\rangle\langle\alpha| := (|\alpha\rangle\langle\alpha^*|)^T \tag{2.34}$$

in which $|\alpha\rangle = e^{\alpha a^\dagger}|0\rangle$ and $\langle\alpha^*| = \langle 0|e^{\alpha^* a}$ are coherent states and α and α^* are complex numbers and we use the fact that the time-reversal operator is simply the complex conjugation, $\mathscr{T} = \mathscr{K}$. This definition for the partial transpose leads to the transformation rule $|m\rangle\langle n| \mapsto |n\rangle\langle m|$ in the occupation number basis, which follows from identifying the same monomials of α and α^* on both sides of the second equality in the above definition. It is easy to see that the associated Wigner distribution function $W(q, p)$ goes into $W(q, -p)$ [197]. Hence, this means that for bosonic systems partial transpose is the same as partial time-reversal or mirror reflection in (q, p)-space. This fact was also used in harmonic chains to calculate the negativity in terms of the covariance matrix [11].

It is worth noting that for a bosonic system either Eqs. (2.23) or (2.34) can be used as a fundamental defining equation for the partial transpose. However, this is not the case for fermions.

[4] A pseudo-Hermitian operator H is defined by $\eta H^\dagger \eta^{-1} = H$ with $\eta^2 = 1$ where η is a uniatry Hermitian operator satisfying $\eta^\dagger \eta = \eta\eta^\dagger = 1$ and $\eta = \eta^\dagger$. Essentially, pseudo-Hermiticity is a generalization of Hermiticity in the sense that it implies Hermiticity when $\eta = 1$.

Due to anti-commuting property of fermions, Eq. (2.23) may acquire an additional minus sign depending on the states being exchanged during transposition. Therefore, we propose to use the fermionic version of the time-reversal transformation as a guiding principle to determine the rules associated with the partial transpose. To begin with, let us consider a single-site system described by complex fermion operators f and $f^\dagger$ which obey the anti-commutation relation $\{f, f^\dagger\} = 1$. The analog of Eq. (2.34) for fermions is given by

$$|\xi\rangle\langle\bar{\xi}| \to |i\bar{\xi}\rangle\langle i\xi| := \left(|\xi\rangle\langle\bar{\xi}|\right)^T \tag{2.35}$$

where $\xi, \bar{\xi}$ are Grassmann variables, $|\xi\rangle = e^{-\xi f^\dagger}|0\rangle$ and $\langle\bar{\xi}| = \langle 0|e^{-f\bar{\xi}}$ are fermionic coherent states. It is important to note that the time-reversal transformation is not just exchanging Grassmann variables between bra and ket states but also multiplying them by a factor of i [5]. The factor of i appears due to anticommuting property of Grassmann variables and is required for keeping the trace (i.e., sum of the diagonal elements of density matrix, in this case 1 and $f^\dagger f$) unchanged after taking the transpose.

It is worth noting that fermionic coherent states are Grassmann even and commute with each other. Therefore, Eq. (2.35) can be readily generalized for a many-particle system.

Definition 2.15. (Fermionic partial transpose in coherent state basis). The partial transpose with respect to the interval A reads as

$$U_A\left(|\{\xi_j\}_{j\in A}, \{\xi_j\}_{j\in B}\rangle\langle\{\bar{\chi}_j\}_{j\in A}, \{\bar{\chi}_j\}_{j\in B}|\right)^{T_A} U_A^\dagger = |\{i\bar{\chi}_j\}_{j\in A}, \{\xi_j\}_{j\in B}\rangle\langle\{i\xi_j\}_{j\in A}, \{\bar{\chi}_j\}_{j\in B}|, \tag{2.36}$$

where U_A acts only on the Hilbert space of A (see below Eq. (2.29)) and $|\{\xi_j\}\rangle = e^{-\sum_j \xi_j f_j^\dagger}|0\rangle$ and $\langle\{\bar{\chi}_j\}| = \langle 0|e^{-\sum_j f_j \bar{\chi}_j}$ are the many-particle fermionic coherent states.

[5] More generally, one can consider $|{-e^{-i\theta}}\bar{\xi}\rangle\langle e^{i\theta}\xi|$ for arbitrary $\theta \in [0, 2\pi)$ as the definition of partial time-reversal transformation. All different definitions lead to the same spectrum for the partial transpose, as they are related by unitary transformations. We choose $\theta = \pi/2$, since the transformation rule for Majorana operators looks simpler.

In closing, we should remind the reader that the three definitions 2.13, 2.14, and 2.15 are identical. In the next chapter, we further explain the significance of the fermionic partial transpose and the associated entanglement quantity. Then, in Chapters 4 and 5, we apply this framework to study critical and topological phases of fermions.

Chapter 3

Entanglement negativity: General remarks

"Not only does God play dice but... he sometimes throws them where they cannot be seen."

— Stephen Hawking

THE spectrum of partial transpose provides information about the entanglement in generic density matrices. This is what we want to study in this chapter. We first show that the entanglement negativity associated with the fermionic partial transpose is an entanglement measure in the sense that it satisfies a required set of quantum information theoretic properties. We explain a general recipe to compute the spectrum (and eventually the entanglement negativity) of the partially transposed density matrix for Gaussian states. Later in this chapter, we give several examples of few-particle and many-particle systems and discuss important differences between bosonic and fermionic partial transpose. We close the chapter by some remarks regarding how the entanglement negativity can guide us towards answering the basic question of dividing the space of mixed states into separable and inseparable subspaces.

Part of the material presented in this chapter was previously published in: H. Shapourian, K. Shiozaki, S. Ryu, Phys. Rev. B 95, 165101 (2017) and H. Shapourian and S. Ryu, Phys. Rev. A 99, 022310 (2019). Some text has been modified. Copyright by the American Physical Society (APS); reuse permitted according to APS copyright policies.

3.1 Entanglement negativity as an entanglement measure

In order for an entanglement measure to be useful, it should satisfy several requirements [29, 66, 216]. We summarize these conditions in Table 3.1. Similar to the usual entanglement negativity, fermionic entanglement negativity introduced in the previous chapter satisfy all the requirements as we have shown in Ref. [189]. Before discussing more about this, let us explain some terminologies.

3.1.1 Local operations and classical communications

We use $\rho_{AB} \in \mathscr{S}(\mathscr{H}^A \otimes \mathscr{H}^B)$ to denote a (possibly entangled) state density matrix between subsystems A and B and we introduce a state ρ_R associated with an ancilla. Local operation and classical communication (LOCC) consist of three types of operations on ρ_{AB} as follows.

1. Appending ancilla: Appending an unentangled local ancilla R is modeled by the following process

$$\rho_{AB} \to (\rho_{AB} \otimes \rho_R), \tag{3.1}$$

   where we add an ancilla in an arbitrary mixed state, denoted by $\rho_R \in \mathscr{S}(\mathscr{H}^R)$, to our original system ρ_{AB} and by local ancilla, we mean that the new global system $R \cup (AB)$ is partitioned to $\tilde{A} = AR$ and B.

2. Local projectors: A local projection operator P_s, $s = A, B$ acting on the Hilbert space $\mathscr{H}^s$ is a physical operator $P \in \mathscr{G}_0(\mathscr{H}^s)$ (recall the definition of physical operators $[(-1)^{F_s}, P_s] = 0$) which satisfies $P_s^2 = P_s$.

   Consider two sets of orthogonal local projectors $\{P_A^\mu\}$ and $\{P_B^\mu\}$ on subsystems A and B. The locally projected density matrices are

$$\rho_{AB}(\mu) = \frac{1}{r_\mu}(P_A^\mu \otimes P_B^\mu)\rho_{AB}(P_A^\mu \otimes P_B^\mu), \tag{3.2}$$

where $r_\mu = \mathrm{Tr}[(P_A^\mu \otimes P_B^\mu)\rho_{AB}(P_A^\mu \otimes P_B^\mu)]$. The completeness of the set of projectors implies $\sum_\mu r_\mu = 1$. Hence, the result of this operation is summarized as

$$\rho_{AB} \to \sum_\mu r_\mu \rho_{AB}(\mu), \tag{3.3}$$

3. Tracing out ancilla: In this operation, an ancilla is entangled to the subsystem A. The process of entangling an ancilla is as follows: We put ancilla together with the subsystem A which is described by $\rho_{AB} \otimes \rho_R$ where ρ_R is the initial state of the ancilla. We let the subsystem $\tilde{A} = AR$ evolve under some unitary evolution $U_{AR} \in \mathscr{G}_0(\mathscr{H}^A \otimes \mathscr{H}^R)$. As a result, we get

$$\rho_{\tilde{A}B} = (U_{AR} \otimes \mathbb{I}_B)\rho_{AB} \otimes \rho_R (U_{AR}^\dagger \otimes \mathbb{I}_B) \tag{3.4}$$

Now, measuring the ancilla and finding it to be in a state $|\mu\rangle_R$ leads to a projected density matrix $\rho_{AB}(\mu)$,

$$\rho_{AB}(\mu) = \frac{1}{r_\mu} {}_R\langle\mu|\, \rho_{\tilde{A}B}\, |\mu\rangle_R \tag{3.5}$$

$$= \frac{1}{r_\mu} {}_R\langle\mu|\, (U_{AR} \otimes \mathbb{I}_B)\rho_{AB} \otimes \rho_R (U_{AR}^\dagger \otimes \mathbb{I}_B)\, |\mu\rangle_R \tag{3.6}$$

where $r_\mu = \mathrm{Tr}_{AB}[\, {}_R\langle\mu|\, U_{AR}(\rho_{AB} \otimes \rho_R)U_{AR}^\dagger\, |\mu\rangle_R]$ is the probability of observing the state $\rho_{AB}(\mu)$. Tracing out ancilla yields

$$\rho_{AB} \to \mathrm{Tr}_R\left(\rho_{\tilde{A}B}\right) = \sum_\mu r_\mu \rho_{AB}(\mu). \tag{3.7}$$

In general, LOCC operations can be used to prepare separable states with zero negativity. However, for bosonic systems there also exists a set of inseparable states which have zero negativity, but since they are inseparable they cannot be prepared using solely LOCC operations. This

phenomenon is known as bound entanglement [101] and suggests that there are other natural restricted classes of operations aside from LOCC. Combining both classes of operators leads to a general class of positive partial transpose preserving operations (PPT operations) which have the property that they map the set of positive partial transpose states into itself. In bosonic partial transpose, the monotonicity under PPT-operations has been shown in Refs. [162, 218].

We have not encountered any example of bound entangled states in fermionic systems. We believe that this is partly due to the fermion-number parity constraint on density matrices (see also the discussion below Eq. (3.53)). In low-dimensional Hilbert spaces, we provide theorems that forbid the existence of such states later in this chapter. For example, for a system of two fermionic modes (Theorem 3.2) or a system of one fermionic mode coupled to arbitrary fermionic Fock space (Theorem 3.3), the fermionic entanglement negativity is a necessary and sufficient condition for the separability, i.e., there is no inseparable state with zero negativity.

Let us now discuss the entanglement measure requirements in Table 3.1. We focus on the properties I and III and refer an interested reader to Ref. [189] for more details about the other requirements. By definition, the fermionic negativity vanishes for separable states. Moreover, it is important to note that similar to the bosonic partial transpose the set of states with zero negativity is convex for the fermionic partial transpose.

Theorem 3.1. *The states of vanishing negativity $\mathcal{N} = 0$ (or $\mathcal{E} = 0$) form a convex set.*

Proof:

Consider a linear interpolation between two states ρ_1 and ρ_2 with a zero negativity, $\rho_p = p\rho_1 + (1-p)\rho_2$, where $\left\|\rho_i^{T_A}\right\| = 1$ and $0 \leq p \leq 1$. We can then write

$$\left\|\rho_p^{T_A}\right\| = \left\|p\rho_1^{T_A} + (1-p)\rho_2^{T_A}\right\| \leq p\left\|\rho_1^{T_A}\right\| + (1-p)\left\|\rho_2^{T_A}\right\| = 1 \tag{3.8}$$

where we use the triangle inequality of the norm. The only solution to the above inequality is when $\left\|\rho_p^{T_A}\right\| = 1$, since $\left\|\rho_p^{T_A}\right\|$ cannot be smaller than one. This means that $\mathcal{N}(\rho_p) = 0$ for all $0 \leq p \leq 1$, which is the statement of convexity. ■

Table 3.1: The required conditions for an entanglement measure.

Property	**Description**
I. Separable states	No entanglement in separable states, $\mathcal{E}(\rho_{\text{sep}}) = 0$.
II. Invariance under local unitary	An entanglement measure must not change under applying a local unitary physical operator, $$\mathcal{E}\left((U_A \otimes U_B)\rho(U_A^\dagger \otimes U_B^\dagger)\right) = \mathcal{E}(\rho). \quad (3.9)$$
III. Additivity	Entanglement of a composite system is equal to the sum of the entanglements of the constituting systems. Consider a combined density matrix $\rho = \rho_{AB} \otimes \rho'_{AB}$, where $\rho_{AB} \in \mathcal{S}(\mathcal{H}^A \otimes \mathcal{H}^B)$ and $\rho'_{AB} \in \mathcal{S}(\mathcal{H}'^A \otimes \mathcal{H}'^B)$ describe entangled states between A and B, respectively. The additivity condition requires that $$\mathcal{E}(\rho_{AB} \otimes \rho'_{AB}) = \mathcal{E}(\rho_{AB}) + \mathcal{E}(\rho'_{AB}). \quad (3.10)$$
IV. Monotonicity under LOCC	An entanglement measure must not increase under LOCC defined in Eqs. (3.1)-(3.7), i.e. $$\mathcal{E}(\rho_{AB} \otimes \rho_R) = \mathcal{E}(\rho_{AB}), \quad (3.11)$$ and $$\mathcal{E}(\rho_{AB}) \geq \sum_\mu r_\mu \mathcal{E}(\rho_{AB}(\mu)). \quad (3.12)$$
V. Continuity	The entanglement measure should be continuous. The Hilbert-Schmidt distance between two density matrices ρ_1 and ρ_2 is defined by $$D_{HS}(\rho_1, \rho_2) = \text{Tr}[(\rho_1 - \rho_2)^2] \quad (3.13)$$ and is used as a measure of proximity of two states in the Hilbert space. It is required that if the Hilbert-Schmidt distance between two states vanishes, the difference between their entanglement should also go towards zero.
VI. Computability	The entanglement measure should be efficiently computable for every state.

We should emphasize that if we treat a density matrix of fermions in the occupation-number basis as a bosonic entity (as is done in Ref. [69]), we may be led to wrong results. For instance, it is possible that an inseparable density matrix of fermions expressed as a separable state within the bosonic formalism. This is, however, wrong, since the local bosonic density matrices are not legitimate fermionic density matrices (see the examples below).

Furthermore, an essential property of the fermionic partial transpose (2.30) is that it preserves the tensor product of fermionic density matrices and we can write

$$(\rho_{AB} \otimes \rho'_{AB})^{T_A} = \rho_{AB}^{T_A} \otimes \rho_{AB}^{\prime T_A}. \tag{3.14}$$

It is worth noting that the bosonic partial transpose of density matrices [69] does not preserve the tensor product structure and hence does not satisfy the additivity condition. This violation is rooted in the fact that the fermionic nature of density matrices was completely ignored in this formalism. Aside from the third requirement, the other conditions also hold for the bosonic partial transpose of density matrices in fermionic systems.

In the remainder of this section, we consider the simplest example of two local fermionic modes. As we will see, the entangled states of two complex fermionic modes shares a lot of similarities with the states of two qubits. In contrast, the entangled states of two Majorana modes has no analog in two-qubit systems.

Let $f_1 \in \mathscr{G}(\mathscr{H}^A)$ and $f_2 \in \mathscr{G}(\mathscr{H}^B)$ be two fermionic sites. A maximally entangled state is given by

$$|\Psi_s\rangle_f = \frac{1}{\sqrt{2}}(f_1^\dagger - f_2^\dagger)\,|0\rangle\,. \tag{3.15}$$

The logarithmic negativity of this state is $\mathscr{E} = \log 2$ using either bosonic or fermionic partial transpose. The corresponding state in a system of two qubits is a spin-singlet,

$$|\Psi_s\rangle_{\text{qubit}} = \frac{1}{\sqrt{2}}(|\uparrow\downarrow\rangle - |\downarrow\uparrow\rangle). \tag{3.16}$$

Now that we see the correspondence between the singlet state of qubits and two fermionic mode, it is instructive to consider Werner states which refer to a one-parameter set of mixed states,

$$\rho = \frac{1}{4}(1-p)\mathbb{I}_A \otimes \mathbb{I}_B + p\,|\Psi_s\rangle\langle\Psi_s| \tag{3.17}$$

where $0 \leq p \leq 1$ is a real parameter which interpolates between a maximally mixed state (identity) and a maximally entangled state (singlet).

It is easy to compute the bosonic negativity

$$\mathcal{E}_b(\rho) = \log\left(\frac{3}{4}(1+p) + \frac{1}{4}|1-3p|\right). \tag{3.18}$$

On the other hand, the Werner state can be considered as a valid density matrix of fermions and so, the fermionic negativity is found to be

$$\mathcal{E}(\rho) = \log\left(\frac{1}{2}(1+p) + \frac{1}{2}\sqrt{5p^2-2p+1}\right). \tag{3.19}$$

The bosonic (3.18) and fermionic (3.19) negativities are compared in Fig. 3.1. We note that these two quantities approach each other as p goes to zero or one and they are tangent at these two extreme points. Also, we observe that $\mathcal{E} \sim p^2$ in the regime $p \ll 1$, i.e. the lowest order term in the fermionic negativity grows quadratically as we depart from a separable state. The quadratic behavior is rather generic and a basis of our proof of Theorem 3.3 in the next section.

A notable difference between the bosonic and fermionic negativities is that $\mathcal{E}$ only vanishes at $p = 0$, whereas $\mathcal{E}_b$ remains zero as long as $p \leq 1/3$. This difference can be understood as a consequence of the fermion-number parity constraint on the density matrices in the

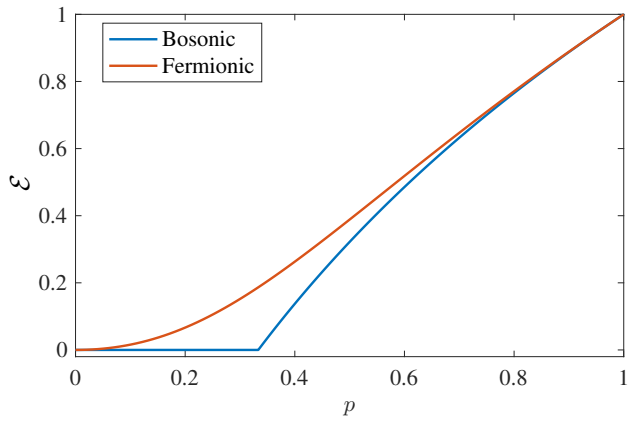

Figure 3.1: Comparison of entanglement negativity associated with fermionic and bosonic partial transpose for the Werner state (3.17).

fermionic Hilbert subspaces. The Werner states can be written in the occupation-number basis $\{|00\rangle, |10\rangle, |01\rangle, |11\rangle\}$ as

$$\rho = \frac{1}{4}\begin{pmatrix} \frac{1-p}{4} & 0 & 0 & 0 \\ 0 & \frac{1+p}{4} & \frac{-p}{2} & 0 \\ 0 & \frac{-p}{2} & \frac{1+p}{4} & 0 \\ 0 & 0 & 0 & \frac{1-p}{4} \end{pmatrix}. \tag{3.20}$$

The density matrix can be decomposed as follows [22]

$$\rho = \frac{p}{2}\sum_{i=x,y,z}\left[\frac{(\mathbb{I}-\sigma^i)_A}{2}\otimes\frac{(\mathbb{I}+\sigma^i)_B}{2}+\frac{(\mathbb{I}+\sigma^i)_A}{2}\otimes\frac{(\mathbb{I}-\sigma^i)_B}{2}\right]+\left(\frac{1-3p}{4}\right)\mathbb{I}_A\otimes\mathbb{I}_B, \tag{3.21}$$

in terms of local operators represented by Pauli matrices in the occupation number basis. If we view it as a bosonic system of qubits, each term is a product state since the operators are valid local density matrices. Therefore, the above decomposition shows that for $p \leq 1/3$ all the coefficients are positive and the density matrix is separable in the bosonic formalism. However, the density matrices $\mathbb{I}\pm\sigma^x = 1+f^\dagger f \pm f \pm f^\dagger$ (similarly, $\mathbb{I}\pm\sigma^y$) are not legitimate density matrices of fermions, because they violate the fermion-number parity symmetry and the above decomposition implies that the density matrix is never separable in the fermionic formalism unless $p = 0$. Therefore,

the separability criterion given by the bosonic partial transpose fails to address the separability of fermionic states correctly.

Let us conclude this part with a general remark about a system of two fermionic modes. The most general form of single-mode fermionic density matrix allowed by fermion-number parity symmetry is

$$\rho = \frac{\mathbb{I} + \alpha\sigma^z}{2}, \tag{3.22}$$

where $|\alpha| \leq 1$ so that ρ is positive definite. Taking two fermionic modes and constructing the full density matrix by tensor product, the resulting matrix contains only diagonal elements and hence, it is evident that a given fermionic density matrix is not separable (from fermionic point of view) unless all off-diagonal elements are zero. Moreover, we find that vanishing logarithmic negativity is a necessary and sufficient condition for separability of a two-fermion density matrix. Therefore, we can put forward the following theorem:

Theorem 3.2. *A two-fermion mixed state ρ is separable if and only if $\mathcal{N}(\rho) = 0$.*

The necessary condition is already evident. The sufficient condition follows immediately from the remark that any inseparable state has to have off-diagonal elements (see Ref. [189] for an explicit proof).

3.2 Entanglement negativity of Gaussian states

In this section, we present a method to calculate the entanglement negativity for noninteracting fermions using the coherent state representation. We will explain how this method can be adapted to quantum field theory calculations in the next chapter. Here, we show that the transformed operator ρ^{T_A} can be written in the Gaussian form (exponentiated bilinear) similar to the original density matrix. Therefore, one can simply compute the eigenvalues of the partially transposed density matrix and obtain the logarithmic negativity.

We consider a general form of quadratic Hamiltonians,

$$\hat{H} = \sum_{i,j} t_{ij} f_i^\dagger f_j + \Delta_{ij} f_i^\dagger f_j^\dagger + \text{H.c.} \tag{3.23}$$

The reduced density matrix of such Hamiltonians can also be recast in a quadratic form

$$\rho = \frac{e^{-\hat{\mathscr{H}}_I}}{\mathscr{Z}} \tag{3.24}$$

where the entanglement Hamiltonian is $\hat{\mathscr{H}}_I = \sum_{i,j} h^1_{ij} f_i^\dagger f_j + h^2_{ij} f_i^\dagger f_j^\dagger + \text{H.c.}$ and $\mathscr{Z}$ is the normalization factor. The eigenvalues of $\hat{\mathscr{H}}_I$ can be found in terms of generalized Green function which includes the pairing correlators [27, 160],

$$G_{ij} = \begin{pmatrix} 1-[C^T]_{ij} & [F^\dagger]_{ij} \\ F_{ij} & C_{ij} \end{pmatrix}, \tag{3.25}$$

where

$$C_{ij} = \langle f_i^\dagger f_j \rangle, \qquad F_{ij} = \langle f_i^\dagger f_j^\dagger \rangle, \tag{3.26}$$

are the ground state two-body correlators and the particle-hole correlators, respectively. By definition, they satisfy $C^\dagger = C$ and $F^T = -F$. The eigenvalues of the G matrix can be recast in the form of pairs $(\alpha_i, 1-\alpha_i)$. It is important to note that G and $\hat{\mathscr{H}}_I$ can be simultaneously diagonalized and the eigenvalues of G are related to those of $\hat{\mathscr{H}}_I$ (denoted by ζ_i) through $\zeta_i = \ln\left(\frac{1-\alpha_i}{\alpha_i}\right)$. Given the eigenvalues of $\hat{\mathscr{H}}_I$, one can easily compute various entanglement measures.

Let us now discuss how to construct the partial transpose in the coherent state representation. The reduced density matrix (3.24) can be represented in the coherent state basis by

$$\rho = \frac{1}{\mathscr{Z}_\rho} \int d[\xi] d[\bar{\xi}]\, e^{\frac{1}{2}\sum_{i,j\in A} \xi_i^T S_{ij} \xi_j} \, |\{\xi_j\}\rangle \langle\{\bar{\xi}_j\}| \tag{3.27}$$

where the S_{ij} matrix is given by

$$S_{ij} = \Gamma_{ij} + i\sigma_2\, \delta_{ij}, \tag{3.28}$$

the matrix Γ is related to the Green function matrix (3.25) through

$$[\Gamma^{-1}]_{ij} = \begin{pmatrix} [F^\dagger]_{ij} & [C^T]_{ij} \\ -C_{ij} & F_{ij} \end{pmatrix}, \tag{3.29}$$

the Grassmannian vector is $\xi_j^T = (\xi_j, \bar{\xi}_j)$ in the particle-hole basis as introduced above and $\mathscr{Z}_\rho = \mathrm{Pf}[S - i\sigma_2] = \mathrm{Pf}[\Gamma]$. Here, σ_2 is the Pauli matrix in the particle-hole basis and appears as the normalization factor $e^{-\bar{\xi}\xi}$ in $e^{-\bar{\xi}\xi}\,|\xi\rangle\langle\bar{\xi}|$. This representation of density matrix manifestly yields the identities in (3.26) and the fact that all higher-order correlators can be computed using the Wick expansion.

Using (2.36), we can write the partial transpose transformation as

$$\rho^{T_A} = \frac{1}{\mathscr{Z}_\rho}\int d[\xi]d[\bar{\xi}]\, e^{\frac{1}{2}\sum_{i,j\in A}\xi_i^T S_{ij}\xi_j}\, |\{i\bar{\xi}_j\}_{j\in A}, \{\xi_j\}_{j\in B}\rangle\langle\{i\xi_j\}_{j\in A}, \{\bar{\xi}_j\}_{j\in B}| \tag{3.30}$$

This transformation can be absorbed into a redefinition of the S_{ij} matrix after introducing the new variables $\xi = U_S\chi$,

$$\rho^{T_A} = \frac{1}{\mathscr{Z}_\rho}\int d[\chi]d[\bar{\chi}]\, e^{\frac{1}{2}\sum_{i,j\in A}\chi_i^T S_{ij}^{T_A}\chi_j}\, |\{\chi_j\}\rangle\langle\{\bar{\chi}_j\}| \tag{3.31}$$

where $S^{T_A} = U_S^T S U_S$ and $U_S = U_S^T$ is a permutation matrix

$$U_S = \begin{pmatrix} 0 & 0 & -i\mathbb{I}_{AA} & 0 \\ 0 & \mathbb{I}_{BB} & 0 & 0 \\ -i\mathbb{I}_{AA} & 0 & 0 & 0 \\ 0 & 0 & 0 & \mathbb{I}_{BB} \end{pmatrix}, \tag{3.32}$$

in the $(\{\xi_j\}_{j\in A},\{\xi_j\}_{j\in B},\{\bar{\xi}_j\}_{j\in A},\{\bar{\xi}_j\}_{j\in B})$ basis. Here, $\mathbb{I}_{AA}$ and $\mathbb{I}_{BB}$ are identity matrices acting on A and B subsystems, respectively. As a result of this transformation, we get the new matrix Γ^{T_A},

$$[\Gamma^{T_A}]^{-1} = (S^{T_A} - i\sigma_2)^{-1} = \begin{pmatrix} F'^{T_A} & [C^{T_A}]^T \\ -C^{T_A} & F^{T_A} \end{pmatrix}, \tag{3.33}$$

which yields the transformed correlators F^{T_A}, F'^{T_A} and C^{T_A}. Generically, $\mathrm{Re}[F^{T_A}] = -\mathrm{Re}[F'^{T_A}]$, while their imaginary parts are not in general related and only share the same eigenvalue spectrum.

In order to obtain the negativity (2.25) of ρ^{T_A}, we need to find the eigenvalues of the composite operator $\Xi = \rho^{T_A}\rho_A^{T_A\dagger}$ which is also Gaussian, since the product of two Gaussian states remain Gaussian. The result is

$$\Xi = \frac{1}{\mathcal{Z}_\rho^2}\int d[\chi]d[\bar{\chi}]\, e^{\frac{1}{2}\sum_{i,j\in A}\chi_i^T\tilde{S}_{ij}\chi_j}\,|\{\chi_j\}\rangle\langle\{\bar{\chi}_j\}| \tag{3.34}$$

Therefore, we determine the reconstructed Green function $\tilde{G}$ associated with $\tilde{S}$ as in

$$\tilde{G} = \begin{pmatrix} 1-\tilde{C}^T & \tilde{F}^\dagger \\ \tilde{F} & \tilde{C} \end{pmatrix}, \tag{3.35}$$

where we read off $\tilde{F}$ and $\tilde{C}$ from analog of Eq. (3.33) for $\tilde{S}$. The $2N = 2(m_A + m_B)$ eigenvalues of $\tilde{G}$ are in the form of pairs $(\lambda_i, 1-\lambda_i)$ where $0 \le \lambda_i \le 1$. Hence, the logarithmic negativity can be easily computed by

$$\begin{aligned}\mathcal{E} &= \ln\left[\frac{\mathrm{Tr}[\sqrt{\rho^{T_A}\rho_A^{T_A\dagger}}]}{\sqrt{\mathrm{Tr}[\rho^{T_A}\rho_A^{T_A\dagger}]}}\sqrt{\mathrm{Tr}[\rho^{T_A}\rho_A^{T_A\dagger}]}\right] \\ &= \sum_{i=1}^{M}\ln\left(\sqrt{\lambda_i}+\sqrt{1-\lambda_i}\right) + \frac{1}{2}\ln\left|\frac{\mathrm{Pf}[\tilde{S}-i\sigma_2]}{\mathrm{Pf}[S-i\sigma_2]^2}\right|,\end{aligned} \tag{3.36}$$

where we use the identity $\mathrm{Tr}\,\Xi = \mathrm{Pf}[\tilde{S} - i\sigma_2]/\mathscr{Z}_\rho^2$ by performing the Gaussian integral in (3.34). We can also determine the moments of partial transpose,

$$\mathrm{Tr}\,\Xi^n = \left[\prod_{i=1}^{M}(\lambda_i^n + (1-\lambda_i)^n)\right]\left(\frac{\mathrm{Pf}[\tilde{S} - i\sigma_2]}{\mathrm{Pf}[S - i\sigma_2]^2}\right)^n. \tag{3.37}$$

At this stage, let us make some remarks about the relation between our partial transpose and the bosonic partial transpose introduced in [69]. The partial transpose of Ref. [69] denoted by $\rho^{T_A^b}$ can be written as

$$\rho^{T_A^b} = \left(\frac{1+i}{2}\right)\rho^{T_A} + \left(\frac{1-i}{2}\right)\rho^{T_A\dagger}. \tag{3.38}$$

For Gaussian states, as we saw, ρ^{T_A} is a Gaussian operator; however, $\rho^{T_A\dagger}$ and ρ^{T_A} do not necessarily commute and $\rho^{T_A^b}$ is not guaranteed to be Gaussian. Nevertheless, for pure states one can show that $[\rho^{T_A\dagger}, \rho^{T_A}] = 0$, and hence, both definitions of the negativity are identical and simplified into $\mathscr{E} = \ln\|\rho^{T_A}\|$. The LN of pure states is in turn identical to the 1/2-Rényi entropy $S_{1/2} = 2\ln\mathrm{Tr}(\rho_A^{1/2})$.

3.3 Examples

In this section, we discuss the logarithmic negativity of two adjacent intervals in two canonical microscopic models: the Kitaev and Su-Schrieffer-Heeger chains. Our choice of models is motivated by the fact that these models offer three distinct regimes: Trivial phase where there is no entanglement between sites, topological phase where nearby sites form singlet or Majorana dimers, and a critical point which is described by CFT. We would like to compare the resulting entanglement negativities due to the fermionic and bosonic partial transpose in each regime. In the meantime, we also discuss a toy example of two-fermion density matrix which can also be used to represent the fixed-point density matrix in the topological and trivial limits of the Kitaev chain.

3.3.1 Kitaev Majorana chain

As the first example, we apply our construction of the partial transpose to the ground state of the Kitaev Majorana chain Hamiltonian [124]

$$\hat{H} = -\sum_j \Big[t f_{j+1}^\dagger f_j + \Delta f_{j+1}^\dagger f_j^\dagger + \text{H.c.} \Big] - \mu \sum_j f_j^\dagger f_j \,, \tag{3.39}$$

which describes a superconducting state of spinless fermions on a one-dimensional chain. For simplicity, here we set $t = \Delta$. It should be noted that the topological phase with Majorana zero-energy edge modes is realized when $|\mu|/t < 2$.

Figure 3.2 shows the entanglement negativity of two adjacent intervals for various values of $\mu/2t = (1+\delta)/(1-\delta)$. As shown in Fig. 3.2(a), deep inside the trivial phase both definitions of partial transpose consistently give zero. On the other hand, in the topological phase realized for $\delta < 0$, and in particular near $\delta = -1$ (i.e., $\mu/t = 0$), the bosonic and fermionic partial transpositions give very different results. For the fixed point wave function in the topological phase at $\mu = 0$, the fermionic partial transpose yields $\mathscr{E} = \ln(\sqrt{2})$. This is expected since A and B share a Majorana dimer (see also Fig. 3.3(a)), which connects the two intervals. On the other hand, the bosonic partial transpose of Ref. [69] does not capture this and simply gives zero. In fact, we numerically check that their result is equal to partial transpose of the bosonic density matrix (2.23) in the equivalent Ising spin chain given by

$$\hat{H} = -\sum_j [J S_{j+1}^x S_j^x + h S_j^z], \tag{3.40}$$

where $S_j^x = (S_j^+ + S_j^-)/2$ and $S_j^z = S_j^+ S_j^- - 1/2$ are spin-1/2 operators related to fermions through the Jordan-Wigner transformation $S_j^- = \exp(i\pi \sum_{l<j} f_l^\dagger f_l) f_l$ and $S_j^+ = \exp(-i\pi \sum_{l<j} f_l^\dagger f_l) f_l^\dagger$. The Hamiltonians in Eqs. (3.39) and (3.40) have identical ground state wave function, for values $t = \Delta = J/4$ and $\mu = h$, provided that we relate their bases so that spin-up state $|\uparrow\rangle = \sigma_j^+ |\downarrow\rangle$ is identified with occupied state of fermion $f_j^\dagger |0\rangle$ and spin-down $|\downarrow\rangle$ with an empty state $|0\rangle$.

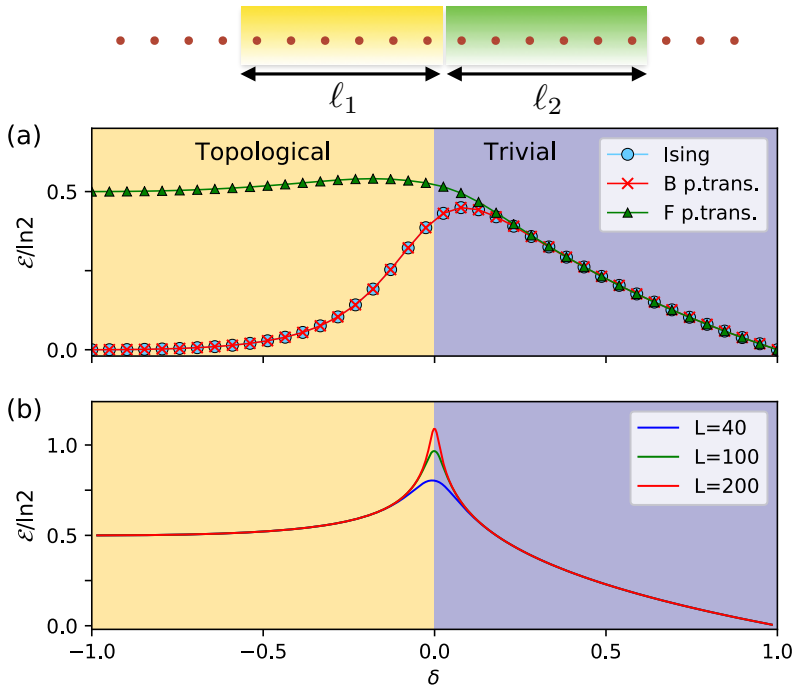

Figure 3.2: Logarithmic negativity of the Kitaev chain as a function of δ for two adjacent intervals with equal length ℓ. Here, $\mu = 1+\delta$ and $t = \Delta = (1-\delta)/2$ in Eq. (3.39). (a) Comparison of different definitions of the partial transpose. From the legend, first curve (blue circles) is computed for the bosonic many-particle density matrix according to Eq. (2.23) in the Ising chain with periodic boundary condition. Second (red crosses) and third (green upward triangles) curves are computed for the fermionic many-particle density matrix according to the rules introduced in Ref. [69] and our definition in Eq. (2.28), respectively. For all curves in this panel, we put $L = 4\ell = 8$. (b) Logarithmic negativity of the fermionic partial transpose as computed in Eq. (3.36) for large systems, $\ell = L/4$. All the data for fermionic chains are shown for anti-periodic boundary condition.

Clearly, we should not expect any entanglement in the Ising chain in the limit $h \to 0$ as it describes a ferromagnetic ordered phase where there is no entanglement between neighboring sites. However, in the fermionic phase we have Majorana modes and the correct entanglement can only be captured in an intrinsic fermionic formalism as derived in the previous chapter. It is worth noting that in the Ising model language, the ground state for infinitesimally small h looks like an equal superposition of two ferromagnetically ordered states, which gives rise to a contribution ln(2) to the (von Neumann) entanglement entropy for a finite interval embedded in the whole system. This correlation seen by the entanglement entropy is however classical one, and hence does not contribute to the entanglement negativity defined by using partial transpose.

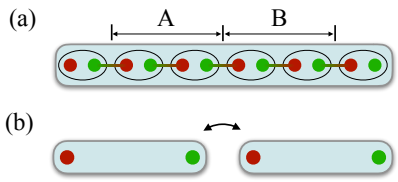

Figure 3.3: Hamiltonian of two coupled Majorana modes, (a) as in the reduced density matrix of two adjacent intervals on a single chain and (b) two coupled chains.

Two Majorana fermions

Here, we consider only two Majorana modes c_1 and c_2. The goal is to clarify the difference between the bosonic and fermionic partial transpose. We take a tunneling Hamiltonian between two Majorana fermion sites,

$$H = -i\Delta c_1 c_2. \tag{3.41}$$

The density matrix associated with the ground state manifold of this Hamiltonian effectively describes the reduced density matrix of two adjacent intervals on a single Kitaev Majorana chain, where the reduced density matrix can be represented in terms of two edge Majorana fermions c_1 and c_2 at the interface between the two intervals [191] (Fig. 3.3(a)). Furthermore, the Hamiltonian (3.41) can be physically related to the low energy modes of two coupled Majorana chains as shown in Fig. 3.3(b).

In order to compute the state density matrix and the corresponding partial transpose, we use a description in which the two coupled Majorana sites are part of two complex fermion modes and represent the density matrix in a basis of two-fermion modes. We combine c_1 and c_2 with the two unentangled Majorana modes c_3 and c_4 (which can be physically thought of as the zero modes at the far end on each interval or chain shown in Fig. 3.3(a) or (b)) to construct the complex fermions $f_1 = (c_1 + ic_3)/2$ and $f_2 = (c_2 + ic_4)/2$, where $f_1 \in \mathcal{G}(\mathcal{H}^A)$ and $f_2 \in \mathcal{G}(\mathcal{H}^B)$. The crucial point is that the entanglement does not depend on the representation. The density matrix can

then be expressed in the occupation-number basis $\{|00\rangle, |10\rangle, |01\rangle, |11\rangle\}$ as in

$$\rho = \frac{1}{4}(1 - ic_1c_2) = \frac{1}{4}\begin{pmatrix} 1 & 0 & 0 & 1 \\ 0 & 1 & 1 & 0 \\ 0 & 1 & 1 & 0 \\ 1 & 0 & 0 & 1 \end{pmatrix}. \tag{3.42}$$

With a little bit of algebra, one can see that $\mathcal{E}(\rho) = \log\sqrt{2}$ while the bosonic negativity vanishes. Let us now get some insights by checking the separability criterion. The density matrix can be expanded in the following form

$$\rho = \frac{1}{8}(\mathbb{I} + \sigma^x)_A \otimes (\mathbb{I} + \sigma^x)_B + \frac{1}{8}(\mathbb{I} - \sigma^x)_A \otimes (\mathbb{I} - \sigma^x)_B. \tag{3.43}$$

We should note that ρ is separable when it is viewed as density matrix of two qubits in the bosonic formalism. However, as already mentioned for the Werner states, $\mathbb{I} \pm \sigma^x = 1 + f^\dagger f \pm f \pm f^\dagger$ are not density matrices of fermions, and the state is not separable in the fermionic formalism. This observation means that the density matrix (3.42) is separable from point of view of bosonic partial transpose while it is entangled from the point of view of fermionic partial transpose.

3.3.2 Su-Schriffer-Heeger model

As the second example, we consider the Su-Schrieffer-Heeger (SSH) model,

$$\hat{H} = -\sum_j [t_2 f_{j+1}^{L\dagger} f_j^R + t_1 f_j^{L\dagger} f_j^R + \text{H.c.}] \tag{3.44}$$

where there are two fermion species living on each site f_j^L and f_j^R. This model realizes two topologically distinct phases: topologically non-trivial phase for $t_2 > t_1$, where the open chain has localized fermion modes at the boundaries, and trivial phase for $t_2 < t_1$ which is just an insulator with no boundary mode. Figure 3.4 compares the logarithmic negativity of two adjacent intervals

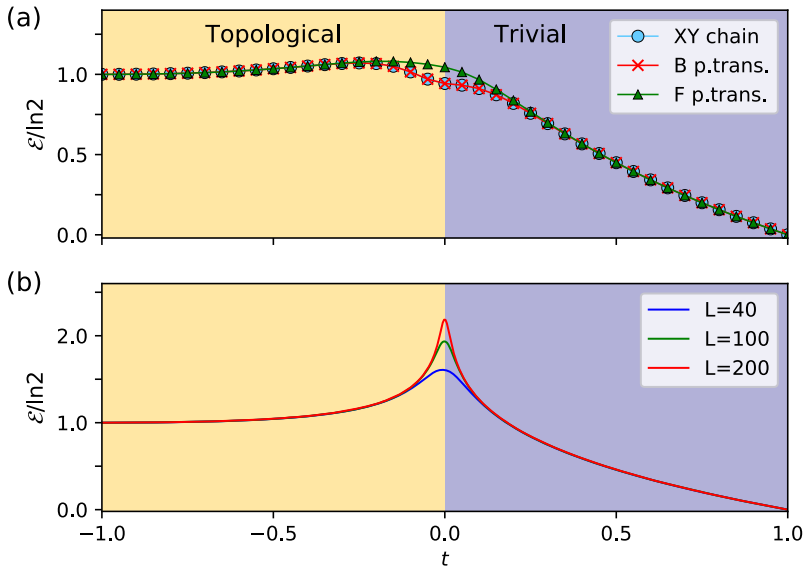

Figure 3.4: Logarithmic negativity of SSH model as a function of t where $t_1 = (1+t)/2$ and $t_2 = (1-t)/2$ in Eq. (3.44) for two adjacent intervals with equal length ℓ. (a) Comparison of different definitions of the partial transpose. See the caption of Fig. 3.2 for details of what each curve represents. For all curves in this panel, we put $L = 4\ell = 8$ (16 fermion sites). (b) Logarithmic negativity of the partial transpose as computed in Eq. (3.36) for large systems, $\ell = L/4$. All the data for fermionic chains are shown for anti-periodic boundary condition.

using different methods. In the topological phase, both bosonic and fermionic partial transpose give ln(2) associated with the complex fermion dimer (or singlet, Eq. (3.15)) at the sharing boundary between two intervals. The fact that the partial transpose can capture the entanglement in the SSH chain, but not the Kitaev chain, can be understood as a result of the violation of additivity (3.10). It is expected that any measure of entanglement S which satisfies (3.10), obeys the identity $S_{\rm SSH} = 2S_{\rm Kitaev}$, since two copies of the Kitaev chain are equivalent to a single copy of the SSH chain. One way to see this is by fusing pairs of Majorana fermions across the two copies of the Kitaev chain to form complex fermions in the SSH chain. Evidently, the negativity associated with the fermionic partial transpose is consistent with this requirement. Also, we again observe in Fig. 3.4(a) that the fermionic partial transpose of Ref. [69] is identical to the bosonic partial transpose. Here, the dual bosonic Hamiltonian after the Jordan-Wigner transformation is the

XY chain with alternating exchange coefficients,

$$\hat{H} = -2t_2 \sum_j [S_{j+1}^{x,L} S_j^{x,R} + S_{j+1}^{x,L} S_j^{y,L}] - 2t_1 \sum_j [S_j^{x,L} S_j^{y,R} + S_j^{y,L} S_j^{y,R}], \tag{3.45}$$

and ln(2) in the bosonic partial transpose comes from breaking the spin singlet $|\uparrow\downarrow\rangle + |\downarrow\uparrow\rangle$ at the interface between the two intervals.

In the remainder of this chapter, we use the machinery of fermionic partial transpose and fermion-number parity symmetry to present some ideas towards classifying pure and mixed states of a system with a few fermionic modes. In the case of two fermionic modes, the story is complete. According to the Theorem 3.2, vanishing negativity is a necessary and sufficient condition for separability.

3.4 Classification of mixed states

Here, we are dealing with a density matrix ρ and the ideal goal is to to classify all possible density matrices. This is clearly a daunting task beyond the scope of this disseration. Instead, we limit our discussion to how the entanglement negativity with respect to each partitioning scheme can constrain the form of the density matrix. For qubit systems, these constraints are found to be sufficient to fix the form of density matrix for certain families of states of three qubits such as generalized Werner states and mixed orthonormal Greenberger–Horne–Zeilinger (GHZ) states [61, 62].

Let us begin with a three-party setup. There have been several attempts at classifying the pure states of three-qubit systems [2, 63, 156, 198]. As we will see, the methods of Refs. [63, 156, 198] can be applied to fermionic systems. However, Ref. [2] introduces a method in which a given state is brought to a certain canonical form by unitary transformations and a generalized Schmidt decomposition are derived for those canonical states. This approach is not applicable to fermionic systems as the mentioned unitary transformation is not a valid operation in the fermionic formalism because of violating the fermion-number parity symmetry.

The classification of mixed states of three qubits is much more complicated and there is no universal framework which addresses all possible states [3, 61, 62, 71, 180]. Due to numerous possibilities of three-qubit mixed states, previous studies have tried to devise technologies to distinguish certain families of density matrices which obey a certain form. For instance, Dür *et. al.* [61, 62] used negativities to classify superposition of GHZ density matrices associated with a set of orthonormal GHZ states and Acín *et. al.* [3] introduced entanglement witnesses to distinguish mixed states of GHZ and W states with positive coefficients. Interestingly, Ref. [3] finds that the W-type mixed states form a subspace of finite volume as opposed to the W-type pure states which occupies a measure-zero subspace in a parameterized Hilbert space. Ref. [71] also provided a classification for a family of GHZ symmetric mixed states (parametrized in a Euclidean space with the Hilbert-Schmidt metric) based on the invariance of entanglement properties under general local operations.

In what follows, we put forward a powerful theorem based on which we can build two important theorems. The latter theorems are particularly helpful in diagnosing separable and biseparable mixed states of three fermions.

Theorem 3.3. *Consider a density matrix $\rho \in \mathscr{S}(\mathscr{H}^A \otimes \mathscr{H}^{\bar{A}})$ where $\mathscr{H}^A$ contains one fermionic mode and $\mathscr{H}^{\bar{A}}$ is an arbitrary Fock space. ρ can be decomposed as*

$$\rho = \sum_i w_i \rho_{A,i} \otimes \rho_{\bar{A},i} \tag{3.46}$$

where $w_i \geq 0$, if and only if $\mathscr{N}(\rho) = 0$.

Proof:

The necessary condition is clearly true, given that the state is separable with respect to such partitioning. For the sufficient condition, one can use perturbation theory to show that for any inseparable state in an immediate vicinity of separable states $\rho = \rho_{\text{sep}} + \rho_{\text{off}}$, the negativity is non-zero to the leading order [189]. Here, $\rho_{\text{sep}} = w_0 |0\rangle\langle 0| \otimes \rho_0 + w_1 f_1^\dagger |0\rangle\langle 0| f_1 \otimes \rho_1$ is a separable part in which $f_1 \in \mathscr{G}(\mathscr{H}^A)$ and $\rho_1, \rho_2 \in \mathscr{S}(\mathscr{H}^{\bar{A}})$ are two fermionic density matrices,

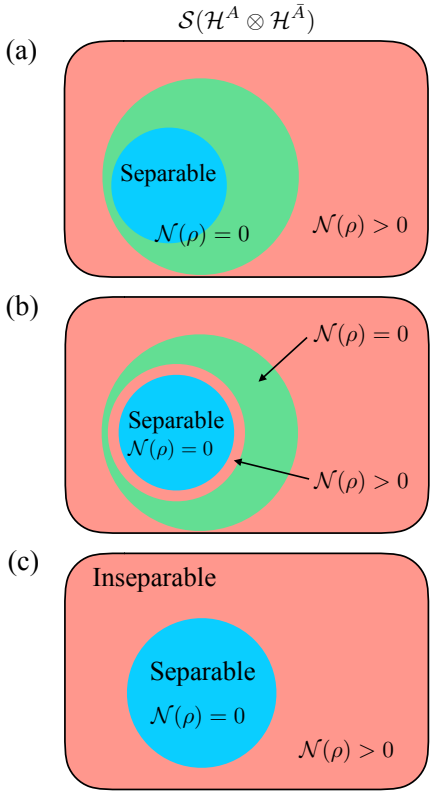

Figure 3.5: Schematic structure of separable and inseparable sets of states and values of the negativity in a bipartite system of one fermion $\mathscr{H}^A$ and a Fock space $\mathscr{H}^{\bar{A}}$ (discussed in Theorem 3.3). (a) A situation in which there exists a subset of inseparable states with zero negativity away from separable states, that results in a contradiction (see the text). Therefore, the correct structure is given by (b), which means zero negativity is a necessary and sufficient condition for separability in this setup.

and $\rho_{\text{off}} = f_1^\dagger |0\rangle \langle 0| \otimes \delta\rho + |0\rangle \langle 0| f_1 \otimes \delta\rho^\dagger$ is an inseparable part where $\delta\rho \in \mathscr{G}_1(\mathscr{H}^{\bar{A}})$ is a fermion-number parity odd operator.

The rest of the proof is a consequence of the convexity of the zero-negativity states (Theorem 3.1). Note that separable states form a convex set as shown in Fig. 3.5(a). Our finding from perturbation theory implies that there exists at least a finite strip of states S_1 right outside the boundary of separable states (shown as a red strip in Fig. 3.5(b)) where $\mathscr{N}(\rho) > 0$. Let us assume that there exists a subset S_2 of states outside this strip (green region) where the negativity vanishes $\mathscr{N}(\rho) = 0$. This immediately contradicts the convexity of the set of states with zero negativity. Therefore, $\mathscr{N}(\rho) > 0$ for all inseparable states (as depicted in Fig. 3.5(c)).

It is worth noting that a special case of Theorem 3.3 is Theorem 3.2 where $\mathscr{H}^{\bar{A}}$ consists of one fermionic mode. Another special case is applicable to the mixed state of three fermions, where $\mathscr{H}^{\bar{A}} = \mathscr{H}^B \otimes \mathscr{H}^C$ containing both f_2 and f_3 modes.

Let us recall that the negativity with respect to each party in a three-fermion system is defined by

$$\mathcal{N}_{A(BC)} = \frac{\mathrm{Tr}|\rho^{T_A}| - 1}{2} \tag{3.47}$$

and similarly for $\mathcal{N}_{B(AC)}$ and $\mathcal{N}_{C(AB)}$.

Corollary 3.1. *ρ can be decomposed as $\rho = \sum_i w_i \rho_{A,i} \otimes \rho_{BC,i}$ where $w_i \geq 0$, if and only if $\mathcal{N}_{A(BC)} = 0$.*

As a result of the above corollary, we arrive at the following two theorems.

Theorem 3.4. *ρ is fully separable,*

$$\rho = \sum_i w_i \ \rho_{A,i} \otimes \rho_{B,i} \otimes \rho_{C,i}, \tag{3.48}$$

if and only if $\mathcal{N}_{A(BC)} = \mathcal{N}_{B(AC)} = \mathcal{N}_{C(AB)} = 0$.

A straightforward consequence of this theorem is a useful criterion for bi-separability

Theorem 3.5. *ρ is bi-separable,*

$$\rho = \sum_i w_i \rho_{A,i} \otimes \rho_{BC,i}, \tag{3.49}$$

where at least one of $\rho_{BC,i}$ are inseparable, if and only if $\mathcal{N}_{A(BC)} = 0$, but $\mathcal{N}_{B(AC)} \neq 0$ and $\mathcal{N}_{C(AB)} \neq 0$.

We conclude our discussion with a few remarks and a conjecture about the structure of reduced density matrices of generic fermionic systems. As we learned, the transformation rule for the *fermionic* partial transpose in the Fock space Eq. (2.28) contains a phase factor in addition to

the *bosonic* partial transpose (i.e., matrix transposition). In the case where each subsystem has the same fermion-number parity on both sides (inside bra and ket) the phase factor is identically one and fermionic partial transpose becomes a matrix transposition. This property is independent of the representation and in general we may say:

Remark 3.1. *For a bipartite state density matrix $\rho \in \mathscr{S}(\mathscr{H}^A \otimes \mathscr{H}^B)$ with even fermion-number parity in each subsystem, i.e.,*

$$[(-1)^{F_A}, \rho] = 0, \tag{3.50}$$

the fermionic and bosonic entanglement negativities are identical.

This in turn leads us to divide the density matrices of fermions into two categories.

Remark 3.2. *There exist two types of states in fermionic systems:*

I. Fermion-number parity of subsystems is even,

$$[(-1)^{F_A}, \rho] = 0, \tag{3.51}$$

II. Fermion-number parity of subsystems is mixed,

$$[(-1)^{F_A}, \rho] \neq 0. \tag{3.52}$$

It is worth noting that there is no density matrix with only terms of odd subsystem fermion-number parity, since ρ must always contain terms with even subsystem parity to guarantee $\mathrm{tr}(\rho) = 1$. It is easy to deduce from the definition of a separable state (2.19) that the first type of states can be either separable or inseparable, whereas the second type is always inseparable. As mentioned, for the first type of states, there is no difference between fermionic and bosonic entanglement negativities and we expect that all the known results about entanglement and separability in the context of qubit systems hold in this case as well. However, type II density matrices

are specific to fermionic systems. A canonical example of this case is when we consider bipartitioning a Hilbert space of dimension 2^N into a single fermionic mode and the rest (i.e., the Hilbert space is decomposed as $2\times 2^{N-1}$ as we did for Theorem 3.3). Any inseparable state in this bipartite system is necessarily type II. We have proven in Theorem 3.3 that the entanglement negativity of such states is positive. Beyond this, we believe that this observation could be generalized to the following conjecture.

Conjecture 3.1. *The entanglement negativity of inseparable states of type II (3.52) is always non-vanishing,*

$$\mathcal{E}(\rho) > 0. \tag{3.53}$$

An immediate consequence of this conjecture is that vanishing fermionic entanglement negativity is a necessary and sufficient condition for separability, as long as type I inseparable states are excluded. This property is particularly relevant to fermionic systems realized in condensed matter setups, where one wants to study the entanglement in the ground state or finite-temperature state of a Hamiltonian. Having type I inseparable states as a ground (finite-temperature) state of a fermionic Hamiltonian requires fine-tuned models which contain only terms that preserve the subsystem fermion-number parity. Therefore, as far as a generic Hamiltonian of fermions possibly with hopping terms, pairing terms, and interactions is concerned, non-zero negativity implies an inseparable state.

3.5 Summary and future directions

In this chapter, we investigate several quantum information theoretic properties of analog of the entanglement negativity in fermionic systems. This quantity was recently introduced [191] as a measure of entanglement in mixed states of fermions based on the fermionic partial time-reversal transformation of the density matrix. Using this analogy, we have called it fermionic entanglement negativity. Among various properties an entanglement measure should satisfy, we

show that the fermionic entanglement negativity is non-increasing (monotone) under LOCCs which preserve the fermion-number parity. Furthermore, the fermionic negativity is additive when the Hilbert space is enlarged by adding extra degrees of freedom through a tensor product and invariant under local unitary operations.

We further discuss the relation between the separability criterion and entanglement negativity in fermionic systems. As expected (and similar to qubit systems), the fermionic negativity of a separable state is identically zero.

We find that the fermionic partial transpose can distinguish the topological phase from the trivial phase in canonical examples of one-dimensional TIs and TSCs. This is in contrast with the bosonic partial transpose which fails to diagnose the entanglement in TSCs.

In order to show the versatility of the fermionic entanglement negativity, we use it to classify entangled states in systems with small Hilbert spaces containing two or three fermionic modes. As we have learned, the fermionic entanglement negativity is a faithful and intrinsic measure of entanglement in such systems; hence, it would be interesting to see applications of the fermionic negativity in characterizing various quantum processes and states for measurement-based fermionic quantum computation [28, 48, 243].

Chapter 4

Entanglement negativity of critical theories

"The [quantum] theory reminds me a little of the system of delusions of an exceedingly intelligent paranoiac."

— Albert Einstein

A notable property of entanglement entropies (EEs) is that the leading order term shows certain universal scaling behaviors as a function of system size. In (1+1)d systems, it is well-known that EEs of gapped states assume a boundary (area) law [93], i.e., they saturate as the system is made larger, while EEs of critical (bosonic or fermionic) states described by CFTs increase logarithmically with system size [32, 33, 98, 217], i.e., $S \sim \ln L$ where the coefficient is proportional to the central charge. In contrast, in higher dimensions, most systems obey a boundary law [65]. However, there are important exceptions to the area law in higher dimensions: Namely, free fermions with a Fermi surface [17, 60, 85, 95, 136, 203, 205, 241] and Fermi

Part of the material presented in this chapter was previously published in: H. Shapourian, K. Shiozaki, S. Ryu, Phys. Rev. B 95, 165101 (2017) and H. Shapourian and S. Ryu, J. Stat. Mech.: Theory Exp. xxxx. Some text has been modified. Copyright by the American Physical Society (APS); reuse permitted according to APS copyright policies.

liquids [204, 206]. In the case of codimension-one Fermi surfaces in d-dimensions, the entanglement entropies to the leading order scale as $S \sim L^{d-1} \ln L$.

Unlike pure states, EEs are not good measures of the useful entanglement in mixed states, e.g. finite temperature states of quantum systems or tripartite entanglement of a pure state. This should be expected since a generic mixed state contains both quantum and classical correlations. The former can be used as a resource for quantum computation (i.e. , useful entanglement), while the latter could be a result of LOCCs and is not a resource for quantum computation. In the case of finite temperature density matrices, the classical correlations are due to thermal fluctuations. At sufficiently high temperatures thermal fluctuations put the system in an equal superposition of all quantum states, which is in essence fully classical. Given this, it is important to distinguish between classical mixing and quantum entanglement. However, it is well-known that the usual bipartite von Neumann or Rényi entropies cannot exclusively capture the quantum entanglement.

As we have seen, the (logarithmic) entanglement negativity defined in terms of partial transpose of the density matrix could be a good candidate to detect the quantum entanglement of mixed states. In this chapter, we study the entanglement negativity of free fermions with a Fermi surface. Our starting point is the Hamiltonian of free fermion chain with nearest neighbor hopping,

$$\hat{H} = -\sum_i [t(f_{i+1}^\dagger f_i + \text{H.c.}) + \mu f_i^\dagger f_i] \tag{4.1}$$

which describes a one-dimensional metal, where the Fermi surface consists of two points. The low energy theory of this model is the massless Dirac fermions in (1+1)d. We discuss the entanglement due to three different ways of partitioning the system. Two bipartite geometries, (1) an interval of length ℓ embedded inside an infinite chain (Fig. 4.1(a)), or (2) a semi-infinite chain (Fig. 4.1(b)), and (3) a tripartite geometry with two adjacent intervals ℓ_1 and ℓ_2 (Fig. 4.1(c)). First, we derive the zero-temperature entanglement negativity of free fermions in (1+1)d which

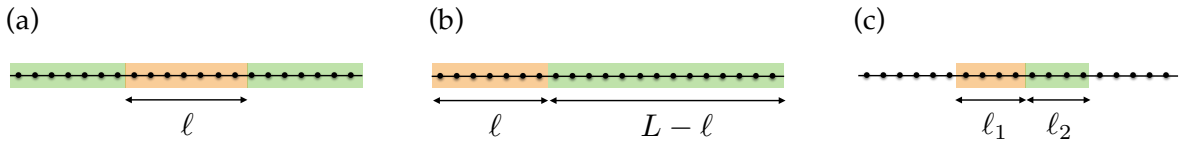

Figure 4.1: Various ways of partitioning the 1d system. Bipartite geometry: (a) One interval in the infinite line and (b) one interval in the semi-infinite line (open boundary condition is assumed). (c) Tripartite geometry. In all cases, the density matrix ρ corresponds to the union of the colored regions, and the partial transpose is applied to the orange region.

shows a logarithmic violation of the area law. Furthermore, we would like to see the fate of this logarithmic term at finite temperatures and also ask how our result in (1+1)d is generalized to higher dimensions. In general, we find that there are two temperature regimes: First, a quantum regime at low temperatures when $L_\beta > L$, where $L_\beta = \hbar v_F / k_B T$ is the length scale associated with thermal fluctuations at temperature T (and v_F is the Fermi velocity) and L is the system size, and the entanglement negativity remains almost unchanged and close to its value at the zero temperature. Second, a classical regime when $L_\beta \sim L$ and the entanglement negativity decays asymptotically to zero. The latter regime is characterized by an area-law entanglement of the form $L^{d-1} \ln L_\beta$. This behavior is a direct signature of quantum-to-classical crossover at finite temperatures. Compared with the general (bosonic) CFT calculations [37] in (1+1)d where the negativity at low temperatures $L < L_\beta$ was difficult to be derived, our analytical results covers both regimes of temperatures and faithfully interpolates between them.

This chapter is organized as follows: In Sec. 4.1, we analytically derive the finite-temperature logarithmic negativity for massless Dirac fermions, which is the continuum theory for the critical point of the SSH model. To this end, we develop a replica approach to relate the negativity to the partition functions on higher genus Riemann spacetime manifold. In Sec. 4.2, we present numerical results for 1d systems which completely match the above expression. Next in Sec. 4.3 we explain how 1d results can be generalized to higher dimensions and explicitly check 2d formulas against numerical calculations. We give a summary and an overview of possible future directions at the end.

4.1 Replica approach

Here, we present a spacetime view of moments of partial transpose, $\mathrm{Tr}(\rho^{T_A}\rho^{T_A\dagger}\rho^{T_A}\rho^{T_A\dagger}\cdots)$, and write them in terms of partition functions. We use quantum field theory techniques such as bosonization to evaluate those partition functions.

Before we proceed, let us briefly review the replica approach to find the regular entanglement entropy. Next, we make connections to our construction of fermionic partial transpose. As we discussed earlier, the Rényi entanglement entropy (REE) of a reduced density matrix ρ is defined by

$$\mathscr{R}_n = \frac{1}{1-n}\ln \mathrm{Tr}[\rho^n]. \tag{4.2}$$

The above expression corresponds to a partition function on the spacetime manifold shown in Fig. 4.2(a), which can be recast as correlators of twist fields. The idea of using the twist fields for the REE of the Dirac fermions was originally initiated by Casini *et. al.* [41]. The fermionic twist field approach was further applied to the entanglement negativity of disjoint intervals [97]. Here, we present an explicit derivation of the twist matrix using the coherent state representation.

A generic density matrix can be represented in the fermionic coherent state as

$$\rho = \int d\alpha d\bar{\alpha}\, d\beta d\bar{\beta}\, \rho(\bar{\alpha},\beta)|\alpha\rangle\langle\bar{\beta}|e^{-\bar{\alpha}\alpha-\bar{\beta}\beta} \tag{4.3}$$

where α, $\bar{\alpha}$, β and $\bar{\beta}$ are independent Grassmann variables and we omit the real-space (and possibly other) indices for simplicity. The trace formula then reads

$$Z_{\mathscr{R}_n} = \mathrm{Tr}[\rho^n] = \int \prod_i d\psi_i d\bar{\psi}_i \prod_i \Big[\rho(\bar{\psi}_i,\psi_i)\Big] e^{\Sigma_{i,j}\bar{\psi}_i T_{ij}\psi_j}, \tag{4.4}$$

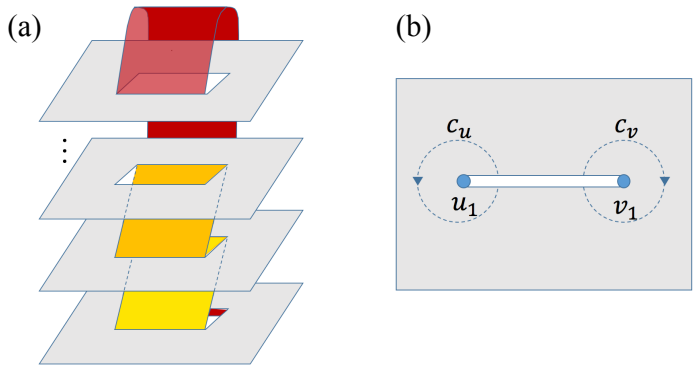

Figure 4.2: Path integral representation of Rényi entropy for (a) multi-sheet and (b) single-sheet spacetime manifold.

where the subscripts in ψ_i and $\bar{\psi}_i$ denote the replica indices and T is called the twist matrix,

$$T = \begin{pmatrix} 0 & -1 & 0 & \dots \\ 0 & 0 & -1 & 0 \\ \vdots & \vdots & \ddots & -1 \\ 1 & 0 & \cdots & 0 \end{pmatrix}. \tag{4.5}$$

Note that the global boundary condition depends on the replica index n, $T^n = (-1)^n$. The above expression can be viewed as a partition function on a n-sheet spacetime manifold where the n flavors (replicas) ψ_i are glued in order along the cuts. Alternatively, one can consider a multi-component field $\Psi = (\psi_1, \cdots, \psi_n)^T$ on a single-sheet spacetime. This way when we traverse a close path through the interval the field gets transformed as $\Psi \mapsto T\Psi$. Hence, each interval can be represented by two branch points $\mathcal{T}_n$ and $\mathcal{T}_n^{-1}$ –the so called twist fields– and the REE of one interval can be written as a two-point correlator [41],

$$Z_{\mathcal{R}_n} = \langle \mathcal{T}_n(u)\mathcal{T}_n^{-1}(v) \rangle, \tag{4.6}$$

where u and v denote the real space coordinates of the two ends of the interval on a chain.

In the remainder of this section, we compute the moments of the partially transposed density matrix ρ^{T_A} and ultimately the logarithmic negativity. We begin with a general point of view

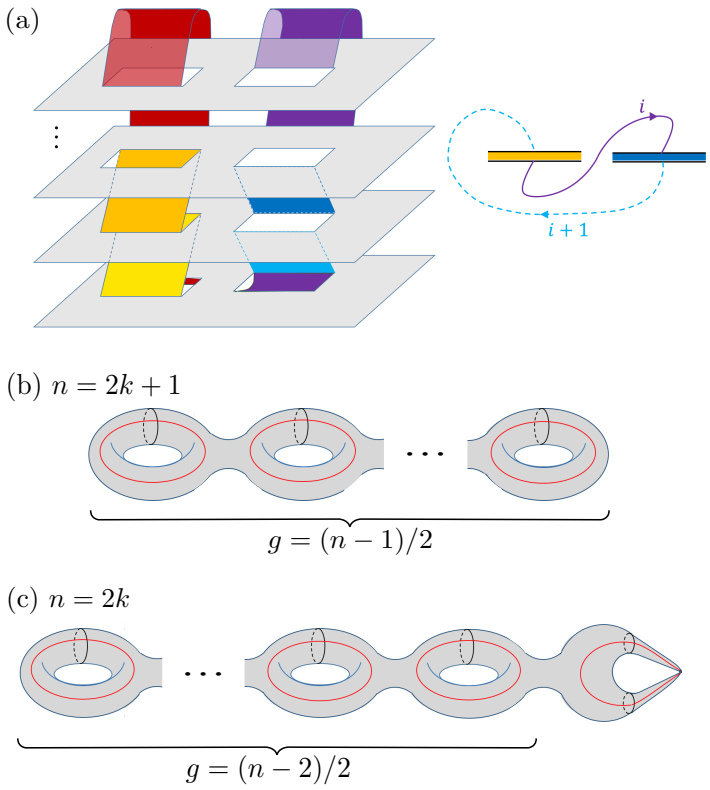

Figure 4.3: (a) Path integral representation of moments of the partial transpose $\mathcal{E}_n$ (4.7). (b) and (c) Equivalent spacetime manifold of $\mathcal{E}_n$ for two adjacent intervals which is a torus Σ_g of genus g when n is odd and Σ_g with an additional pinched torus when n is even.

based on the replica approach [35, 36, 97] and provide an equivalent spacetime picture of the Rényi negativity.

One can derive an analogous relation to Eq. (4.4) for the transpose. We define moments of the partial transpose (aka, Rényi negativity) for any integer powers as follows

$$\mathcal{E}_n := \begin{cases} \ln \mathrm{Tr}(\rho^{T_A}\rho^{T_A\dagger}\cdots\rho^{T_A}\rho^{T_A\dagger}) & n \text{ even}, \\ \ln \mathrm{Tr}(\rho^{T_A}\rho^{T_A\dagger}\cdots\rho^{T_A}) & n \text{ odd}. \end{cases} \tag{4.7}$$

Thus, the analytic continuation to obtain the logarithmic negativity (2.25) is

$$\mathcal{E}(\rho) = \lim_{n\to 1/2} \mathcal{E}_{2n}. \tag{4.8}$$

To proceed, we recall the transposed density matrix

$$\rho^T = \int d\alpha d\bar{\alpha}\, d\beta d\bar{\beta}\, \rho(\bar{\alpha},\beta)|i\bar{\beta}\rangle\langle i\alpha|e^{-\bar{\alpha}\alpha-\bar{\beta}\beta}, \tag{4.9}$$

and

$$(\rho^T)^\dagger = \int d\alpha d\bar{\alpha}\, d\beta d\bar{\beta}\, \rho(\bar{\alpha},\beta)|-i\bar{\beta}\rangle\langle -i\alpha|e^{-\bar{\alpha}\alpha-\bar{\beta}\beta}. \tag{4.10}$$

Therefore, we can write for a product of n density matrices (composed of ρ^T and $\rho^{T\dagger}$ alternating)

$$\begin{aligned}
&\mathrm{Tr}(\rho^T\rho^{T\dagger}\rho^T\rho^{T\dagger}\cdots)\\
&=\int\prod_i d\alpha_i d\bar{\alpha}_i d\beta_i d\bar{\beta}_i\, \rho(\bar{\alpha}_i,\beta_i)e^{-\sum_{i=1}^n(\bar{\alpha}_i\alpha_i+\bar{\beta}_i\beta_i)}\langle i\alpha_1|-i\bar{\beta}_2\rangle\ldots\langle i\alpha_{n-1}|-i\bar{\beta}_n\rangle\langle i\alpha_n|(-1)^n i\bar{\beta}_1\rangle\\
&=\int\prod_i d\alpha_i d\bar{\alpha}_i\prod_i[\rho(\bar{\alpha}_i,\alpha_i)]e^{\sum_{i,j}\bar{\alpha}_i T^R_{ij}\alpha_j},
\end{aligned} \tag{4.11}$$

which leads to the following twist matrix

$$\widetilde{T} = \begin{pmatrix} 0 & \cdots & 0 & (-1)^{n-1}\\ 1 & \ddots & \vdots & \vdots\\ 0 & 1 & 0 & 0\\ \cdots & 0 & 1 & 0 \end{pmatrix}. \tag{4.12}$$

Putting these together, we can write the general expression for moments of the partial transpose as

$$Z^{(\mathrm{r})}_{\mathscr{E}_n} = \mathrm{Tr}(\rho^{T_A}\rho^{T_A\dagger}\rho^{T_A}\rho^{T_A\dagger}\cdots) = \int\prod_i d\psi_i d\bar{\psi}_i\, \rho(\bar{\psi}_i,\psi_i)e^{\sum_{i,j}\bar{\psi}^A_i\widetilde{T}_{ij}\psi^A_j}e^{\sum_{i,j}\bar{\psi}^B_i T_{ij}\psi^B_j} \tag{4.13}$$

where $\psi^{A(B)}$ refers to the sites in A and B intervals. Figure 4.3(a) shows the spacetime picture of this quantity. Therefore, it can be written as a four-point correlator

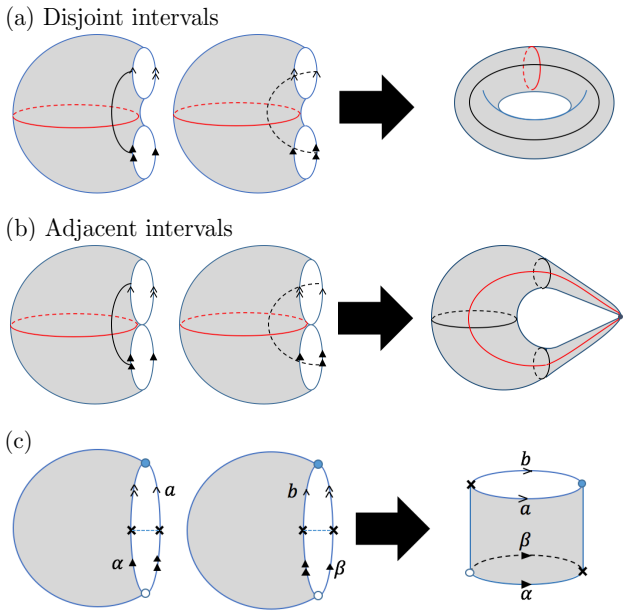

Figure 4.4: Spacetime manifold of $\mathrm{Tr}[\rho^{T_A}\rho^{T_A\dagger}]$ or $\mathrm{Tr}[(\rho^{T_A})^2]$ for (a) two disjoint intervals and (b) two adjacent intervals. In each panel, equivalent loops appear in the same color. (c) Spacetime manifold of $\rho^{T_A}\rho^{T_A\dagger}$ or $(\rho^{T_A})^2$ for two adjacent intervals as a generator of $\mathcal{E}_n$ shown in Figs. 4.3(b) and (c).

$$Z^{(\mathrm{r})}_{\mathcal{E}_n} = \langle \tilde{\mathcal{T}}_n^{-1}(u_A)\tilde{\mathcal{T}}_n(v_A)\mathcal{T}_n(u_B)\mathcal{T}_n^{-1}(v_B)\rangle\,. \tag{4.14}$$

where $\tilde{\mathcal{T}}_n$ and $\tilde{\mathcal{T}}_n^{-1}$ are twist fields associated with $\tilde{T}$. Note that the order of twist fields are reversed for the first interval. For fermions with a global $U(1)$ gauge symmetry (i.e., particle-number conserving systems) there is a freedom to twist boundary condition along the fundamental cycles (e.g. the path shown in the right panel of Fig. 4.3(a)) of the spacetime manifold by a $U(1)$ phase. The boundary conditions are independent and in principle can be different. If we assume a replica symmetry (i.e. uniform boundary conditions) $\psi \mapsto e^{i\alpha}\psi$, the corresponding expression in the operator formalism is given by

$$Z_{\mathcal{E}_n}(\alpha) = \mathrm{Tr}[(\rho^{T_A}e^{i\alpha F_A})^n]. \tag{4.15}$$

From this, we get a family of Rényi negativities (RNs) parametrized by α. However, for a generic fermionic system (including superconductors), the $U(1)$ symmetry is reduced to $\mathbb{Z}_2$ fermion-

number parity symmetry. Hence, $\alpha = 0$ or π are the most general allowed values. We should reemphasize that either quantities are described by a partition function on the same spacetime manifold (Fig. 4.3) as in the case of bosonic systems [36], while they differ in the boundary condition for fundamental cycles of the manifold. In other words, $Z^{(\mathrm{ns})}_{\mathscr{E}_n}$ and $Z^{(\mathrm{r})}_{\mathscr{E}_n}$ correspond to anti-periodic (Neveu-Schwarz, NS) and periodic (Ramond, R) boundary conditions, respectively. This can be readily seen by comparing the corresponding twist matrices. In what follows, we compute the two RNs for various partitioning schemes:

- Two **disjoint intervals** as introduced above which are given by four-point correlators.

- Two **adjacent intervals** which are described by three twist fields. Hence, the RNs are given in terms of three-point correlators

$$Z^{(\mathrm{r})}_{\mathscr{E}_n} = \langle \widetilde{\mathscr{T}}_n^{-1}(u_A)\mathscr{Q}_n^2(v_A)\mathscr{T}_n^{-1}(v_B)\rangle\,, \tag{4.16}$$

  where we introduce the fusion of unlike twist fields,

$$\mathscr{Q}_n^2 := \mathscr{T}_n\widetilde{\mathscr{T}}_n. \tag{4.17}$$

- The **bipartite geometry** where the two intervals combined form the entire system which is in the ground state. The RNs are given by the two-point correlators

$$Z^{(\mathrm{r})}_{\mathscr{E}_n} = \langle \mathscr{Q}_n^{-2}(u_A)\mathscr{Q}_n^2(v_A)\rangle\,. \tag{4.18}$$

Let us make a few remarks as to why the choice $[\rho^{T_A}\rho^{T_A\dagger}\rho^{T_A}\cdots]$ is a more desirable quantity from the quantum field theory point of view. First and foremost, the above choice can be written as a partition function on the same spacetime manifold (Fig. 4.3(a)) as the one originally proposed for the entanglement negativity in bosonic systems [36]. Moreover, only this quantity has a smooth behavior as we bring two disjoint intervals closer to each other to obtain two adjacent

intervals. To illustrate this, let us consider the case of two replicas and the following quantities: $E_0 = \mathrm{Tr}\rho^2$, $E_1 = \mathrm{Tr}(\rho^{T_A}\rho^{T_A\dagger})$, and $E_2 = \mathrm{Tr}(\rho^{T_A})^2$. For two disjoint intervals, these quantities correspond to the toroidal spacetime (Fig. 4.4(a)), and for two adjacent intervals, E_0 defines the partition function on a sphere, while E_1 and E_2 define the partition function on a pinched torus (which is homeomorphic to a sphere with two points being identified, see Fig. 4.4(b)). Before we continue our discussion, it is worth mentioning that one can also consider another quantity $E_3 = \mathrm{Tr}(\rho U_{A_1}\rho^{T_A}U_{A_1}^\dagger)$. Although this quantity is a very useful measure in other contexts such as detecting the many-body topological invariants in time-reversal symmetric SPT phases (see Chapter 5), it is not qualified for our interest here, mainly for two reasons: First, it corresponds to the partition function on non-orientable spacetime manifolds, while we want to consider orientable manifolds (Fig. 4.3(a)) in analogy to what is considered for bosonic systems [36]. Second, we are interested in an entanglement measure which can be defined for a generic system (possibly with no symmetry), while E_3 is only well-defined for time-reversal symmetric systems and vanishes otherwise. Returning to our earlier argument, we should note that the difference between E_1 and E_2 is in the boundary condition for the black loop in Fig. 4.4(b) (that is the loop between two successive replicas as shown in Fig. 4.3(a)). E_1 and E_2 correspond to periodic and anti-periodic boundary conditions along such a loop, respectively. As a result, E_2 requires inserting a π-flux through the black loop around the pinched torus (to get a periodic boundary condition) whereas E_1 does not. However, this loop is contractible to a point as shown in Fig. 4.4(b), and this means that E_2 contains a singularity at the identification point. Hence, it is natural to choose E_1 (over E_2) that has no singularity in the limit of adjacent intervals.

Therefore, the consecutive presence of $\rho^{T_A\dagger}$ and ρ^{T_A} in Eq.(4.7) implies periodic boundary condition along the cycle between two replicas i and $i+1$, as shown in Fig. 4.3(a). We further find that the spacetime manifold for $\mathscr{E}_n$ is a higher genus torus shown in Figs. 4.3(b) and (c) for even and odd values of n, where the boundary condition is periodic for all fundamental cycles. One way to see how these manifolds emerge is by noticing that the composite operator $\rho_A^{T_A}\rho_A^{T_A\dagger}$, for two adjacent intervals, forms a cylinder as shown in Fig. 4.4(c) and by combining these cylinders

we construct the corresponding manifold for $\mathscr{E}_n$ which is sketched in Figs. 4.3(b) and (c). In the case of $n=2$, it is easy to see that the identity

$$\mathrm{Tr}(\rho^2) = \mathrm{Tr}(\rho^{T_A}\rho^{T_A\dagger}) \tag{4.19}$$

holds in general.

For generic noninteracting systems with conserved particle number, we can transform the trace formulas into a product of n partition functions. Let us first illustrate this idea for the REE [41]. We can diagonalize the twist matrix T in Eq. (4.5) and rewrite the REE in terms of n-decoupled copies,

$$\mathrm{tr}[\rho^n] = \int \prod_k d\psi_k d\bar{\psi}_k \prod_i \left[\rho(\bar{\psi}_k,\psi_k)\right] e^{\sum_k \lambda_k \bar{\psi}_k \psi_k}, \tag{4.20}$$

where $\lambda_k = e^{i2\pi\frac{k}{n}}$ for $k=(n-1)/2,\cdots,(n-1)/2$ are eigenvalues of the twist matrix. In this new basis, the transformation rule, $\Psi \to T\Psi$, for the field passing through the interval becomes a pure phase, $\psi_k \mapsto \lambda_k \psi_k$ (Fig. 4.5(a)). Therefore, the REE can be decomposed into sum of separate terms as

$$\mathscr{R}_n = \frac{1}{1-n} \sum_{k=-(n-1)/2}^{(n-1)/2} \ln Z_k \tag{4.21}$$

where Z_k is the partition function containing an interval with the twist phase $2\pi k/n$ (Fig. 4.5(a)). For the zero-temperature case, Z_k can be computed as a ground state expectation value,

$$Z_k = \langle\Psi|\hat{T}_k|\Psi\rangle \tag{4.22}$$

where

$$\hat{T}_k = \exp\left(i\frac{2\pi k}{n}\sum_{j\in A} f_j^\dagger f_j\right), \tag{4.23}$$

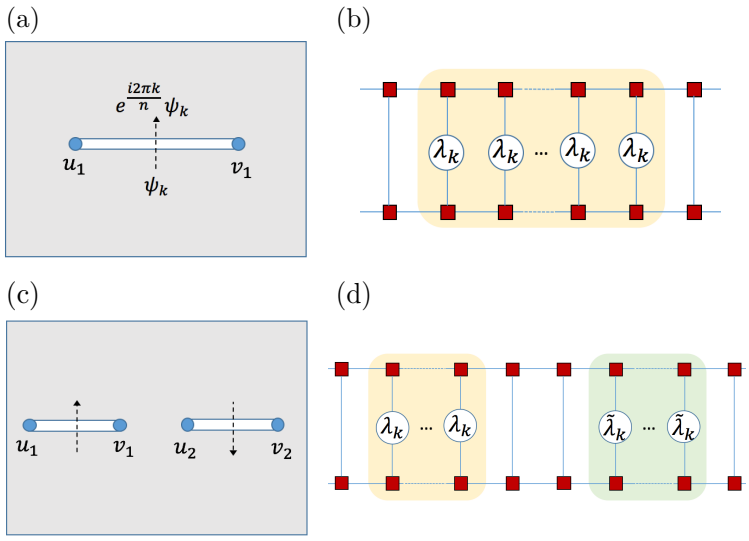

Figure 4.5: Decomposition of the path integral formulation of (a) and (b) Rényi entropy, (c) and (d) Rényi negativity (4.7) in terms of n decoupled partition functions with twist defects. (a) and (c) are spacetime picture, (b) and (d) are MPS representation, $\lambda_k = e^{i2\pi k/n}$ and $\tilde{\lambda}_k = e^{i\delta}\lambda_k^*$ where $\delta = \pi$ or $\frac{\pi(n-1)}{n}$ for n even or odd.

is a phase twist operator which only acts on the A interval. This quantity can also be implemented in the MPS representation as shown in Fig. 4.5(b). The ground state expectation values in Eq. (4.22) for free fermions can be written as a determinant of a Toeplitz matrix, and REE on lattice can be evaluated exactly using the Fisher-Hartwig conjecture [18]. See Ref. [191] for explicit derivation.

As shown in Eq. (4.13), for the n-th RN $\mathscr{E}_n$, we are dealing with two intervals where the twist matrices are T and $\widetilde{T}$. Fortunately, these matrices are simultaneously diagonalizable and we can reduce the n coupled sheets to decoupled copies where the phase factors are different for the two intervals. Therefore, we can write

$$\mathscr{E}_n = \sum_{k=-(n-1)/2}^{(n-1)/2} \ln Z_{R,k} \tag{4.24}$$

where $Z_{R,k}$ is the partition function containing two intervals with the twisting phases $e^{i2\pi k/n}$ and $e^{\delta - i2\pi k/n}$ (Fig. 4.5(c)). At zero temperature, the above expression can again be written in terms

of a ground state expectation value as shown in Fig. 4.5(d), or equivalently,

$$Z_{R,k} = \langle \Psi | \hat{T}_{R,k} | \Psi \rangle \tag{4.25}$$

where

$$\hat{T}_{R,k} = \exp\left[i\frac{2\pi k}{n} \sum_{j\in A_2} f_j^\dagger f_j + i(\delta - \frac{2\pi k}{n}) \sum_{j\in A_1} f_j^\dagger f_j \right], \tag{4.26}$$

where $\delta = \pi$ or $\pi(n-1)/n$ for n even or odd, respectively. From this, one can recast $Z_{R,k}$ for free fermion in the form of a determinant of a Toeplitz matrix and apply the Fisher-Hartwig conjecture [18] to exactly compute the zero-temperature negativity [191]. Here, we choose a different approach based on the quantum field theory which is also applicable to finite-temperature states.

Following Casini *et. al* [41], we note that the partition function in the presence of phase twisting intervals can be formulated as a theory subject to an external gauge field. The external gauge field is a pure gauge everywhere, except at the points u_i and v_i where it is vortex-like. The idea is to get rid of the phase twists by performing a singular gauge transformation

$$\psi_k(x) \to e^{i\int_{x_0}^{x} dx'^{\mu} A_\mu^k(x')} \psi_k(x), \tag{4.27}$$

where x_0 is an arbitrary reference point. The new field is now single-valued everywhere. Hence, we can absorb the boundary conditions for C_{v_i} and C_{u_i} circuits into an external gauge field. For free fermions (4.1), the resulting Lagrangian density reads

$$\mathscr{L}_k = \bar{\psi}_k \gamma^\mu \left(\partial_\mu + i A_\mu^k \right) \psi_k. \tag{4.28}$$

From the boundary conditions on ψ_k defined over the spacetime, the gauge fields are constrained as in

$$\oint_{C_{u_i}} dx^\mu A^k_\mu(x) = -\frac{2\pi k}{n}, \tag{4.29}$$

$$\oint_{C_{v_i}} dx^\mu A^k_\mu(x) = \frac{2\pi k}{n}. \tag{4.30}$$

One subtlety in this approach is that we can add phase shifts of $2\pi m$, with m an integer, to the right hand side of the above expressions and yet it does not change the total phase factor along the circuits. It turns out that this ambiguity in general leads to different representations of the partition function Z_k [38, 78, 114, 157]. Hence, Z_k can be written as a summation over all representations. The asymptotic behavior of each term in the thermodynamic limit (large (sub-)system size) is a power law $\ell^{-\alpha_m}$ and the leading order term corresponds to the smallest exponent. For instance, the leading order term in the Rényi entropy of the ground state is given by the $m = 0$ term. See Appendix A of Ref. [188] for more discussion on this. As we will see in the case of entanglement negativity, we need to consider $m \neq 0$ for some values of k.

The magnetic flux of the gauge fields satisfying Eqs. (4.29) and (4.30) is given by

$$\epsilon^{\mu\nu}\partial_\nu A^k_\mu(x) = 2\pi\frac{k}{n}\sum_{i=1}^{p}\big[\delta(x-u_i)-\delta(x-v_i)\big]. \tag{4.31}$$

The above formula is for p intervals and as we see each interval is represented by a vortex-antivortex pair of strength $2\pi\frac{k}{n}$. The goal here is to compute the partition function as thermal expectation value in the free Dirac theory

$$Z_k = \left\langle e^{i\int A^k_\mu j^\mu_k d^2x}\right\rangle, \tag{4.32}$$

where $j^\mu_k = \bar{\psi}_k\gamma^\mu\psi_k$ is the Dirac current and A^k_μ satisfies (4.31).

In order to evaluate (4.32), we use the bosonization technique to express the current j_k^μ as

$$j_k^\mu \to \frac{1}{2\pi}\epsilon^{\mu\nu}\partial_\nu\phi_k\,, \tag{4.33}$$

where ϕ_k is a real scalar field. For a free massless Dirac field, the theory for the dual field ϕ_k is simply

$$\mathscr{L}_\phi = \frac{1}{8\pi}\partial_\mu\phi\partial^\mu\phi\,. \tag{4.34}$$

Therefore we have to evaluate

$$Z_k = \left\langle e^{i\int A_\mu^k \frac{1}{2\pi}\epsilon^{\mu\nu}\partial_\nu\phi d^2x}\right\rangle = \left\langle \prod_{i=1}^{p} V_k(u_i)V_{-k}(v_i)\right\rangle \tag{4.35}$$

where $V_k(x) = e^{-i\frac{k}{n}\phi(x)}$ is the vertex operator and the expectation values correspond to the scalar-field theory (4.34). Hence, the finite-temperature partition function of a Dirac fermion can be described by a compactified boson with radius $R = 2$ (Here, the self-dual radius is $R = \sqrt{2}$). We consider the spacetime torus by identifying $z \sim z+1$ and $z \sim z+\tau$ where $\tau = i\beta/L$ is the dimensionless inverse temperature. The fermionic theory is specified by the two boundary conditions along the two cycles of the spacetime torus

$$\psi_k(z+1) = e^{i\pi\nu_1}\psi_k(z), \qquad \psi_k(z+\tau) = e^{i\pi\nu_2}\psi_k(z), \tag{4.36}$$

where $\nu_i = 0$ or 1. We denote the four possible boundary conditions (spin structures) by $\nu \equiv \{\nu_1\nu_2\} = \{00,01,11,10\} \equiv \{1,2,3,4\}$ cases, respectively. The correlation function of the vertex operators on the torus in sector ν is found by [58]

$$\langle V_{e_1}(z_1,\bar{z}_1)\cdots V_{e_N}(z_N,\bar{z}_N)\rangle = \prod_{i<j}\left|\frac{\partial_z\vartheta_1(0|\tau)}{\vartheta(z_j-z_i|\tau)}\right|^{-2e_ie_j}\left|\frac{\vartheta_\nu(\sum_i e_iz_i|\tau)}{\vartheta_\nu(0|\tau)}\right|^2 \tag{4.37}$$

in terms of the Jacobi theta functions for $R = 2$ where $V_e(z,\bar{z}) = e^{ie\phi(z,\bar{z})}$ is the vertex operator. Hence, we can write for the partition function in sector ν

$$Z_k^{(\nu)} = \left| \frac{\prod_{i<j} \vartheta_1(u_i - u_j|\tau)\vartheta_1(v_i - v_j|\tau)}{\prod_{i,j} \vartheta_1(u_i - v_j|\tau)} \cdot (\epsilon \partial_z \vartheta_1(0|\tau))^p \right|^{2\frac{k^2}{n^2}} \cdot \left| \frac{\vartheta_\nu(\frac{k}{n}\sum_i (u_i - v_i)|\tau)}{\vartheta_\nu(0|\tau)} \right|^2, \tag{4.38}$$

where the partition function is normalized such that $Z_k^{(\nu)} = 1$ in the absence of any branch points. The dimensionless UV cutoff $\epsilon = a/L$ is introduced as a UV-cutoff to resolve the coincident points since the theta function behaves as $\vartheta_1(z|\tau) \sim z$ when $z \to 0$. As a result, the Rényi entropy reads

$$S_n^{(\nu)} = S_{n,0} + S_{n,1}^{(\nu)} \tag{4.39}$$

where the first term is universal

$$S_{n,0} = -\frac{n+1}{6n} \ln \left| \frac{\prod_{i<j} \vartheta_1(u_i - u_j|\tau)\vartheta_1(v_i - v_j|\tau)}{\prod_{i,j} \vartheta_1(u_i - v_j|\tau)} (\epsilon \partial_z \vartheta_1(0|\tau))^p \right|, \tag{4.40}$$

and the second term depends on the spin structure ν,

$$S_{n,1}^{(\nu)} = \frac{2}{1-n} \sum_{k=-\frac{n-1}{2}}^{\frac{n-1}{2}} \ln \left| \frac{\vartheta_\nu(\frac{k}{n}\sum_i (u_i - v_i)|\tau)}{\vartheta_\nu(0|\tau)} \right|. \tag{4.41}$$

We should note that the Rényi entropies in the $\nu = 1$ sector are divergent, since $\vartheta_1(0|\tau)$ in the denominator of $S_{n,1}^{(\nu)}$ is zero. This is related to the fermion zero mode in this sector.

Let us now look at various limits of the above result. For simplicity, we shall consider a single interval and the sector $\nu = 3$ which is the usual anti-periodic boundary condition in both spacetime directions.

In the low temperature limit $\tau = i\beta/L \to i\infty$, we have

$$S_{n,0} = \frac{n+1}{6n} \ln \left| \frac{L}{\pi a} \sin(\frac{\pi \ell}{L}) \right| + O(e^{-2\pi/(LT)}), \tag{4.42}$$

where we use the relation

$$\lim_{\beta \to \infty} \vartheta_1(z|i\beta) = 2e^{-\pi\beta/4} \sin \pi z + O(e^{-2\pi\beta}). \tag{4.43}$$

The second term $S^{(\nu)}_{n,1}$ is vanishing and we arrive at the usual expression for the ground state of CFT.

In the high temperature limit where $\tau = i\beta/L \to 0$, we obtain

$$S_{n,0} = \frac{n+1}{6n} \left[-\frac{\pi \ell}{\beta} \frac{\ell}{L} + \ln \left| \frac{\beta}{\pi a} \sinh(\frac{\pi \ell}{\beta}) \right| \right] + O(e^{-\pi LT}), \tag{4.44}$$

for the universal part and

$$S^{(3)}_{n,1} = \frac{(1+n)}{6n} \frac{\pi \ell^2}{\beta L} - \frac{2}{1-n} \sum_{j=1}^{\infty} \frac{(-1)^j}{j} \frac{1}{\sinh(\frac{\pi j}{\beta})} \left(\frac{\sinh(\frac{\pi j \ell}{\beta})}{\sinh(\frac{\pi j \ell}{n\beta})} - n \right) \tag{4.45}$$

for the second part (similar results can be derived for other sectors). We should note that the first terms in (4.44) and (4.45) precisely cancel each other. Here, we use the modular transformation rules for the theta functions,

$$\vartheta_1(z|\tau) = -(-i\tau)^{-1/2} e^{-\pi i z^2/\tau} \vartheta_1(z/\tau|-1/\tau), \tag{4.46}$$

and the asymptotic form of the theta function in the small β limit

$$\vartheta_1(z/\tau|-1/\tau) = -2i\, e^{-\frac{\pi L}{4\beta}} \sinh(\frac{\pi z L}{\beta}) + O(e^{\frac{3\pi L}{\beta}(z-3/4)}), \tag{4.47}$$

for $0 \le z \le 1/2$.

Let us now move on to the calculations of the RN (4.7). In order to compute the moments, we need to consider two intervals with different twist matrices T and $\widetilde{T}$. Note that the overall boundary condition due to the twist matrices is identical $T^n = \widetilde{T}^n = (-1)^{n-1}$. As mentioned, we carry out a similar procedure and decompose RN into n decoupled copies where the phase twists are different for the two intervals (see Eq. (4.24) and Fig. 4.5(c)). In the following parts, we compute the entanglement negativity for various geometries as shown in Fig. 4.1.

Tripartite geometry

Here, we consider two adjacent intervals partitioned from a long chain (see Fig. 4.1(c)). Hence, the gauge field appearing in (4.28) for such configuration is given by

$$\frac{1}{2\pi}\epsilon^{\mu\nu}\partial_\nu A^k_\mu(x) = \left(\frac{k}{n}-\frac{\varphi_n}{2\pi}\right)\delta(x-u_1) - \left(\frac{2k}{n}-\frac{\varphi_n}{2\pi}\right)\delta(x-v_1) + \frac{k}{n}\delta(x-v_2) \tag{4.48}$$

where we place the branch points at $u_1 = -\ell_1$, $v_1 = u_2 = 0$, and $v_2 = \ell_2$. Similar to the previous derivation, we find

$$\begin{aligned} Z^{(\nu)}_{R,k} = &|\vartheta_1(T_A|\tau)|^{-2(|\frac{k}{n}|-\frac{\varphi_n}{2\pi})(|\frac{2k}{n}|-\frac{\varphi_n}{2\pi})} \cdot |\vartheta_1(r_2|\tau)|^{-2|\frac{k}{n}|(|\frac{2k}{n}|-\frac{\varphi_n}{2\pi})} |\vartheta_1(T_A+r_2|\tau)|^{2|\frac{k}{n}|(|\frac{k}{n}|-\frac{\varphi_n}{2\pi})} \\ &\times |\epsilon\partial_z\vartheta_1(0|\tau)|^{-\Delta_k} \cdot \left|\frac{\vartheta_\nu\left(\frac{k}{n}(r_2-T_A)+\mathrm{sgn}(k)\frac{\varphi_n}{2\pi}T_A|\tau\right)}{\vartheta_\nu(0|\tau)}\right|^2, \end{aligned} \tag{4.49}$$

where

$$\Delta_k = -\frac{6k^2}{n^2} + \frac{3\varphi_n}{2\pi}\left|\frac{k}{n}\right| - \frac{\varphi_n^2}{2\pi^2}. \tag{4.50}$$

It is important to note that for $k < 0$, we modified the flux at u_1 and v_1 by inserting an additional 2π and -2π fluxes, respectively, where the scaling exponent α_m takes its minimum value. One can also see this independently in a separate derivation in terms of the Toepltiz matrix [191]. Putting together, the moments of negativity are given by $\mathscr{E}_n = \mathscr{E}_{n,0} + \mathscr{E}_{n,1}$ where the universal

part is

$$\mathcal{E}_{n_o,0} = -\left(\frac{n_o^2-1}{12n_o}\right)\ln\left|\vartheta_1(T_A|\tau)\vartheta_1(r_2|\tau)\vartheta_1(T_A+r_2|\tau)\cdot(\epsilon\partial_z\vartheta_1(0|\tau))^{-3}\right|, \tag{4.51}$$

$$\begin{aligned}\mathcal{E}_{n_e,0} = &-\left(\frac{n_e^2-4}{12n_e}\right)\ln\left|\vartheta_1(T_A|\tau)\vartheta_1(r_2|\tau)(\epsilon\partial_z\vartheta_1(0|\tau))^{-2}\right| \\ &-\left(\frac{n_e^2+2}{12n_e}\right)\ln\left|\vartheta_1(T_A+r_2|\tau)(\epsilon\partial_z\vartheta_1(0|\tau))^{-1}\right|,\end{aligned} \tag{4.52}$$

for n odd or even and the spin structure dependent term is

$$\mathcal{E}_{n,1}^{(\nu)} = 2\sum_{k=-\frac{n-1}{2}}^{\frac{n-1}{2}}\ln\left|\frac{\vartheta_\nu\left(\frac{k}{n}(r_2-T_A)+\mathrm{sgn}(k)\frac{\varphi_n}{2\pi}T_A|\tau\right)}{\vartheta_\nu(0|\tau)}\right|. \tag{4.53}$$

In the above expressions, $r_i = \ell_i/L$ are the dimensionless lengths. Hence, the logarithmic negativity is given by $\mathcal{E}^{(\nu)} = \mathcal{E}_0 + \mathcal{E}_1^{(\nu)}$ where

$$\mathcal{E}_0 = \lim_{n_e\to 1}\mathcal{E}_{n_e,0} = \frac{1}{4}\ln\left|\frac{\vartheta_1(T_A|\tau)\vartheta_1(r_2|\tau)}{\vartheta_1(T_A+r_2|\tau)}(\epsilon\partial_z\vartheta_1(0|\tau))^{-1}\right| \tag{4.54}$$

is the universal part. There is no closed-form expression for the non-universal part $\mathcal{E}_1^{(\nu)} = \lim_{n_e\to 1}\mathcal{E}_{n_e,1}^{(\nu)}$ in a generic case other than when $\ell_1 = \ell_2$. In the case of intervals with equal lengths the negativity is simplified into

$$\mathcal{E}^{(\nu)} = \frac{1}{4}\ln\left|\frac{\vartheta_1(r|\tau)^2}{\vartheta_1(2r|\tau)}(\epsilon\partial_z\vartheta_1(0|\tau))^{-1}\right| + 2\ln\left|\frac{\vartheta_\nu(\frac{r}{2}|\tau)}{\vartheta_\nu(0|\tau)}\right|. \tag{4.55}$$

where $r = \ell/L$.

Let us now examine the limiting behaviors. In the low temperature limit where $\tau = i\beta/L \to \infty$, we get

$$\mathcal{E}_0 = \frac{1}{4}\ln\left|\frac{L}{\pi a}\frac{\sin(\frac{\pi\ell_1}{L})\sin(\frac{\pi\ell_2}{L})}{\sin(\frac{\pi(\ell_1+\ell_2)}{L})}\right| + O(e^{-2\pi/(LT)}), \tag{4.56}$$

while in the high temperature limit where $\tau = i\beta/L \to 0$, we obtain

$$\mathscr{E}_0 = \frac{1}{4}\left[\frac{2\pi\ell_1\ell_2}{\beta L} + \ln\left|\frac{\beta}{\pi a}\frac{\sinh(\frac{\pi\ell_1}{\beta})\sinh(\frac{\pi\ell_2}{\beta})}{\sinh(\frac{\pi(\ell_1+\ell_2)}{\beta})}\right|\right] + O(e^{-\pi LT}). \tag{4.57}$$

As we will see below, the the first term in the above expression is cancelled by the contribution from $\mathscr{E}_1$. In the following, we evaluate the spin structure dependent term (4.53) for the $\nu = 3$ sector and even $n = n_e$. Similar expressions can be derived for other sectors. So, the low temperature limit of (4.53) is found by

$$\mathscr{E}^{(3)}_{n_e,1} = 2\sum_{j=1}^{\infty}\frac{(-1)^{j+1}}{j\sinh(\pi\beta j)}\left(\frac{\sin(\pi j r_2) - \sin(\pi j T_A)}{\sin(\pi j(r_2 - T_A)/n_e)} - n_e\right). \tag{4.58}$$

To the leading order, the above expression contributes to the negativity as

$$\mathscr{E}^{(3)}_1 = \lim_{n_e\to 1}\mathscr{E}^{(3)}_{n_e,1} = 4e^{-\pi/(LT)}\left(\frac{\cos(\pi(r_2+T_A)/2)}{\cos(\pi(r_2-T_A)/2)} - 1\right). \tag{4.59}$$

This is reminiscent of the universal thermal corrections found for the Rényi entropies [96]. The high temperature limit is determined by

$$\begin{aligned}\mathscr{E}^{(3)}_{n_e,1} = &-\frac{\pi}{2\beta L}\left[\left(\frac{n_e^2-1}{3n_e}\right)(\ell_2-\ell_1)^2 + n_e\ell_1(\ell_2-\ell_1) + n_e\ell_1^2\right] \\ &-2\sum_{j=1}^{\infty}\frac{(-1)^j}{j}\frac{1}{\sinh(\frac{\pi j}{\beta})}\left(\frac{\sinh\left[(\varphi_{n_e}\ell_1 + \pi(\ell_2-\ell_1))\frac{j}{\beta}\right] - \sinh(\varphi_{n_e}\ell_1 j/\beta)}{\sinh\left(\frac{\pi(\ell_2-\ell_1)j}{n_e\beta}\right)} - n_e\right)\end{aligned} \tag{4.60}$$

and hence, we get

$$\mathscr{E}^{(3)}_1 = -\frac{\pi\ell_1\ell_2}{2\beta L}. \tag{4.61}$$

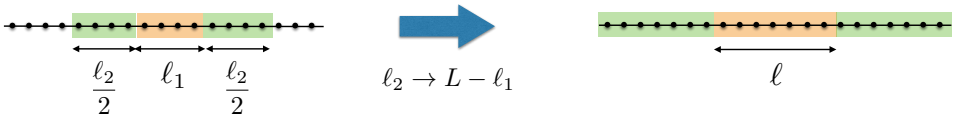

Figure 4.6: Bipartite geometry (right) of a single interval on a chain of length L which can be derived from the limit $\ell_2 \to L-\ell_1$ of the tripartite geometry (left).

To sum up, we have shown that the logarithmic negativity of two adjacent intervals are given by

$$\mathcal{E}(LT \ll 1) = \frac{1}{4}\ln\left|\frac{L}{\pi a}\frac{\sin(\frac{\pi\ell_1}{L})\sin(\frac{\pi\ell_2}{L})}{\sin(\frac{\pi(\ell_1+\ell_2)}{L})}\right| + O(e^{-2\pi/(LT)}), \tag{4.62}$$

$$\mathcal{E}(LT \gg 1) = \frac{1}{4}\ln\left|\frac{\beta}{\pi a}\frac{\sinh(\frac{\pi\ell_1}{\beta})\sinh(\frac{\pi\ell_2}{\beta})}{\sinh(\frac{\pi(\ell_1+\ell_2)}{\beta})}\right| + O(e^{-\pi LT}), \tag{4.63}$$

in the low and high temperature regimes, which is identical to the bosonic results obtained for Harmonic chains [68]. The logarithmic negativity of two adjacent intervals with equal lengths is simplified further into

$$\mathcal{E} = \frac{1}{4}\ln\left[\frac{\beta}{\pi a}\tanh\left(\frac{\pi\ell}{\beta}\right)\right] + O(e^{-\pi LT}). \tag{4.64}$$

We should note that there is no term linear in ℓ in the tripartite case (compared to the bipartite case in Eqs. (4.77) and (4.79) as we will see shortly). In the language of Ref. [37], this is because we sew together only parts of spacetime sheets and taking higher powers of twist fields T and T^R does not create a new manifold.

Bipartite geometry

In order to evaluate the bipartite negativity of a single interval (Fig. 4.1(a)), we start by considering a tripartite geometry where an interval of length ℓ_1 is symmetrically embedded inside another interval of length ℓ_2 shown in Fig. 4.6(left). Eventually, we take the limit $\ell_2 \to L-\ell_1$ in our calculations, where L is the total length of the chain (see Fig. 4.6).

The tripartite configuration (Fig. 4.6(left)) implies four branch points at $u_1 = -r_2/2,\ v_1 = 0,\ u_2 = r_1$, and $v_2 = r_2/2 + r_1$ such that the gauge field in (4.28) must obey

$$\frac{1}{2\pi}\epsilon^{\mu\nu}\partial_\nu A^k_\mu(x) = \left(\frac{2k}{n} - \frac{\varphi_n}{2\pi}\right)(\delta(x-v_1) - \delta(x-u_2)) + \frac{k}{n}(\delta(x-v_2) - \delta(x-u_1)). \tag{4.65}$$

Therefore, we can find k-th term in the moments of partial transpose as

$$\begin{aligned} Z^{(\nu)}_{R,k} = &|\vartheta_1(T_A|\tau)|^{-2(|\frac{2k}{n}| - \frac{\varphi_n}{2\pi})^2} \left|\frac{\vartheta_1(\frac{r_2}{2}|\tau)}{\vartheta_1(\frac{r_2}{2}+T_A|\tau)}\right|^{-4|\frac{k}{n}|(|\frac{2k}{n}| - \frac{\varphi_n}{2\pi})} \cdot |\vartheta_1(T_A + r_2|\tau)|^{-2\frac{k^2}{n^2}} \\ &\times |\epsilon\partial_z\vartheta_1(0|\tau)|^{-\Delta_k} \cdot \left|\frac{\vartheta_\nu\left(\frac{k}{n}(r_2 - T_A) + \mathrm{sgn}(k)\frac{\varphi_n}{2\pi}T_A|\tau\right)}{\vartheta_\nu(0|\tau)}\right|^2, \end{aligned} \tag{4.66}$$

where Δ_k is

$$\Delta_k = -10\frac{k^2}{n^2} + \frac{8\varphi_n}{2\pi}\left|\frac{k}{n}\right| - \frac{\varphi_n^2}{2\pi^2}. \tag{4.67}$$

This leads to

$$\mathscr{E}_{n_o,0} = -\left(\frac{n_o^2-1}{6n_o}\right)\ln\left|\frac{\vartheta_1(T_A|\tau)\vartheta_1(\frac{r_2}{2}|\tau)\vartheta_1(T_A+r_2|\tau)}{\vartheta_1(\frac{r_2}{2}+T_A|\tau)}(\epsilon\partial_z\vartheta_1(0|\tau))^{-2}\right|, \tag{4.68}$$

$$\begin{aligned} \mathscr{E}_{n_e,0} = &-\left(\frac{n_e^2-4}{6n_e}\right)\ln\left|\frac{\vartheta_1(T_A|\tau)\vartheta_1(\frac{r_2}{2}|\tau)}{\vartheta_1(\frac{r_2}{2}+T_A|\tau)}(\epsilon\partial_z\vartheta_1(0|\tau))^{-1}\right| \\ &-\left(\frac{n_e^2-1}{6n_e}\right)\ln\left|\vartheta_1(T_A+r_2|\tau)(\epsilon\partial_z\vartheta_1(0|\tau))^{-1}\right|, \end{aligned} \tag{4.69}$$

for the universal part and

$$\mathscr{E}^{(\nu)}_{n,1} = 2\sum_{k=-\frac{n-1}{2}}^{\frac{n-1}{2}} \ln\left|\frac{\vartheta_\nu\left(\frac{k}{n}(r_2 - T_A) + \mathrm{sgn}(k)\frac{\varphi_n}{2\pi}T_A|\tau\right)}{\vartheta_\nu(0|\tau)}\right|, \tag{4.70}$$

for the spin structure dependent term. Taking the replica limit, the universal part of the logarithmic negativity reads

$$\mathcal{E}_0 = \frac{1}{2}\ln\left|\frac{\vartheta_1(T_A|\tau)\vartheta_1(\frac{r_2}{2}|\tau)}{\vartheta_1(\frac{r_2}{2}+T_A|\tau)}(\epsilon\partial_z\vartheta_1(0|\tau))^{-1}\right|. \tag{4.71}$$

As mentioned earlier, for the bipartite geometry (Fig. 4.1(a)), we need to take $r_2 = 1-T_A$, which gives

$$\begin{aligned}\mathcal{E}_0 &= \frac{1}{2}\ln\left|\frac{\vartheta_1(T_A|\tau)\vartheta_1(\frac{1-T_A}{2}|\tau)}{\vartheta_1(\frac{1+T_A}{2}|\tau)}(\epsilon\partial_z\vartheta_1(0|\tau))^{-1}\right| \\ &= \frac{1}{2}\ln\left|\frac{\vartheta_1(T_A|\tau)}{\epsilon\partial_z\vartheta_1(0|\tau)}\right|,\end{aligned} \tag{4.72}$$

where in the second line, we use the properties of theta functions to further simplify the original expression. The low temperature limit of the second term is

$$\mathcal{E}_1^{(3)} = \lim_{n_e\to 1}\mathcal{E}_{n_e,1}^{(3)} = 4e^{-\pi/(LT)}\left(\frac{\cos(\pi(r_2+T_A)/2)}{\cos(\pi(r_2-T_A)/2)}-1\right). \tag{4.73}$$

Let us now derive the high temperature expansion of the bipartite entanglement negativity. Similar to the previous section, the universal part can be simplified into

$$\mathcal{E}_0 = \frac{1}{2}\left[-\frac{\pi\ell_1^2}{\beta L}+\ln\left|\frac{\beta}{\pi a}\sinh(\frac{\pi\ell_1}{\beta})\right|\right]+O(e^{-\pi LT}). \tag{4.74}$$

The second term in the $\nu=(3)$ sector can be evaluated as follows

$$\begin{aligned}\mathcal{E}_{n_e,1}^{(3)} =& -\frac{\pi}{2\beta L}\left[\left(\frac{n_e^2-1}{3n_e}\right)(L-2\ell_1)^2+n_e\ell_1(L-2\ell_1)+n_e\ell_1^2\right] \\ &-2\sum_{j=1}^{\infty}\frac{(-1)^j}{j}\frac{1}{\sinh(\frac{\pi j}{\beta})}\left(\frac{\sinh\left[(\varphi_{n_e}\ell_1+\pi(L-2\ell_1))\frac{j}{\beta}\right]-\sinh(\varphi_{n_e}\ell_1 j/\beta)}{\sinh\left(\frac{\pi(L-2\ell_1)j}{n_e\beta}\right)}-n_e\right)\end{aligned} \tag{4.75}$$

which simplifies into

$$\mathscr{E}_1^{(3)} = \frac{\pi \ell_1}{2\beta L}(\ell_1 - L) + O(e^{-\pi LT}). \tag{4.76}$$

Therefore, we find that

$$\mathscr{E}(LT \gg 1) = \frac{1}{2}\left[\ln\left|\frac{\beta}{\pi a}\sinh(\frac{\pi \ell_1}{\beta})\right| - \frac{\pi \ell_1}{\beta}\right] + O(e^{-\pi LT}), \tag{4.77}$$

which agrees (bosonic) CFT results derived in Ref. [37].

From the above result (4.72), we can find the negativity of the semi-infinite geometry by noting that the semi-infinite geometry (Fig. 4.1(b)) can be obtained from the infinite geometry (Fig. 4.1(a)) by cutting the ℓ_1 interval in half; therefore, the entanglement of each cut is equal to half of the value in Eq. (4.72). This gives the entanglement of a finite interval with length $\ell_1/2$ to a semi-infinite interval. Hence, the entanglement negativity of a finite interval with length ℓ_1 to an adjacent semi-infinite interval becomes

$$\mathscr{E}_0 = \frac{1}{4}\ln\left|\frac{\vartheta_1(2T_A|\tau)}{\epsilon \partial_z \vartheta_1(0|\tau)}\right|, \tag{4.78}$$

the high temperature limit of which is given by

$$\mathscr{E}(LT \gg 1) = \frac{1}{4}\left[\ln\left|\frac{\beta}{\pi a}\sinh(\frac{2\pi \ell_1}{\beta})\right| - \frac{2\pi \ell_1}{\beta}\right] + O(e^{-\pi LT}). \tag{4.79}$$

This is also in agreement with the bosonic results of Ref. [37].

4.2 One-dimensional systems

In this section, we numerically calculate the logarithmic negativity associated with the partial transpose (2.28) for free fermions on a lattice and compare it with the analytical results derived above.

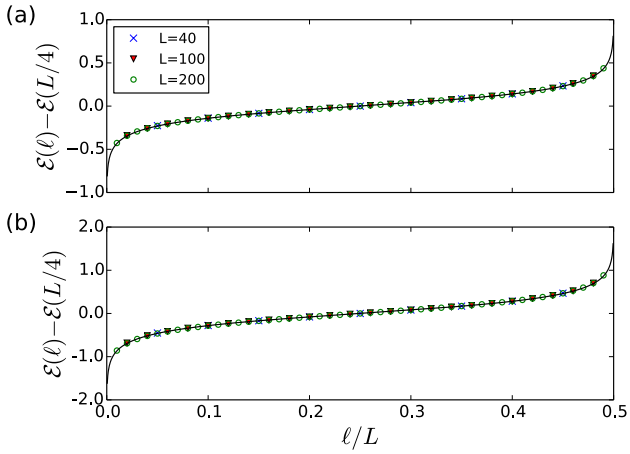

Figure 4.7: Zero-temperature logarithmic negativity of two adjacent intervals for free fermion CFTs. (a) Kitaev chain (3.39) at $\mu = -2t$ where $c = 1/2$, and (b) SSH model (3.44) at $t_2 = t_1$ where $c = 1$. Here c is the central charge of CFT. The solid curves are the analytical expression $\mathcal{E} = \frac{c}{4} \ln \tan(\frac{\pi \ell}{L})$ from Eq. (4.62). The data are shown for a closed chain with anti-periodic boundary condition.

Let us first sketch the steps of numerically computing the partial transpose and entanglement negativity for non-interacting systems. The following procedure works efficiently for any quadratic Hamiltonian of the form $\hat{H} = \sum_{i,j} t_{ij} f_i^\dagger f_j + \text{H.c.}$ which spans a variety of non-interacting models with a conserved total particle number. A more general (less efficient) procedure which does not require particle number conservation was already described in Chapter 3. For free fermions, the reduced density matrix can be completely characterized by the single particle correlation function [160],

$$C_{ij} = \langle f_i^\dagger f_j \rangle = \text{tr}(\rho f_i^\dagger f_j), \tag{4.80}$$

for the ground state $\rho = |GS\rangle \langle GS|$ or a thermal ensemble described by the density matrix $\rho = e^{-\beta \hat{H}}$. For a thermal state, the single-particle correlator reads

$$C_{ij} = \sum_n f(\epsilon_n)\, u_n^*(i) \cdot u_n(j), \tag{4.81}$$

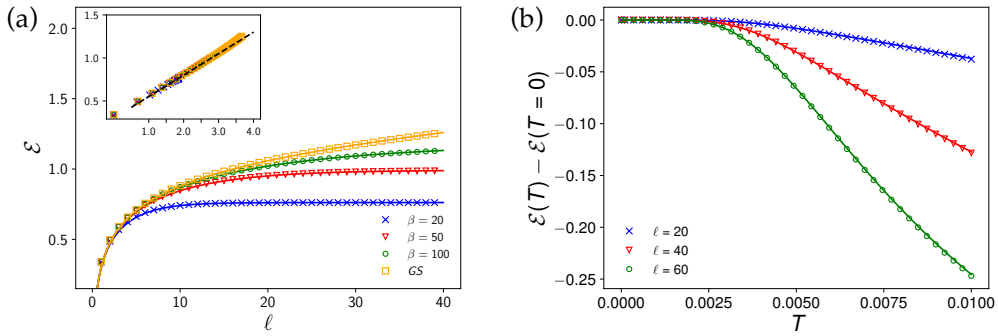

Figure 4.8: Logarithmic negativity of the tripartite geometry for two adjacent intervals with equal length ℓ on the free fermion lattice model (4.1). The negativity as a function of (a) interval length and (b) temperature. The solid lines are analytical results (4.55). The inset of panel (a) shows the linear behavior when $\mathcal{E}$ is plotted against $x = \ln\left[\frac{\beta}{\pi}\tanh\left(\frac{\pi\ell}{\beta}\right)\right]$. The dashed line in the inset is a reference line with the slope of $c/4 = 1/4$. We set $L = 200$.

where $|u_n\rangle$ are single particle eigenstates $H|u_n\rangle = \epsilon_n|u_n\rangle$, $u_n(j) = \langle j|u_n\rangle$ is the value of the wave function at site j, and $f(x) = (1+\exp(\epsilon_n/T))^{-1}$ is the Fermi-Dirac distribution. For the ground state, the Fermi-Dirac distribution at zero temperature automatically enforces the summation to be over the occupied states.

We should note that the functional form of our analytical results is universal (especially for quantities involving two and three point correlators) although we compute them for a special CFT, namely, the free fermion CFT. Hence, the expressions for $\mathcal{E}$ can be modified by putting the central charge c of CFT in front of the functions. For instance, we check the zero-temperature logarithmic negativity of two adjacent intervals (4.1(c)) in two cases: The critical point of the Kitaev chain where $c = 1/2$ and the SSH model where $c = 1$. The results are shown in Figs. 4.7(a) and (b), where the agreement between numerics and analytical formulas is evident.

For finite temperature calculations, we mainly focus on the free fermion chain. Again, the functional forms are universal (see for example some general CFT results in [37]). We choose $t = 1$ and set $\mu = 0$ in the lattice Hamiltonian (4.1). In Fig. 4.8, we compute the logarithmic negativity for two adjacent intervals (Fig. 4.1(c)). The analytical results (solid lines) and lattice calculations (points) match over a range of temperatures and interval lengths. As we see in Fig. 4.8(a), the negativity saturates, i.e., obeys an area law, at any finite temperature once $\ell \gg 1/T$. This means

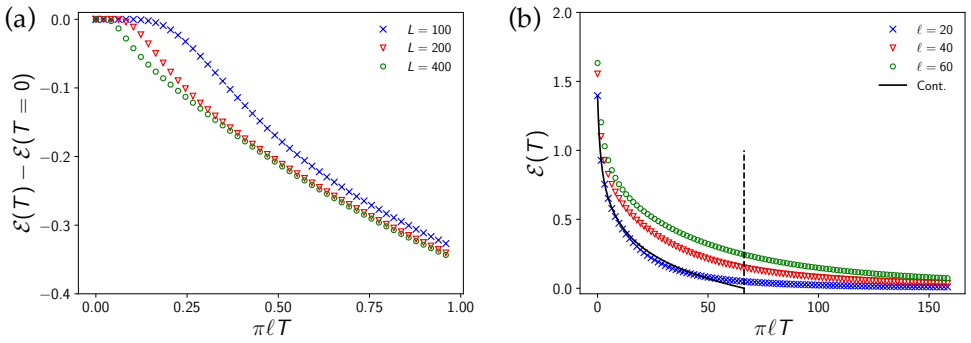

Figure 4.9: Logarithmic negativity of the bipartite geometry for one interval in the semi-infinite line (Fig. 4.1(b)). (a) The subsystem size $\ell = 20$ is fixed, while T is varied for different total system sizes L. The initial plateau is due to finite length of chain. (b) The total system size is fixed, while T is varied for different subsystem sizes ℓ. Absence of sudden death in the fermionic negativity is evident. The dashed vertical line indicates the point at which the continuum limit expression (4.79) starts to become negative.

that at finite temperatures the quantum coherence can only be maintained for length scales of order $\beta = 1/T$, beyond which thermal fluctuations completely wash it out. Another interesting point is the collapse of high-temperature negativity for various values of ℓ and T onto the universal curve (4.64) as shown by the inset of Fig. 4.8(a). We also observe that the negativity curves (e.g., Fig. 4.8(b)) generically start off with a plateau at low temperatures. This corresponds to the limit $T \ll 1/L$ when the temperature is less than the finite-size gap ($\sim 1/L$) in the energy spectrum and the system behaves as if it is at the zero temperature. Figure 4.9(a) illustrates this finite-size effect, where the negativity remains a plateau until some temperature, and then it falls off. The onset of decay (length of the finite-size plateau) is decreased as we make the system larger.

Next, we look at the high temperature limit in Fig. 4.9(b), where we observe that the fermionic logarithmic negativity decays to zero smoothly without any sudden death, as opposed to the bosonic case [37]. We believe that this is related to the fermion-number parity constraint on the fermionic density matrices [189]. One can explicitly check in a system of two fermionic sites how this constraint limits the form of density matrix and modifies the notion of separability, which ultimately lead to the absence of sudden death [188]. Further, it is evident that for high temperatures and at a fixed ℓ, the continuum limit Eq. (4.79) is valid only until we reach the lattice scale (i.e., as long as $\beta \gg a$).

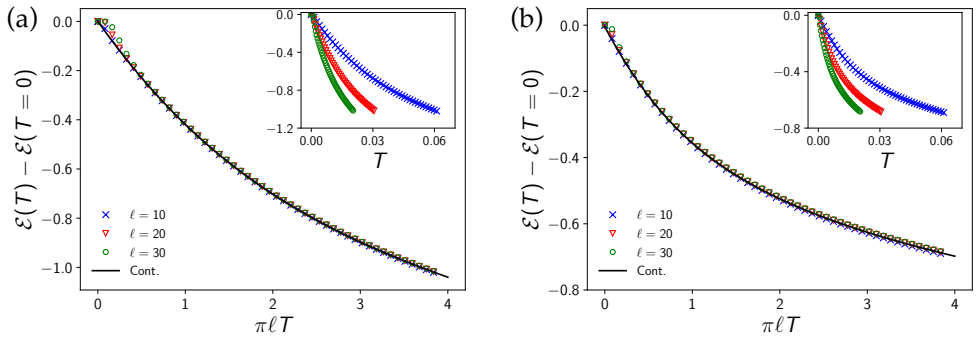

Figure 4.10: Collapse of logarithmic negativity of the bipartite geometry on a universal curve. (a) One interval in the infinite line (Fig. 4.1(a)). (b) One interval in the semi-infinite line (Fig. 4.1(b)). In each panel, the inset shows the $\mathcal{E}$ against temperature (without scaling). This is to be compared with the universal curve when the horizontal axis is normalized as $\pi \ell T$. Here, the numerics are done for the free fermion lattice model where $L = 400$.

An important implication of Eqs. (4.77) and (4.79) for the logarithmic negativity of the bipartite geometries (c.f., Fig. 4.1(a) and (b)) is that the entanglement difference $\mathcal{E}(T) - \mathcal{E}(0)$ is a universal function of $\pi \ell T$. We verify this behavior in Fig. 4.10 by looking at various interval sizes and showing that they all collapse on the same curve. For reference, we also plotted the analytical expressions (4.77) and (4.79).

4.3 Higher dimensional systems

In this section, we would like to extend our result for the finite-temperature entanglement negativity of one-dimensional metals to higher dimensions. Our idea is motivated by similar results discussed by Swingle [203, 206] for generalizing entanglement entropies to higher dimensional Fermi surfaces.

The general result for the zero-temperature is as follows: the Rényi entanglement entropy of a subregion of size ℓ for a $(d+1)$ metallic system with a codimension one Fermi surface is [85],

$$S_n(\ell) = C_d(\mu) \left(\frac{n+1}{6n} \right) \ell^{d-1} \ln \ell, \tag{4.82}$$

where

$$C_d(\mu) = \frac{1}{4(2\pi)^{d-1}} \int_{\partial\Omega} \int_{\partial\Gamma(\mu)} dS_k dS_x |n_x \cdot n_k|, \tag{4.83}$$

Ω is the volume of the subregion normalized to one, $\Gamma(\mu)$ is the volume enclosed by the Fermi surface, and the integration is carried out over the surface of both domains.

In particular, the entanglement entropy of a two dimensional metal reads as

$$S_n(\ell) = \left(\frac{n+1}{6n}\right) C_2(\mu) \cdot \ell \ln \ell. \tag{4.84}$$

The filled Fermi surface of a two dimensional metal may be viewed as a collection of one dimensional gapless modes [24, 163, 187] and the entanglement can be understood as a sum of 1d segments (ℓ of them) each of which contributes $(n+1)/6n \cdot \ln(\ell)$ up to a geometrical coefficient (4.83). The above formula was shown to be in a remarkable agreement with numerical simulations of various microscopic lattice models [17, 136]. As we have seen for a one-dimensional metal, the finite temperature Rényi entropy has the same form as the zero temperature entropy provided that we replace $\ln(\ell)$ by $\ln[(\beta/\pi)\sinh(\pi\ell/\beta)]$. Hence, we can follow the same lines of argument as those we use for the zero temperature to deduce that the Rényi entropy of a two-dimensional metal should obey the following form [203, 206],

$$S_n(\ell, T) = \left(\frac{n+1}{6n}\right) C_2(\mu) \cdot \ell \ln \left| \frac{\beta}{\pi a} \sinh\left(\frac{\pi\ell}{\beta}\right) \right|. \tag{4.85}$$

Let us now consider the bipartite logarithmic negativity. By a similar reasoning, we expect that the two dimensional negativity should obey the same form in terms of the one dimensional negativity. So, for finite temperature negativity we can write

$$\mathcal{E}(\ell, T) = C_2(\mu) \cdot \frac{\ell}{2} \left[\ln\left(\frac{\beta}{\pi a} \sinh\left(\frac{\pi\ell}{\beta}\right)\right) - \frac{\pi\ell}{\beta} \right]. \tag{4.86}$$

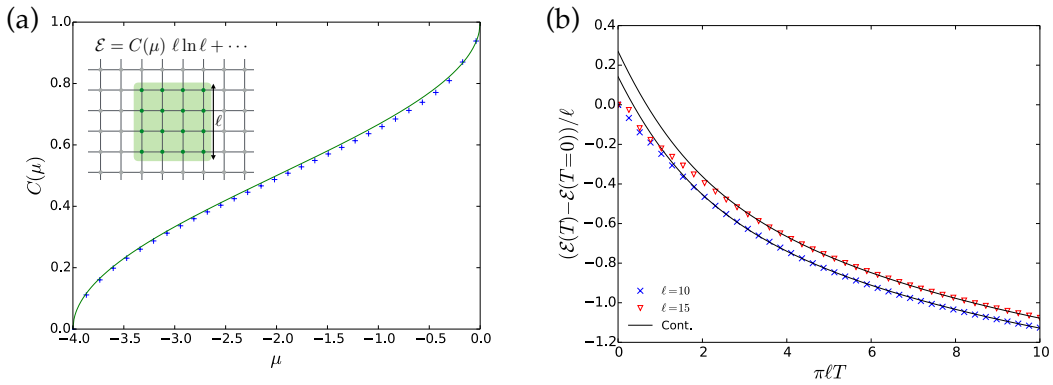

Figure 4.11: Logarithmic negativity of the bipartite geometry on a 2d square lattice. (a) The slope of zero-temperature negativity as a function of chemical potential. The solid line is the continuum expression (4.88). Here, we carry out numerics for the infinite size system and the slope is found for $\mathscr{E}$ vs. ℓ over the range $40 \leq \ell \leq 80$. (b) Finite temperature negativity as a function of rescaled (dimensionless) temperature. The solid lines are Eq. (4.86) which are shifted vertically to fit the low-temperature value. The system size is 30×30.

We should note that the bipartite logarithmic negativity is equal to the 1/2-Rényi entropy at zero temperature. However, there is an important difference between the logarithmic negativity and the Rényi entropy. Entanglement negativity has an extra term linear in ℓ inside the parenthesis compared to the 1/2-Rényi entropy and this term exactly cancels the volume law term in the high temperature limit, i.e., the negativity eventually vanishes while Rényi entropy grows as a volume law.

4.3.1 Numerical results

A canonical model to benchmark two-dimensional entropies is a simple tight-binding model on a 2d square lattice described by the Hamiltonian,

$$\hat{H} = -\sum_{\mathbf{x},\mathbf{e}_i} [f^\dagger_{\mathbf{x}+\mathbf{e}_i} f_{\mathbf{x}} + f^\dagger_{\mathbf{x}} f_{\mathbf{x}+\mathbf{e}_i}] - \mu \sum_{\mathbf{x}} f^\dagger_{\mathbf{x}} f_{\mathbf{x}}. \tag{4.87}$$

The zero-temperature Rènyi negativities of this model for various tripartite geometries have been studied in [70]. The geometric coefficient in the entanglement entropy (4.83) of a square segment

is found to be

$$C_2(\mu) = \frac{2}{\pi}\Big[\pi - \cos^{-1}(\frac{\mu}{2}+1)\Big]. \tag{4.88}$$

The bipartite entanglement negativity of a square subregion is computed in Fig. 4.11. As mentioned, the zero-temperature negativity is the same as 1/2-Rényi entropy and we confirm in Fig. 4.11(a) that it obeys Eq. (4.84) over a wide range of chemical potential. The agreement between the numerically computed negativity at finite temperature and analytical results in the continuum limit (4.86) is shown in Fig. 4.11(b).

4.4 Summary and future directions

In this chapter, we study the entanglement negativity of free fermions with a Fermi surface of codimension one. We observe that there are two temperature regimes which are defined by the ratio L_β/L of the length scale associated with the thermal fluctuations $L_\beta = \hbar v_F/k_B T$ to the system size L. We find that the leading order term in the negativity (irrespective of dimensionality) consists of two kinds of contributions: a logarithmic term and a linear term (volume law) in system size. The logarithmic term is simplified to the usual logarithmic violation of area law at zero (and low) temperature, while it becomes a volume law at high temperatures (when $L_\beta \ll L$). It is interesting that these two contributions cancel each other at high temperatures which means that the entanglement negativity asymptotically vanishes. This coincides with the fact that although finite temperature states of quantum systems are highly correlated, these correlations are mostly due to thermal fluctuations and do not include any amount of quantum entanglement. In other words, the decaying behavior of the negativity indicates its very characteristic as a measure of quantum entanglement. Moreover, this property of the negativity is in stark contrast with the entanglement entropies such the von Neumann and Rényi entropies where there is only the logarithmic contribution which eventually turns into a volume law at high temperatures.

The above observation suggests that the entanglement negativity could shed light on the quantum-to-classical crossover [207] as the temperature is increased. The cross-over temperature can then be studied in various phases of a given phase diagram away from the critical point. For example, one direction could be to investigate the finite-temperature states of Hamiltonians which have symmetry protected topological phases or topological order as their ground states. The question is to what extent the entanglement properties of such phases survive at temperatures away from zero. Along the same line, it would also be interesting to use the current framework and study massive quantum field theories [26] at finite temperatures. Out-of-equilibrium dynamics [53, 68, 99, 229] of fermions is another interesting avenue for research.

Throughout all numerical simulations of fermionic systems in this work, we have not experienced any sudden death in the entanglement negativity. This is consistent with Conjecture 3.1 regarding the absence of sudden death in a fermionic lattice with hopping terms where the fermion-number parity remains mixed, i.e., the necessary condition is always satisfied.

Chapter 5

Many-body topological invariants

"Make Physics as simple as possible, but no simpler."

— Albert Einstein

In this chapter, by making use of the fermionic partial transpose introduced in Chapter 2, we construct nonlocal order parameters which detect fermionic SPT phases of various kinds. Our strategy for the construction of many-body topological invariants is to find a way – within the operator formalism – to *simulate* the Euclidean path-integral on generating manifolds of the cobordism groups. The phases of the partition functions are the desired topological invariants. We are interested in the topological phases protected by various symmetry groups, such as time-reversal, charge conjugation, or space-group symmetry. The gapped phases of matter refer to the many-body ground state of gapped quantum systems.

The basic principle is that low-energy long-wavelength physics of the gapped phases is governed by TQFTs of some sort. In general, we consider a topological phase protected or enriched by a set of global symmetries, which form a symmetry group $\widetilde{G}$. It is convenient to decompose the symmetry group $\widetilde{G}$ into two parts: The first part consists of unitary on-site (or "internal")

Part of the material presented in this chapter was previously published in: H. Shapourian, K. Shiozaki, S. Ryu, Phys. Rev. Lett. 95, 165101 (2017), Phys. Rev. B 95, 205139 (2017), and K. Shiozaki, H. Shapourian, K. Gomi S. Ryu, Phys. Rev. B 98, 035151(2018). Some text has been modified. Copyright by the American Physical Society (APS); reuse permitted according to APS copyright policies.

symmetries (call it G), and the second part contains symmetry transformations which reverse the orientation of spacetime manifolds, such as TRS and inversion. If the underlying system includes fermions, it is convenient to include the fermion number parity to the latter part.

In order to probe the topological properties of the ground state of a gapped system, a typical approach is to couple the system to a external gauge field associated with the on-site symmetry G. Let us denote a generic topological matter field by ϕ_i. Formally, the matter field can be integrated out leading to the partition function,

$$Z(X,\eta,A) = \int \prod_i D\phi_i e^{-S_X(\{\phi_i\},\eta,A)} \tag{5.1}$$

where X is a closed $(d+1)$-dimensional spacetime manifold, $\{\phi_i\}$ includes all matter fields, A is the background G gauge field which couples to the matter fields via a *minimal coupling* scheme. For relativistic fermions, the spacetime manifold X is called the spin manifold. In this case, X must be accompanied by extra information such as an orientation and boundary conditions along cycles of X. This information is collectively denoted by η and called the "structure" of the manifold. In short, the partition function of a given gapped (topological) phase depends on the input data (X,η,A).

For a gapped phase, when the correlation length of the system is much shorter than the system size, we expect that the partition function do not depend strongly on the local details of the spacetime manifold X, and the background gauge field A. In particular, for gapped topological phases, we expect that $Z(X,\eta,A)$ includes a topological term, which is independent of local data (e.g., metric),

$$Z(X,\eta,A) \sim \exp[iS_{top}(X,\eta,A) + \cdots]. \tag{5.2}$$

Here, we observe that the topological part appears, in the Euclidean signature, as a phase of the partition function $Z(X,\eta,A)$. [2] The pure imaginary part of the partition function defines a TQFT. For our purpose of distinguishing different gapped (topological) phases, the topological phase part $e^{iS_{top}}$ can be used as a (many-body) topological invariant or non-local order parameter of SPT phases.

Let us mention a few examples of the topological phase factor (5.2) of the Euclidean path integral.

– In integer quantum Hall phases, the path integral of electron degrees of freedom in the presence of a background $U(1)$ gauge field A gives rise to the Chern-Simons term, $S_{top}(X,A) = \frac{k}{4\pi}\int_X AdA$ where $k =$ integer is the quantized Hall conductance in unit of e^2/h.

– Another simple example is provided by $(1+1)d$ TSCs (e.g., the non-trivial phase of the Kitaev chain [124]); Putting the Kitaev chain on the spatial circle, the imaginary time path-integral over gapped BdG fermionic quasiparticles gives rise to $Z(T^2,\eta)$ where $X = T^2$ is the spacetime torus, and η specifies four possible boundary conditions (i.e., periodic/antiperiodic boundary conditions in space and temporal directions) for BdG fermions. If BdG quasiparticles are considered as relativistic fermions, to give a specific boundary condition η is equivalent to give a spin structure of the spacetime torus. The topological term in this case is given by the Arf invariant of a spin structure η. [196]

– For $(1+1)d$ bosonic SPT phases protected by TRS such as the Haldane spin chain, the phase of the path integral on the real projective plane $\mathbb{R}P^2$ is either 0 or π, and hence serves as a $\mathbb{Z}_2$-valued topological invariant. [164, 193]

– In Ref. [190], the discretized imaginary time path integral, in the presence of a cross-cap, was evaluated for $(1+1)d$ TSCs in symmetry class BDI. The spacetime is effectively $\mathbb{R}P^2$. It was shown that the phase of the partition function yields correctly the $\mathbb{Z}_8$ SPT topological invariant for $(1+1)d$ class BDI TSCs. [76, 118]

[2] In the Euclidean signature, the real (and positive) part of the effective action $-\ln Z(X,\eta,A)$ is the Boltzmann weight, and hence related to energetics. As energetics is usually local, global and topological properties of the field configurations should not enter into the real part of the effective action.

In the above discussion, it is of crucial importance to choose proper input data or "background", (X,η,A). Namely, (X,η,A) must be a suitable manifold such that the topological term $S_{top}(X,\eta,A)$ of the partition function, when evaluated for (X,η,A), is non-zero. In addition, it is desirable to find backgrounds (X,η,A) for which the topological phase factor $e^{iS_{top}(X,\eta,A)}$ takes the "smallest possible" or "most fundamental" value; for example, for SPT phases for which we have $\mathbb{Z}_N$ classification (N is an integer), we naturally expect the topological invariant $e^{iS_{top}(X,\eta,A)}$ to take N possible values (i.e., $e^{iS_{top}(X,\eta,A)}$ should be an N-th root of unity). Were the input (X,η,A) not chosen properly, while $e^{iS_{top}(X,\eta,A)}$ could be non-zero, it would take only a subset of possible values and hence would not distinguish all possible phases in the $\mathbb{Z}_N$ classification.

For SPT phases of our interest here the ground state is unique on any space manifold. This implies that we are dealing with TQFTs of special kind, the so-called invertible TQFTs. A remarkable fact [80, 117] is that the classification of invertible TQFTs with a background field falls under the cobordism classification of manifolds. Hence, we can use this fact to classify SPT phases. The cobordism theory [84, 199] provides a classification of manifolds in the presence of a background field A, which is introduced by gauging the onsite symmetry G, under the equivalence relation known as the cobordant. Two d-dimensional manifolds (X_i,η_i,A_i) $(i=1,2)$ with the structure η_i and background field A_i are said to be cobordant iff there exists a $(d+1)$-dimensional manifold $(\tilde{X},\tilde{\eta},\tilde{A})$ with the structure $\tilde{\eta}$ and the background field $\tilde{A}$ on $\tilde{X}$ so that its boundary $\partial\tilde{X}$ agrees with $X_1 \sqcup (-X_2)$ as well as the structure $\tilde{\eta}|_{\partial\tilde{X}}$ and the background field $\tilde{A}|_{\partial\tilde{X}}$. The abelian group structure is introduced by the disconnected sum $[X_1,\eta_1,A_1]+[X_2,\eta_2,A_2] = [(X_1,\eta_1,A_1)\sqcup(X_2,\eta_2,A_2)]$, which results in the cobordism group $\Omega_d^{\mathrm{str}}(BG)$, the equivariant cobordism group over the classifying space of G for a given type of structures. We illustrate the geometric significance of the cobordism through an example in Fig. 5.1, which shows the equivalence relation between a single circle and a pair of disjoint circles. This relation can then be used to define the equivalence classes.

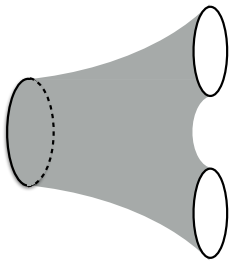

Figure 5.1: A cobordism in $(0+1)$-dimensions between a single circle (left) and a pair of disjoint circles (right).

The partition function Z of an invertible TQFT can be considered as a homomorphism $\Omega_d^{\mathrm{str}}(BG) \to U(1)$, $(X,\eta,A) \mapsto Z(X,\eta,A)$. [3] Cobordism invariant partition functions are thus labeled by elements in $\mathrm{Hom}(\Omega_d^{\mathrm{str}}(BG), U(1))$. The free part of the coboridims group leads to the theta term $e^{i\theta n}$, $n \in \mathbb{Z}$, parametrized by $\theta \in \mathbb{R}/2\pi\mathbb{Z}$. On the other hand, the torsion part $\mathrm{Tor}\,\Omega_d^{\mathrm{str}}(BG)$ classifies TQFT and in turn SPT phases.

In order to construct the order parameter of SPT phases, generating manifolds, that are generators of the cobordism groups, are of particular importance. The partition function, when evaluated for the generator of the cobordism group, gives rise to the most fundamental phase factor. Hence, the partition function on the generating manifolds serves as the order parameter of SPT phases.

In the cobordism theory, η represents spin or pin structures (and proper generalizations thereof). Invertible TQFTs which are expected to give an effective description of fermionic SPT phases depend on spin, pin, etc. structures (i.e., we are considering spin TQFTs, etc.). The precise definition of pin structures is explained in Sec. 5.1.

It should be noted that, in defining these structures in relativistic contexts, fermion fields are assumed to be transformed as a spinor under $SO(d+1)$ or $O(d+1)$ (in the Euclidean signature). In contrast, in condensed matter physics, there is no *a priori* Poincaré (relativistic) invariance, and hence fermions in condensed matter systems are not always sensitive to spin structures. There-

[3] In typical situations when we want to compute SPT topological invariants, there are gapped excitations that contribute to the amplitude of the partition function. The cobordism invariant appears in the complex $U(1)$ phase $Z(X,\eta,A)/|Z(X,\eta,A)|$ of the partition function $Z(X,\eta,A)$.

fore, it is not obvious if the classification of SPT phases by the cobordism group works for condensed matter systems. Nevertheless, as we discuss in Sec. 5.1, there exist analogs of "structures" even in non-relativistic contexts. They are symmetry twists, i.e., twisting boundary conditions by using the symmetry of the problem. For example, for fermionic SPT phases (without any symmetry other than fermion number parity conservation), it is known that twisting boundary conditions by fermion number parity symmetry is a useful diagnostic tool. Such twisting in the path integral picture gives rise to periodic or antiperiodic boundary conditions of fermions fields. Non-trivial SPT phases may "respond" to such twist in a non-trivial way and may be characterized such a response. The twisting by fermion number parity is precisely a non-relativistic analogue of spin structures, and coincides with spin structures if we consider relativistic fermions.

Put differently, while fermions in condensed matter systems are not relativistic and not always sensitive to spin (and pin) structures, when some sort of topological media (topological phases) are realized, effective relativistic fermions can emerge, which do depend on spin structures. In short, spin may emerge from short-range entanglement in quantum ground states. Now, the emergent spin is described by different relativistic structures (spin, pin, and their variants) [80, 240], corresponding to different definitions of TRS in the AZ symmetry classes. This correspondence is summarized in Table 5.3, and will be discussed in detail in Sec. 5.1.

Instead of the spacetime path integral, one can also adopt the canonical operator formalism which is the focus of this chapter. In the canonical formalism, the partition functions, and hence the topological invariants can be expressed in terms of (a set of) ground state wave functions or reduced density matrices constructed thereof and symmetry operators. Summarizing, our guiding principle is

($\star$) *Simulating* the path-integral (the partition function) on the generating spacetime manifold of the cobordism group with the use of the ground state wave function and symmetry transformations in question.

For example, the many-body Chern number [12, 152] for the quantum Hall effect in two spatial dimensions is the prototype of the many-body topological invariant written in terms of

ground state wave functions. The electric polarization operator (Resta's z) [122, 172] is also known as a many-body characterization of short-range entangled phases in the presence of the electromagnetic $U(1)$ symmetry. More generically, the characterization of SPT phases in terms of their ground state wave functions has been discussed both for bosons [91, 105, 108, 164, 193, 228, 246] and fermions. [190, 196, 228] For instance, Refs. [190, 196] use this strategy to construct many-body topological invariants for various fermionic SPT phases.

To detect non-trivial SPT phases protected by TRS, it is necessary to consider the Euclidean path integral (5.1) on various non-orientable spacetime. It was noted previously that, in the operator formalism, non-orientable spacetimes can be effectively realized by using *partial transpose*. For example, for $(1+1)d$ bosonic SPT phases protected by TRS such as the Haldane chain, the generating manifold of the relevant cobordism group is the real projective plane $\mathbb{R}P^2$. It was shown that the corresponding many-body topological invariant is given by using the partial transpose of the density matrix. [164, 193]

For fermionic systems, the notion of partial transpose must be properly introduced, i.e., the definition of partial transpose for fermionic systems does not simply follow from the definition of partial transpose for bosonic systems – as we discuss in previous chapters, because of the fermion sign, the fermionic Fock space does not simply factorize locally, and hence there is an extra complication in defining the notion of partial transpose.

As mentioned, the main goal of this chapter is to construct many-body topological invariants for fermionic SPT phases protected by TRS or other antiunitary symmetries. See Table 5.1 and 5.2 for a summary of the many-body topological invariants. There are two main technical steps for our goal which are discussed in Sec. 5.1 and in Sec. 5.2, respectively: First, in Sec. 5.1, we give detailed descriptions of the variants of pin structures. We discuss their origin in systems with a given TRS in the AZ classes, which are not necessarily relativistic at microscopic scales, following Ref. [80]. Those readers who are interested in the explicit formulas for many-body topological invariants can safely skip this section. Second, in Sec. 5.2, we use the fermionic partial transpose and antiunitary transformations, associated with orientation-reversing symmetries in the

AZ symmetry classes to construct many-body topological invariants in the operator formalism. After these technical preliminaries, we will present our formula for many-body topological invariants for various SPT phases in one, two, and three dimensions.

Table 5.1: List of many-body topological invariants for one-dimensional fermionic topological phases. The first column specifies the AZ symmetry class. The second column shows the cobordisms of pin structures. [80] The bold $\mathbf{Z}_2$ represents topological phases which appear only in the presence of interaction. KB and $\mathbb{R}P^2$ represent the Klein bottle and the real projective plane, respectively.

AZ class	Cobordism	Generating spacetime manifold	Topological invariant
BDI	$\Omega_2^{\mathrm{Pin}_-} = \mathbb{Z}_8$	$\mathbb{R}P^2$	$\mathrm{Tr}\left[\rho_I C_T^{I_1} \rho_I^{\mathsf{T}_1} [C_T^{I_1}]^\dagger\right]$ Adjacent partial transpose.
DIII	$\Omega_2^{\mathrm{Pin}_+} = \mathbb{Z}_2$	KB, (R,R) sector	$\mathrm{Tr}\left[\rho_{I_1\cup I_3}\left((-1)^{F_2}\right) C_T^{I_1} \rho_{I_1\cup I_3}^{\mathsf{T}_1}\left((-1)^{F_2}\right)[C_T^{I_1}]^\dagger\right]$ Disjoint partial transpose with intermediate fermion parity twist.
AIII	$\Omega_2^{\mathrm{Pin}^c} = \mathbb{Z}_4$	$\mathbb{R}P^2$, the flux threading $\mathbb{R}P^2$ is quantized to $\pm i$	$\mathrm{Tr}\left[\rho_I U_S^{I_1} \rho_I^{\mathsf{T}_1} [U_S^{I_1}]^\dagger\right]$ Adjacent partial transpose.
AI	$\Omega_2^{\mathrm{Pin}_-^{\tilde{c}}} = \mathbb{Z} \times \mathbf{Z}_2$	$\mathbb{R}P^2$ for $\mathbf{Z}_2$ and a 2-manifold with a unit magnetic flux for $\mathbb{Z}$	$\mathrm{Tr}\left[\rho_I C_T^{I_1} \rho_I^{\mathsf{T}_1} [C_T^{I_1}]^\dagger\right]$ for $\mathbf{Z}_2$ Adjacent partial transpose. $\mathbf{Z}_2$ phase is an interaction enabled SPT phase which is equivalent to the Haldane phase.
AII	$\Omega_2^{\mathrm{Pin}_+^{\tilde{c}}} = \mathbb{Z}$	$\mathbb{R}P^2$ with a half magnetic flux $\int_{RP^2} F = \pi$	$\mathrm{Tr}\left[\rho_I \prod_{x\in I_1} e^{\frac{\pi i x \hat{n}(x)}{2\lvert I_1\rvert}} C_T^{I_1} \rho_I^{\mathsf{T}_1} [C_T^{I_1}]^\dagger \prod_{x\in I_1} e^{\frac{-\pi i x \hat{n}(x)}{2\lvert I_1\rvert}}\right]$ Adjacent partial transpose with the twist operator.

5.1 Variants of pin structures and their origins in non-relativistic systems

In this section, we will discuss various kinds of TRS in the AZ symmetry classes, and the corresponding variants of pin structures in relativistic fermion theories. These structures are im-

Table 5.2: List of many-body topological invariants for fermionic topological phases in higher dimensions. The first column specifies a AZ symmetry class. The second column shows the cobordisms of pin structures. [80] The bold $\mathbf{Z}_2$ represent topological phases which appear only in the presence of interaction. KB and $\mathbb{R}P^2$ represent the Klein bottle and the real projective plane, respectively.

AZ class	dim.	Cobordism	Generating spacetime manifold	Topological invariant
DIII	2	$\Omega_3^{\mathrm{Pin}_+} = \mathbb{Z}_2$	$KB(x,y) \times S^1(z)$ with periodic boundary conditions in spatial directions	$\mathrm{Tr}\left[\rho_{R_1\cup R_3}\left((-1)^{F_2}\right) C_T^{R_1} [\rho_{R_1\cup R_3}\left((-1)^{F_2}\right)]^{\mathsf{T}_1} [C_T^{R_1}]^\dagger\right]$ Disjoint partial transpose with intermediate fermion parity twist.
AII	2	$\Omega_3^{\mathrm{Pin}_+^{\tilde{c}}} = \mathbb{Z}_2$	$KB[(x,y) \sim (1-x, y+1)] \times S^1(z)$ with a unit magnetic flux $\int F_{zx} = 2\pi$	$\mathrm{Tr}_{R_1\cup R_3}\left[\rho^+_{R_1\cup R_3} C_T^{R_1} [\rho^-_{R_1\cup R_3}]^{\mathsf{T}_1} [C_T^{R_1}]^\dagger\right]$, $\rho^\pm_{R_1\cup R_3} = \mathrm{Tr}_{\overline{R_1\cup R_3}}\left[\prod_{(x,y)\in R_2} e^{\pm \frac{2\pi i y}{L_y} \hat{n}(x,y)} \lvert GS\rangle \langle GS\rvert\right]$ Disjoint partial transpose along the x-direction with intermediate $U(1)$ twist which varies in the y-direction as $e^{2\pi i y/L_y}$.
D+I	3	$\Omega_4^{\mathrm{Pin}^+} = \mathbb{Z}_{16}$	$\mathbb{R}P^4$	$\langle GS \lvert I_D \rvert GS\rangle$ Partial inversion.
A+I	3	$\Omega_4^{\mathrm{Pin}^c} = \mathbb{Z}_8 \times \mathbf{Z}_2$	$\mathbb{R}P^4$ for subgroup $\mathbb{Z}_8$	$\langle GS \lvert I_D \rvert GS\rangle$ Partial inversion. $U(1)$ phase associated with I is chosen so that $I^2 = (-1)^F$.

portant input for the cobordism classification of fermionic TQFTs (spin or pin TQFTs), which provides the classification of cobordism invariant partition functions obtained by the Euclidean path integral of fermionic quantum field theories. This section may be skipped, if the reader is interested mostly in the explicit formulae of many-body topological invariants of fermionic SPT phases, which can be found in the later sections.

In Sec. 5.1.1, we start by discussing TRS in the Euclidean path integral for generic systems without assuming relativistic invariance. Within the Euclidean path integral, TRS can then be used to twist boundary conditions, leading to non-orientable spacetime such as the real projective plane, Klein bottle, etc. (Sec. 5.1.1.) As discussed in the beginning of this chapter, the path integral on these spacetime manifolds can serve as topological invariants of fermionic SPT phases. Although this can be done without assuming relativistic invariance, it is worth understanding this process in relativistic quantum field theories. In the relativistic context, in order to consider

fermionic theories on non-orientable spacetime, we can start from local definitions of fermionic spinors (on each coordinate patch). They can be then glued together to give the global definitions of fermionic spinors on non-orientable spacetime. As we will see, in this construction, TRS constitutes a part of this gluing operation. This consideration allows us to establish a connection between (twisting or gluing by) TRS in the AZ symmetry classes and (variants of) pin structures in relativistic quantum field theory.

5.1.1 Time-reversal symmetry in Euclidean path integral

In this part, we consider how TRS can be implemented in the Euclidean path integral. This should be contrasted with TRS in the operator formalism, where TRS is given by an anti-linear and anti-unitary operator acting on the Hilbert space. The path-integral formulation is particularly useful when discussing twisting boundary conditions by TRS to generate non-orientable spacetimes. Here, we will take both real and complex fermion fields as examples.

Let $\{\hat{\psi}_j^\dagger, \hat{\psi}_j\}$ be a set of fermionic creation and annihilation operators. Here, the index j labels collectively all degrees of freedom including the spatial coordinates, and internal degrees of freedom. Suppose that anti-unitary time-reversal $\hat{T}$ acts on these operators as

$$\hat{T}\hat{\psi}_j^\dagger \hat{T}^{-1} = \hat{\psi}_k^\dagger [\mathcal{U}_T]_{kj}, \quad \hat{T} i \hat{T}^{-1} = -i. \tag{5.3}$$

The Hermite conjugate of (5.3) leads to the transformation rule for the fermion annihilation operators, $\hat{\psi}_j$. Here, $\mathcal{U}_T$ is a unitary matrix and satisfies

$$\mathcal{U}_T \mathcal{U}_T^* = \pm 1. \tag{5.4}$$

The $\pm$ signs correspond to time-reversal which squares to $+1$, $\hat{T}^2 = 1$ (non-Kramers), and to the fermion number parity $(-1)^F$, $\hat{T}^2 = (-1)^F$ (Kramers), respectively.

Let us now consider a free fermionic Hamiltonian $\hat{H} = \sum_{jk} \hat{\psi}_j^\dagger h_{jk} \hat{\psi}_k$. By the standard coherent state path-integral, the partition function Z can be expressed as the Euclidean path integral,

$$Z = \int D\bar{\psi} D\psi e^{-S} = \mathrm{Det}(\partial_\tau \delta_{jk} + h_{jk}), \tag{5.5}$$

$$S = \int d\tau \bar{\psi}_j(\tau) \big[\partial_\tau \delta_{jk} + h_{jk}\big] \psi_k(\tau), \tag{5.6}$$

where $\bar{\psi}_j(\tau)$ and $\psi_k(\tau)$ are independent Grassmann variables. Requiring TRS, $\hat{T}\hat{H}\hat{T}^{-1} = \hat{H}$, which is equivalent to $\mathcal{U}_T h^* \mathcal{U}_T^\dagger = h$, implies that the action S is invariant under the following renaming of path-integral variables,

$$\begin{aligned} T_E: \ \psi_j(\tau) &\mapsto i\bar{\psi}_k(-\tau)[\mathcal{U}_T]_{kj}, \\ \bar{\psi}_j(\tau) &\mapsto i[\mathcal{U}_T^\dagger]_{jk} \psi_k(-\tau), \end{aligned} \tag{5.7}$$

which looks like a composition of reflection in the imaginary time direction and a particle-hole transformation. It is evident that time-reversal in the operator formalism is translated into reflection along the imaginary time direction in the Euclidean path integral. [4] It should be noted that, in contrast to the operator formalism, both the first and second equations in (5.7) are needed to define the Euclidean TRS since the Grassmann fields ψ_j and $\bar{\psi}_j$ are independent.

Another important point to note is that, when TRS is translated into the particle-hole reflection symmetry in the Euclidean path integral, (5.7), the additional pure imaginary phase factor $\pm i$ must be introduced. This is to compensate the minus sign arising from the anti-commutation of Grassmann variables. We have seen in Chapter 2 that a similar phase factor arises when we introduce the fermionic partial transpose. We also note that the square of the Euclidean TRS T_E is $T_E^2 = 1$ for $\hat{T}^2 = (-1)^F$ and $T_E^2 = -1$ for $\hat{T}^2 = 1$.

[4] Here, we consider the quadratic Hamiltonian for simplicity. However, including interactions in the Hamiltonian gives rise to no extra difficulties, and leads to the same result, (5.7).

Twisting boundary condition by TRS

Unitary on-site symmetries in quantum many-body systems (described by quantum field theories) can be used to twist boundary conditions, or to introduce symmetry-twist defects, by introducing a branch cut (or branch sheet). In the presence of a symmetry-twist defect, quantum fields, when adiabatically transported across a branch cut (sheet), will be acted upon by the symmetry operator. Twisted boundary conditions and symmetry-twist defects have been proven to be useful diagnostic tools to detect properties of the systems. In particular, different SPT phases protected by symmetries respond differently to the twisted background, and hence can be distinguished and characterized this way.

Twisting boundary conditions is most commonly done in particle number conserving systems, where boundary conditions can be twisted by adding a $U(1)$ phase. For example, in the context of the quantum Hall effect, from the response of the system to the twisted boundary condition, one can extract the quantized Hall conductance. One can also introduce a symmetry-twist defect in this context, a small flux tube carrying unit flux quantum, which accumulates/depletes charge. The quantized response to the flux tube can be used as a characterization of the quantum Hall system.

For fermionic systems without particle number conservation, e.g., those described by the BdG Hamiltonians, boundary conditions can still be twisted by using fermion number parity – by adding $\pm$ signs corresponding to periodic/anti-periodic boundary conditions. Twisting by fermion number parity can be used, for example, to detect the non-trivial topological superconductor phase of the Kitaev chain.

An orientation reversing symmetry, such as TRS or spatial reflection, can be used to twist boundary conditions as well. This procedure effectively leads to spacetime manifolds which are not orientable in general. Different SPT phases protected by an orientation reversing symmetry can then be distinguished and characterized by their responses to non-orientable geometry/topology of spacetime manifold. For example, the $\mathbb{Z}_8$ SPT invariant of (1+1)d TSCs in

symmetry class BDI can be detected by the discretized imaginary time path-integral in the presence of a cross-cap (the relevant spacetime is $\mathbb{R}P^2$).

Spin and pin structures, and their variants

Spin and pin structures The above construction of the path-integral on non-orientable spacetime manifolds through twisting boundary conditions by an orientation reversing symmetry can be applied to systems without relativistic invariance. On the other hand, in the presence of relativistic invariance, the construction of fermionic, relativistic quantum field theories on generic (both orientable and non-orientable) spacetime can be done once we specify how we glue local definitions of fermionic spinors. The data needed to specify the gluing rule consists of structures, such as spin or pin structures. We will now see that TRS constitutes a part of this gluing operation, and hence a specific choice of TRS corresponds to a specific type of pin structures (and variants thereof).

To be specific, let us start by recalling the standard construction of (non-orientable) spacetime manifolds, and quantum fields on them. We first focus on real fermion fields, i.e., systems without particle-number conservation, and discuss spin and $\text{pin}_{\pm}$ structures. We start from a collection of "patches", $\{U_i\}$. These patches are glued together to give a global definition of a Riemannian manifold X. (Here, we adopt the Euclidean signature.) When two patches intersect, there is a transition function relating two patches. The transition functions take their values in $SO(d+1)$ for an oriented, $(d+1)$-dimensional Riemannian manifold. Here, $SO(d+1)$ is the structure group acting on the frame fields (vielbein) on the tangent spaces. Similarly, global definition of a quantum field on the manifold can be made by first considering quantum fields on individual patches and then gluing them together. For a relativistic fermion field on X, $SO(d+1)$ is lifted to its double cover, $\text{Spin}(d+1)$, which is generated by $\Sigma_{ab} = [\gamma^a, \gamma^b]/4i$ where $\gamma^{a=1,\ldots,d+1}$ are gamma matrices. The choice of signs that arises in this lifting defines a spin structure.

Similarly, for an non-orientable, $(d+1)$-dimensional Riemannian manifold X, the transition functions are members of $O(d+1)$, i.e., the structure group is $O(d+1)$. To define relativistic

fermion fields on X, $O(d+1)$ should be lifted to its double cover, $\mathrm{Pin}_+(d+1)$ or $\mathrm{Pin}_-(d+1)$. Here, these are two different double covers of $O(d+1)$. Once again, sign ambiguities that arise in the lifting define the pin structures. In addition to continuous spinor rotations generated by Σ_{ab}, $\mathrm{Pin}_\pm(d+1)$ has an element which reverses the orientation, and squares to ± 1. To be more specific, $\mathrm{Pin}_\pm(n)$ groups are defined as follows. Let $\mathrm{Cliff}_{\pm n}$ be the algebra over $\mathbb{R}$ generated by $e_1,\dots,e_n$ subject to the relations $e_i e_j + e_j e_i = \pm 2\delta_{ij}$. Introduce the "mode space" $M := \{\sum_i x_i e_i | x_i \in \mathbb{R}\}$ with an inner product $(x,y) = \frac{1}{2}(xy+yx), x, y \in M$. The $\mathrm{Pin}_\pm(n)$ group is defined by

$$\mathrm{Pin}_\pm(n) := \{v_1 \cdots v_r | v_i \in M, (v_i, v_i) = \pm 1\}. \tag{5.8}$$

Summarizing, relativistic fermion fields can be defined globally on an non-orientable manifold, by patching and gluing local definitions by $\mathrm{Pin}_\pm(d+1)$. The gluing by the orientation-reversing element in $\mathrm{Pin}_\pm(d+1)$ is an analogue of twisting by orientation-reversing symmetry which we discussed without assuming relativistic invariance. As mentioned, an orientation reversing symmetry in the Euclidean signature which squares to ± 1 corresponds to TRS which squares to $(-1)^F$ and $+1$, respectively, in the operator formalism. That is to say, symmetry classes DIII and BDI correspond to $\mathrm{Pin}_+(d+1)$ and $\mathrm{Pin}_-(d+1)$ respectively in the relativistic context.

It once again should be stressed that in the above definitions, fermion fields are assumed to transform as a spinor under $SO(d+1)$ or $O(d+1)$. The main difference between condensed matter systems and relativistic systems is the absence of *a priori* rotation symmetry in condensed matter systems. Put differently, fermion fields in condensed matter systems do not know the transformation rule under $O(d+1)$ rotations because of the lack of rotation symmetry. [5] It is thus not obvious that the classification of SPT phases by the cobordism group still works for condensed matter systems. Nevertheless, when some sort of topological media (topological phases) are realized, effective relativistic fermions can emerge, which are sensitive to spin and pin structures. In short, spin may emerge from short-range entanglement in quantum ground states.

[5] In lattice systems, the degrees of freedom obey a representation of space group under consideration.

Symmetry	AZ class	Relativistic pin structure
$(-1)^F$	D	Spin
$(-1)^F, \hat{T}, \hat{T}^2 = 1$	BDI	Pin_-
$(-1)^F, \hat{T}, \hat{T}^2 = (-1)^F$	DIII	Pin_+
$U(1)$	A	Spin^c
$U(1) \rtimes \hat{T}, \hat{T}^2 = 1$	AI	$\mathrm{Pin}^{\tilde{c}}_-$
$U(1) \rtimes \hat{T}, \hat{T}^2 = (-1)^F$	AII	$\mathrm{Pin}^{\tilde{c}}_+$
$U(1) \times \hat{C}\hat{T}$	AIII	Pin^c

Table 5.3: Orientation reversing symmetries in the Altland-Zirnbauer (AZ) classification [6] and corresponding relativistic spin and pin structures in fermionic systems. Here, $(-1)^F$ is the fermion number parity, $\hat{T}$ is antiunitary time-reversal, and $\hat{C}$ is unitary particle-hole symmetry. The semidirect product $U(1) \rtimes \hat{T}$ means that the $U(1)$ charge e^{iQ} is flipped under $\hat{T}$ as $\hat{T} e^{iQ} \hat{T}^{-1} = e^{-iQ}$.

Variants of spin/pin structures and AZ symmetry classes The above correspondence between orientation reversing symmetries and pin structures can be extended to other T and CT symmetries in AZ symmetry classes: There is a one-to-one correspondence between AZ symmetry classes and types of spin and pin structures in Euclidean relativistic quantum field theories, as summarized in Table 5.3.

Let us give a brief overview of Table 5.3. More details can be found in Appendix D of Ref. [195]. First, for the symmetry class in which only fermion number parity is conserved, i.e., class D, the corresponding structures are spin structures. Next, if, in addition to fermion number parity conservation, there is TRS, the corresponding AZ class is either class DIII or BDI, depending on if $T^2 = (-1)^F$ or $T^2 = 1$, respectively. For these classes, we associate pin_+ or pin_- structures. These structures are associated to Pin_+ or Pin_- groups, respectively.

We now add the electric charge $U(1)$ conservation, and consider symmetry classes A, AIII, AI, and AII. First, for symmetry class A, we consider spin^c structures. This means that fermions on manifolds endowed with a spin^c structure, in which states obey the so-called spin-charge relation. [185] Next, let us consider symmetry class AIII. Symmetry class AIII respects CT (the combination of TRS and unitary PHS). The corresponding structures are called pin^c structures. Finally, symmetry classes AII and AI respect, in addition to the $U(1)$ charge conservation, TRS

which squares to $(-1)^F$ and 1, respectively. The corresponding structures are called $\text{pin}^{\tilde{c}}_{\pm}$ structures. $\text{pin}^{\tilde{c}}_{\pm}$ structures are variants of ordinary $\text{pin}_{\pm}$ structures, which were introduced by Refs. [80, 145], and will be discussed in detail shortly. To be precise, the pin^c and $\text{pin}^{\tilde{c}}_{\pm}$ structures are associated with the patch transformations of fermionic fields which are elements of $\text{Pin}^c(n)$ and $\text{Pin}^{\tilde{c}}_{\pm}(n)$ group, respectively.

In addition to these symmetry classes and their corresponding structures, there remain symmetry classes (C, CI and CII) and structures ($G_{0,\pm}$). G_0, G_+, and G_- structures are $SU(2)$ analogs of spin^c and pin^c structures, where $U(1)$ is replaced by the internal $SU(2)$ symmetry.

5.2 Non-orientable spacetime path-integral in the operator formalism

In this section, we first give an overview of the use of the fermionic partial time-reversal and anti-unitary transformations to construct non-local order parameters within the operator formalism that correspond to the partition functions on non-orientable spacetime manifolds. In the subsequent section, we present the many-body topological invariants which are also summarized in Table 5.1. For each case, we demonstrate that our formula detects non-trivial SPT phases, by using analytical calculations for fixed point wave functions and numerics for free fermion models.

In the case of SPT phases protected by an orientation-reversing spatial symmetry (e.g., reflection and inversion) [190, 191], a way to implement the path-integral on non-orientable spacetimes in the operator formalism, based on which we propose formulas for many-body topological invariants, is by applying *partial* symmetry operation (e.g., partial reflection and inversion) which acts only on a subregion of the total space and can be used to simulate the non-orientable spacetime path integral, e.g., path-integrals on $\mathbb{R}P^2$ (see Fig. 5.2) and $\mathbb{R}P^4$. Naively pursing the analogy with this approach that works for orientation-reversing spatial symmetries, one would then be tempted to consider a *partial* time-reversal or CT transformation to construct topological invariants for SPT phases protected by these symmetries. However, due to the anti-unitary nature

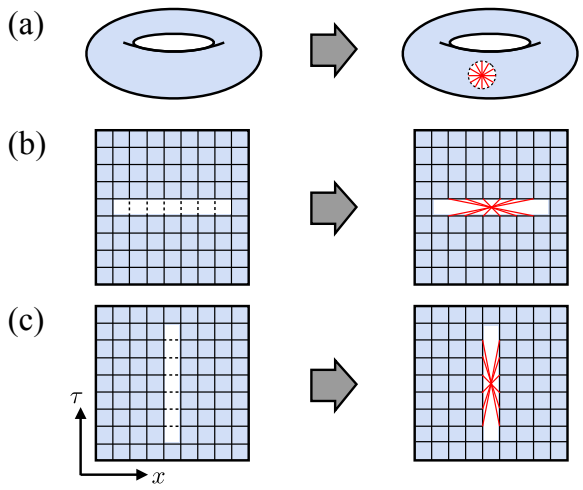

Figure 5.2: (a) Introducing a cross-cap, i.e., generator of $\mathbb{R}P^2$, in the spacetime. (b) Partial reflection and (c) partial time inversion. First and second columns show the original connectivity after cutting and the twisted bonding after gluing, respectively.

of T and CT transformations, simply restricting these transformations to a given spatial region would not work. One may ask: What is the meaning of restricting complex conjugation to a given region?

In this section, we show how partial transpose introduced in Chapter 2, can be properly used to generate the necessary non-orientable spacetime path integral. We also discuss how topological invariants can be expressed in terms of the fermion coherent states. For the case of non-interacting fermionic systems, topological invariants can be expressed as a fermionic Gaussian integral, and can be computed efficiently [190, 191].

Why partial transpose?

Let us begin with the following question: what is a physical observable associated with time-reversal T? Since T is anti-unitary, for a pure quantum state $|\psi\rangle$, a naive expectation value $\langle\psi|T|\psi\rangle$ is not a physical observable as it depends on an unphysical $U(1)$ phase ambiguity of the state $|\psi\rangle$. Instead, we find that the amplitude $|\langle\psi|T|\psi\rangle|$ is physical. We note that amplitude

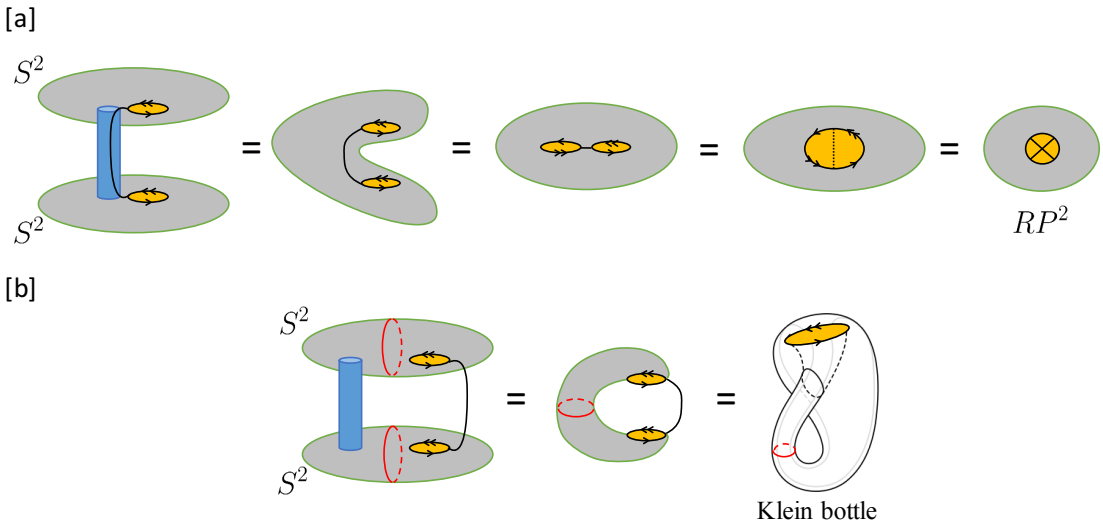

Figure 5.3: The topological equivalence of the spacetime manifolds associated with the partial transpose on [a] two adjacent intervals and [b] two disjoint intervals to the real projective plane and the Klein bottle, respectively. The red curve represents the holonomy from the temporal boundary condition on the intermediate region of the disjoint two intervals (See Fig. 5.5).

square can be written as

$$|\langle\psi|T|\psi\rangle|^2 = \mathrm{Tr}\Big[\rho U_T \rho^* U_T^\dagger\Big] = \mathrm{Tr}\Big[\rho U_T \rho^T U_T^\dagger\Big], \tag{5.9}$$

where U_T is the unitary matrix defined by $[U_T]_{jk} = \langle j|T|k\rangle$, $\rho = |\psi\rangle\langle\psi|$, ρ^* is the complex conjugate of ρ, and ρ^T is the matrix transpose $\big(|i\rangle\langle j|\big)^T = |j\rangle\langle i|$ in the many body Hilbert space. Here, we have used the hermiticity $\rho^\dagger = \rho$ of the density matrix. The quantity $|\langle\psi|T|\psi\rangle|$ is useful for determining whether time-reversal symmetry is spontaneously broken. However, it does not help us to differentiate topological phases protected by TRS, since $|\langle\psi|T|\psi\rangle|$ is identically one for time-reversal symmetric states, i.e., $T|\psi\rangle \sim |\psi\rangle$.

For the purpose of differentiating and detecting SPT phases protected by TRS, it is necessary to consider the expectation value involving *partial transpose* or *partial time-reversal transformation* of the reduced density matrix [164], which, when interpreted in the path-integral picture, corresponds to the path-integral on non-orientable spacetime. [193]

Let us discuss how this can be done first for bosonic SPT phases defined on a one-dimensional space or one-dimensional lattice I_{tot}. We consider a given region (segment) in I_{tot}, call it I, and consider the reduced density matrix ρ_I, which is obtained by integrating all degrees of freedom outside of I, $\rho_I = \mathrm{Tr}_{\bar{I}} |GS\rangle\langle GS|$ where $|GS\rangle$ is the ground state on I_{tot}. We now consider bipartitioning I, $I = I_1 \cup I_2$. Here, I_1 and I_2 can be two adjacent or disjoint intervals within I_{tot}. The many body Hilbert space is the tensor product of sub Hilbert spaces on I_1 and I_2, $\mathscr{H}_I = \mathscr{H}_{I_1} \otimes \mathscr{H}_{I_2}$. By considering the partial transpose of the reduced density matrix followed by the unitary transformation only on the subsystem I_1, we define the quantity

$$Z = \mathrm{Tr}_I \Big[\rho_I U_T^{I_1} \rho_I^{T_1} [U_T^{I_1}]^\dagger \Big], \tag{5.10}$$

where $\rho_I^{T_1}$ is the partial transpose defined in Chapter 2. and $U_T^{I_1}$ is the unitary matrix associated with TRS T on the subsystem I_1.

The quantity (5.10) can be viewed as the partition function on a non-orientable spacetime. In the case of adjacent intervals, the corresponding manifold is $\mathbb{R}P^2$ (Fig. 5.3 [a]), and in the case of disjointed intervals, the corresponding manifold is the Klein bottle [35, 190, 193] (Fig. 5.3 [b]). Hence, the phase of the quantity (5.10) can serve as a topological invariant for $(1+1)d$ bosonic SPT phases protected by TRS.

In the above discussion, we have considered bosonic cases while our focus in this dissertation is fermions. We should note that the partial transposition introduced in Eq. (2.23), which is simply swapping indices of the first interval, is strictly defined for bosons. In order to define a consistent definition for fermions, one needs to take into account the anti-commuting property of fermion operators, as discussed in Chapter 2.

As we show, by using the fermionic partial transpose and related operations developed there, we can construct many-body topological invariants for fermionic SPT phases. In the next two subsubsections, we introduce a fermionic counterpart of (5.10) both for adjacent and disjoint intervals. When considering the Klein bottle, we can insert a π-flux through a non-trivial cycle (red

loops in Fig. 5.3) which leads to two possible boundary conditions: the periodic boundary condition (the "Ramond" sector) and the anti-periodic boundary condition (the "Neveu-Schwarz" sector). As we see in the following, these two boundary conditions can be realized in our calculations by applying the fermion number parity twist operator on the intermediate interval separating the two disjoint intervals.

Two adjacent intervals: cross-cap

Let us consider two states $|\psi_{1,2}\rangle \in \mathscr{H}_{S^1}$ in the Hilbert space defined on the space manifold S^1, and $\rho = |\psi_1\rangle\langle\psi_2|$. When $|\psi_1\rangle = |\psi_2\rangle$, ρ is a pure state density matrix. Let us introduce two adjacent intervals $I_{1,2}$, and trace out the degrees of freedom outside $I = I_1 \cup I_2 \subset S^1$ to obtain a reduced density matrix. The reduced density matrix can be interpreted as a path-integral on a cylinder with a slit as

$$\rho_I = \mathrm{Tr}_{S^1\setminus I}\big(|\psi_1\rangle\langle\psi_2|\big) = \quad . \tag{5.11}$$

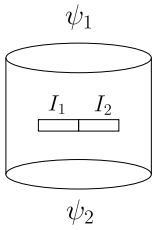

We now consider the fermionic partial transpose of ρ_I with respect to the subregion I_1. Explicitly, it is given, in the coherent state representation, as

$$\begin{aligned} C_T^{I_1}\rho_I^{T_1}[C_T^{I_1}]^\dagger = \int \prod_{j\in I} d\bar{\xi}_j d\xi_j d\bar{\chi}_j d\chi_j e^{-\sum_{j\in I}(\bar{\xi}_j\xi_j+\bar{\chi}_j\chi_j)} \langle\{\bar{\xi}_j\}_{j\in I}|\rho_I|\{\chi_j\}_{j\in I}\rangle \\ \times |\{i[\mathscr{U}_T]_{jk}\bar{\chi}_k\}_{j\in I_1}, \{\xi_j\}_{j\in I_2}\rangle\langle\{i\xi_k[\mathscr{U}_T^\dagger]_{kj}\}_{j\in I_1}, \{\bar{\chi}_j\}_{j\in I_2}|. \end{aligned} \tag{5.12}$$

Let $\rho' = |\psi_3\rangle\langle\psi_4|$ be another density matrix composed of pure states $|\psi_3\rangle, |\psi_4\rangle$. The quantity

$$\mathrm{Tr}_I\left[\rho_I' C_T^{I_1}\rho_I^{T_1}[C_T^{I_1}]^\dagger\right] \tag{5.13}$$

is associated with the spacetime manifold, which is topologically equivalent to the four point function with a cross-cap as shown in Fig. 5.3. By using the coherent state basis, the quantity (5.13) can be expressed as

$$\mathrm{Tr}_I\left[\rho'_I C_T^{I_1}\rho_I^{T_1}[C_T^{I_1}]^\dagger\right]=\int\prod_{j\in\text{full}}[d\alpha_j d\beta_j d\gamma_j d\delta_j]e^{\Sigma_{I_1}[\alpha_j[i\mathscr{U}_T]_{jk}\gamma_k+\beta_j[i\mathscr{U}_T^\dagger]_{jk}\delta_k]}e^{\Sigma_{I_2}[\alpha_j\delta_j+\beta_j\gamma_j]}e^{\Sigma_{S^1\setminus I}[\alpha_j\beta_j+\gamma_j\delta_j]}$$
$$\times\psi_1(\{\alpha_j\})\psi_2^*(\{\beta_j\})\psi_3(\{\gamma_j\})\psi_4^*(\{\delta_j\}). \tag{5.14}$$

The corresponding tensor network representation is presented in Fig. 5.4. When ρ and ρ' are composed of the ground state $|GS\rangle$, $\rho=\rho'=|GS\rangle\langle GS|$, Eq. (5.15) can be interpreted as the partition function on the real projective plane $\mathbb{R}P^2$. (To see this, we note that $|GS\rangle$ is the state defined on the boundary of the disc, and obtained by performing the path-integral inside the disc.)

Finally, it is also possible and useful to turn on an additional symmetry flux along the nontrivial $\mathbb{Z}_2$ cycle of the cross-cap. We insert the unitary operator $U_g^{I_1}$ of g symmetry on the subsystem I_1 and consider

$$\mathrm{Tr}_I\left[\rho'_I U_g^{I_1} C_T^{I_1}\rho_I^{T_1}[C_T^{I_1}]^\dagger[U_g^{I_1}]^\dagger\right]\sim$$

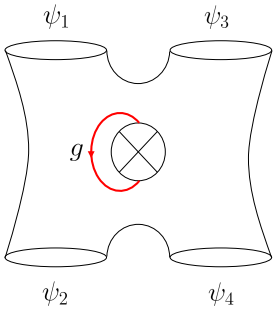

. (5.15)

Two disjoint intervals: the Klein bottle

Let us consider $\rho=|\psi_1\rangle\langle\psi_2|$ as before. We introduce three adjacent intervals $I=I_1\cup I_2\cup I_3\subset S^1$ and trace out the degrees of freedom outside of I. Subsequently, we trace out the interval I_2 after acting with a unitary transformation U^{I_2}. Here, U^{I_2} can be any unitary operator, but we focus on

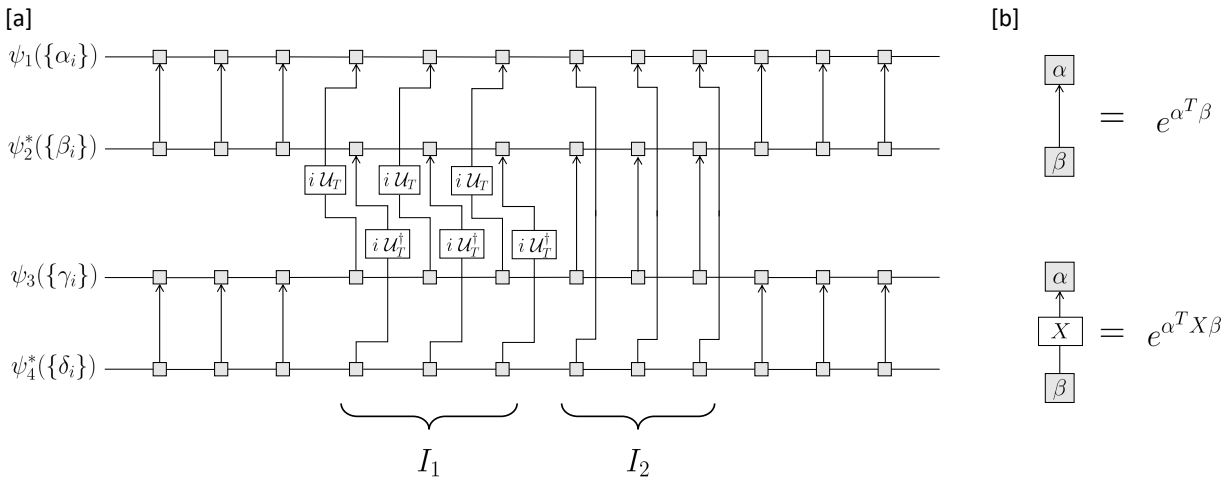

Figure 5.4: [a] Adjacent partial transpose associated with the TRS. [b] Connecting matrices.

the $U(1)$ transformation $U_\theta^{I_2} = e^{\sum_{j\in I_2} i\theta f_j^\dagger f_j}$. The resulting reduced density matrix can be viewed as the path-integral on a cylinder with two slits and an intermediate symmetry defect:

$$\rho_{I_1\cup I_3}(e^{i\theta}) = \mathrm{Tr}_{S^1\setminus I_1\cup I_3}\left(e^{i\theta\sum_{j\in I_2} f_j^\dagger f_j}\ |\psi_1\rangle\langle\psi_2|\right) = \quad , \tag{5.16}$$

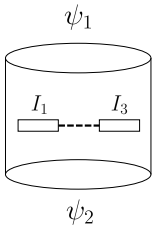

where the dashed line represents the symmetry twist: when passing this twist the complex fermion fields acquire the phase $e^{i\theta}$. Let $\rho' = |\psi_3\rangle\langle\psi_4|$ be another density matrix and consider the density matrix $\rho'_{I_1\cup I_3}(e^{-i\theta})$ with the symmetry twist by the inverse of $U_\theta^{I_2}$. The spacetime manifold associated with the quantity

$$\mathrm{Tr}_{I_1\cup I_3}\left[\rho'_{I_1\cup I_3}(e^{-i\theta})C_T^{I_1}\rho_{I_1\cup I_3}^{T_1}(e^{i\theta})[C_T^{I_1}]^\dagger\right] \tag{5.17}$$

is topologically equivalent to the four point function on the Klein bottle with the twist by $U_\theta^{I_2}$;

$$\mathrm{Tr}_{I_1\cup I_3}\Big[\rho'_{I_1\cup I_3}(e^{-i\theta})C_T^{I_1}\rho^{T_1}_{I_1\cup I_3}(e^{i\theta})[C_T^{I_1}]^\dagger\Big]\sim$$

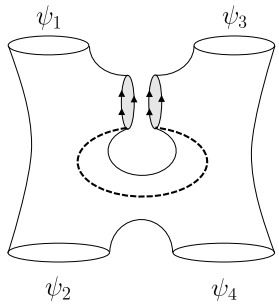

. (5.18)

See Fig. 5.3, and also Fig. 5.5 for a tensor network representation. For the ground states $|\psi_i\rangle = |GS\rangle\,(i=1,2,3,4)$, the four point function (5.18) is the partition function over the Klein bottle. It should be noticed that the $U(1)$ twist $e^{i\theta}$ is arbitrary in the cases of $\mathrm{pin}^{\tilde{c}}_{\pm}$ structures due to the flip of the $U(1)$ charge on the orientation reversing patches. On the other hand, in the case of pin^c structures, the $U(1)$ holonomy along the $\mathbb{Z}_2$ nontrivial cycle is quantized to 0 or π flux. As in (5.14), the quantity (5.18) can be expressed in terms of the fermion coherent state as

$$\begin{aligned}
&\mathrm{Tr}_{I_1\cup I_3}\Big[\rho'_{I_1\cup I_3}(e^{-i\theta})C_T^{I_1}\rho^{T_1}_{I_1\cup I_3}(e^{i\theta})[C_T^{I_1}]^\dagger\Big]\\
&=\int\prod_{i\in\mathrm{full}}[d\alpha_i d\beta_i d\gamma_i d\delta_i]e^{\sum_{I_1}\alpha_i[i\mathscr{U}_T]_{ij}\gamma_j}e^{\sum_{I_1}\beta_i[i\mathscr{U}_T^\dagger]_{ij}\delta_j}e^{\sum_{I_2}\alpha_i e^{-i\theta}\beta_i}e^{\sum_{I_2}\gamma_i e^{i\theta}\delta_i}e^{\sum_{I_3}\alpha_i\delta_i}e^{\sum_{I_3}\beta_i\gamma_i}e^{\sum_{I_4}\alpha_i\beta_i}e^{\sum_{I_4}\gamma_i\delta_i}\\
&\quad\times\psi_1(\{\alpha_i\})\psi_2^*(\{\beta_i\})\psi_3(\{\gamma_i\})\psi_4^*(\{\delta_i\}).
\end{aligned} \tag{5.19}$$

5.3 One dimensional systems

In this section, we explicitly show how the framework explained above can be utilized to characterize different topological phases in four symmetry classes BDI, DIII, and AIII, and AII. The calculation for AI can be found in Ref. [195].

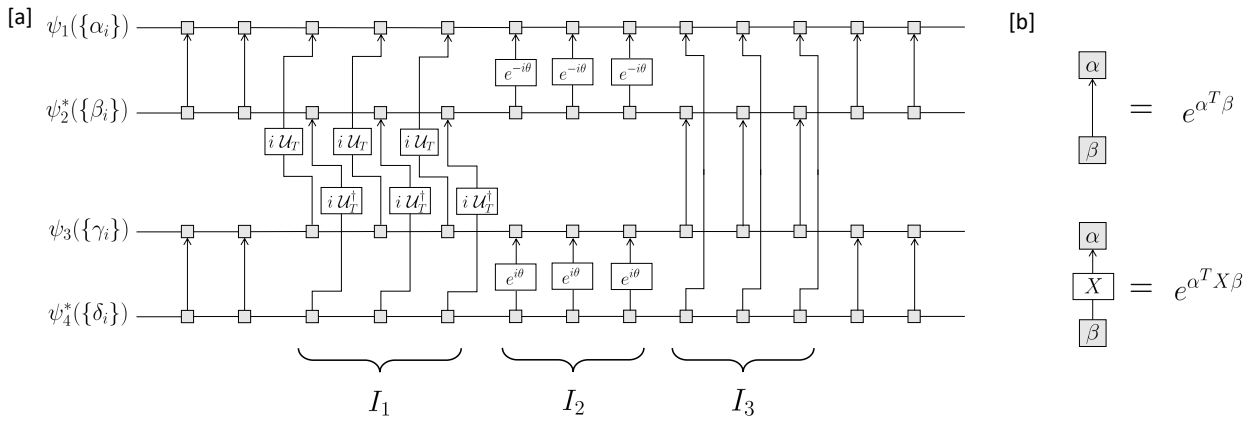

Figure 5.5: [a] Disjoint partial transpose with intermediate $U(1)$ flip for TRS. [b] Connecting matrices.

5.3.1 Class BDI

Let us consider superconducting chains with TRS $T^2 = 1$. The pioneering work by Fidkowski and Kitaev [75] showed that the ground state of the eight copies of the Kitaev Majorana chain [124] can be adiabatically connected into a trivial ground state. In the subsequent work [76, 214], it was pointed out that the operator algebra with fermion parity and TRS realized in the entanglement Hilbert space is classified by $\mathbb{Z}_8$. More recently, Kapustin *et al.* [118] argued that the $\mathbb{Z}_8$ classification is identified with the pin_ cobordism, which gives the classification of the cobordism invariant topological actions of Euclidean quantum field theory of real fermions with reflection symmetry $R^2 = (-1)^F$ or $T^2 = +1$ (See also [31, 120]).

For our purpose, the generating manifold $\mathbb{R}P^2$ of the pin_ cobordism $\Omega_2^{\text{Pin}_-} = \mathbb{Z}_8$ plays an important role. The $\mathbb{Z}_8$ classification implies that the partition function of Euclidean quantum field theory on $\mathbb{R}P^2$ is given by

$$Z(\mathbb{R}P^2, \pm) = |Z(\mathbb{R}P^2, \pm)| e^{\pm i 2\pi\nu/8}, \quad \nu \in \{0, \dots, 7\}, \tag{5.20}$$

where $\pm$ specifies one of two pin_ structure on $\mathbb{R}P^2$, [6] and $\nu \in \mathbb{Z}_8$ labels distinct topological phases. As discussed in the previous section, this path-integral can be simulated by using partial transpose for disjoint interval, and hence the many-body topological invariant in the operator formalism is given by Eq. (5.13) with $\rho' = \rho = |GS\rangle\langle GS|$:

$$Z = \mathrm{Tr}_I \left[\rho_I C_T^{I_1} \rho_I^{T_1} [C_T^{I_1}]^\dagger \right]. \tag{5.21}$$

Moreover, the $\mathbb{Z}_4$ subgroup is generated by the Klein bottle with periodic boundary condition in the S^1 direction. [196] As we discussed in the previous subsection such a spacetime manifold can be prepared by taking partial transpose for disjoint intervals with the fermion parity twist in the intermediate region [193]:

$$Z = \mathrm{Tr}_{I_1 \cup I_3} \left[\rho_{I_1 \cup I_3} (e^{-i\pi}) C_T^{I_1} \rho_{I_1 \cup I_3}^{T_1} (e^{+i\pi}) [C_T^{I_1}]^\dagger \right]. \tag{5.22}$$

Numerical calculations

A canonical model of non-trivial SPT phases in this symmetry class is given by the Kitaev chain [124]

$$H = -\sum_i \left[t f_{i+1}^\dagger f_i - \Delta f_{i+1}^\dagger f_i^\dagger + \mathrm{H.c.} \right] - \mu \sum_i f_i^\dagger f_i \,, \tag{5.23}$$

which describes a superconducting state of spinless fermions. TRS can be introduced as

$$T f_i^\dagger T^{-1} = f_i^\dagger, \quad T^2 = 1. \tag{5.24}$$

For simplicity, we set $t = \Delta$ in the following. (Δ is taken as a real parameter unless stated otherwise.) The SPT phase in this model is realized when $|\mu|/t < 2$ and protected by the time-reversal.

[6] There is a bijection between the set of pin_ structures on M and $H^1(M;\mathbb{Z}_2)$. For $\mathbb{R}P^2$, $H^1(M;\mathbb{Z}_2) = \mathbb{Z}_2$.

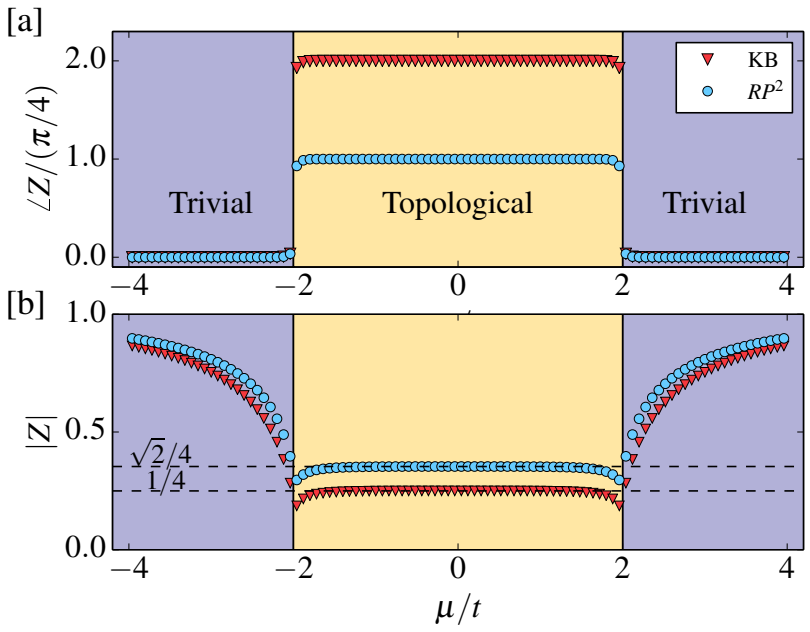

Figure 5.6: [a] Complex phase and [b] amplitude of the $\mathbb{R}P^2$ (5.21) and Klein bottle (5.22) partition functions in class BDI. The generating model is given by Eq. (5.23). The total number of sites is $N = 80$. Each of the I_1, I_2 and I_3 (only Klein bottle) intervals has 20 sites.

Figure 5.6 shows the evaluated complex phase and amplitude of adjacent intervals (5.21) and disjoint intervals (5.22) in the Ramond sector (the r sector). In the non-trivial phase, we observe that the quantization of the complex phase matches with the $e^{i\pi/4}$ and $e^{i\pi/2}$ phases associated with the spacetime manifolds $\mathbb{R}P^2$ and Klein bottle, respectively.

It is also interesting to observe that the amplitude reaches 1 deep in the trivial limit, while it plateaus at values $\sqrt{2}/4$ and $1/4$ in the non-trivial phase. We attribute this to the fact that we choose a normalization convention such that $\mathrm{Tr}(\rho_I) = 1$ where the spacetime manifold is actually not a sphere but a torus. We find that the overall amplitude is multiplied by the factor $d^{-(n-1)}$ in the non-trivial phase where n is the number of cycles of the spacetime manifold and $d = \sqrt{2}$ is the quantum dimension of the Majorana edge modes. Let us check this for various examples: For the partial reflection (for class D in the presence of reflection which is CRT equivalent of BDI), manifold is $\mathbb{R}P^2$ with a handle which gives two independent cycles, hence, the amplitude is $1/\sqrt{2}$ (as expected, see Refs. [190, 196]). For adjacent intervals, there are two handles (one per ρ_I) giving

AZ class	Edge mode	Quant. dim (d)	Adjacent	Disjoint
BDI	Majorana Fermion	$\sqrt{2}$	$\sqrt{2}/4$	$1/4$
DIII	Complex Fermion	2	—	$1/16$
AIII	Complex Fermion	2	$1/8$	$1/16$

Table 5.4: Amplitude of the partition functions on $\mathbb{R}P^2$ and the Klein bottle for various symmetry classes in $(1+1)d$ is given by $d^{-(n-1)}$ where d is the quantum dimension of the edge modes and n is the number of one-cycles of the spacetime manifold. There are 4 and 5 cycles in the manifolds associated with adjacent and disjoint intervals, respectively.

4 cycles overall; thus, the amplitude is $\sqrt{2}/4$. For disjoint intervals there is an additional cycle (associated with the Klein bottle) leading to overall 5 cycles, which implies that the amplitude is $1/4$. The $d^{-(n-1)}$ factor can also be applied to other symmetry classes where d is not necessarily $\sqrt{2}$ and does not depend on the boundary conditions along cycles. For clarity, we summarize all these results in Table. 5.4.

Analytical calculations for the fixed-point wave function

We can also verify analytically the numerical results by using the fixed-point wave function with vanishing correlation length. This state is realized as the ground state of the Hamiltonian (5.23) in the $\mu = 0$ limit,

$$H = -\sum_i \left[f_i^\dagger f_{i+1} + f_i f_{i+1} + \text{H.c.} \right]. \tag{5.25}$$

$\mathbb{Z}_8$ invariant: Partition function on real projective plane Let $I = I_1 \cup I_2$ be two adjacent intervals on closed chain S^1. According to the cut and glue construction [169] of the reduced density matrix, we focus on the 6 real fermions at the boundary of I as in

$$\cdots c_0^R \ \underbrace{c_1^L \cdots\cdots c_1^R}_{I_1} \ \underbrace{c_2^L \cdots\cdots c_2^R}_{I_2} \ c_0^L \cdots \tag{5.26}$$

Introducing the complex fermions inside the intervals as

$$f_i^\dagger = \frac{c_i^R + i c_i^L}{2}, \quad (i = 0, 1, 2), \tag{5.27}$$

we have the gluing Hamiltonian which is essentially identical to (5.25),

$$H = \frac{i}{2}\sum_{i=0}^{2} c_i^R c_{i+1}^L = -\frac{1}{2}\sum_{i=0}^{2}\left[f_i^\dagger f_{i+1} + f_i f_{i+1} + h.c.\right], \tag{5.28}$$

where $c_3^L = c_0^L, f_3 = f_0$. This is the fixed point (which here means zero correlation length) Kitaev chain with the periodic boundary condition. The ground state is given by

$$|\Psi\rangle = \frac{1}{2}\left[(1 + f_1^\dagger f_2^\dagger) f_0^\dagger + (f_1^\dagger + f_2^\dagger)\right]|0\rangle, \tag{5.29}$$

where $|0\rangle$ is the Fock vacuum of f_i fermions. The reduced density matrix for the adjacent intervals I is given by

$$\rho_I = \mathrm{Tr}_0\left(|\Psi\rangle\langle\Psi|\right) = \frac{1}{4}(1 + i c_1^L c_2^R). \tag{5.30}$$

The unitary part $C_T^{I_1}$ of T is given by $C_T^{I_1} = c_1^R$ and the fermionic partial transpose is $\rho_I^{T_1} = \frac{1}{4}(1 - c_1^L c_2^R)$. We hence obtain

$$\mathrm{Tr}_I\left(\rho_I C_T^{I_1} \rho_I^{T_1} [C_T^{I_1}]^\dagger\right) = \frac{1}{2\sqrt{2}} e^{\pi i/4}. \tag{5.31}$$

This $\mathbb{Z}_8$ phase agrees with the pin_ cobordsim group $\Omega_2^{\mathrm{Pin}_-} = \mathbb{Z}_8$.

$\mathbb{Z}_4$ invariant: Partition function on the Klein bottle Let $I = I_1 \cup I_2 \cup I_3$ be three adjacent intervals on closed chain S^1. In a way similar to the previous calculation, we focus on the 8 Majorana

fermions at the boundary of three intervals I_1, I_2 and I_3:

$$\cdots c_0^R \underbrace{c_1^L \cdots\cdots c_1^R}_{I_1} \underbrace{c_2^L \cdots\cdots c_2^R}_{I_2} \underbrace{c_3^L \cdots\cdots c_3^R}_{I_3} c_0^L \cdots \tag{5.32}$$

Introducing the complex fermions inside the intervals as

$$f_i^\dagger = \frac{c_i^R + i c_i^L}{2}, \quad (i = 0, 1, 2, 3), \tag{5.33}$$

and the gluing Hamiltonian as

$$H = \frac{i}{2}\sum_{i=0}^{3} c_i^R c_{i+1}^L = -\frac{1}{2}\sum_{i=0}^{3}\left[f_i^\dagger f_{i+1} + f_i f_{i+1} + h.c.\right], \tag{5.34}$$

where $c_4^L = c_0^L, f_4 = f_0$, the ground state of H is given by

$$|\Psi\rangle = \frac{1}{\sqrt{8}}[(f_1^\dagger + f_3^\dagger) + (1 - f_1^\dagger f_3^\dagger) f_2^\dagger + (1 + f_1^\dagger f_3^\dagger) f_0^\dagger + (f_1^\dagger - f_3^\dagger) f_2^\dagger f_0^\dagger]|0\rangle\,. \tag{5.35}$$

We introduce the reduced density matrix $\rho_{I_1 \cup I_3}\left((-1)^{F_2}\right)$ on the disjoint intervals $I_1 \cup I_3$ with fermion party twist on the I_2 interval by

$$\begin{aligned} \rho_{I_1 \cup I_3}\left((-1)^{F_2}\right) &= \mathrm{Tr}_{0,2}\left((-1)^{f_2^\dagger f_2} |\Psi\rangle \langle\Psi|\right) \\ &= \frac{i}{4} c_1^L c_3^R. \end{aligned} \tag{5.36}$$

We have the partition function on the Klein bottle from the partial transposition as

$$\mathrm{Tr}_{1,3}\left[\rho_{I_1 \cup I_3}\left((-1)^{F_2}\right) C_T^{I_1} \rho_{I_1 \cup I_3}^{T_1}\left((-1)^{F_2}\right)[C_T^{I_1}]^\dagger\right] = \frac{1}{4} e^{\pi i/2}. \tag{5.37}$$

This is the $\mathbb{Z}_4$ invariant as expected. On the other hand, if we do not associate the fermion parity twist on I_2, the reduced density matrix on $I_1 \cup I_3$ is unentangled one:

$$\rho_{I_1 \cup I_3} = \mathrm{Tr}_{0,2}\big(|\Psi\rangle \langle\Psi| \big) = \frac{1}{4}, \tag{5.38}$$

which leads to a trivial topological $U(1)$ phase of the Klein bottle partition function

$$\mathrm{Tr}_{1,3}\Big(\rho_{I_1 \cup I_3} C_T^{I_1} \rho_{I_1 \cup I_3}^{T_1} [C_T^{I_1}]^\dagger \Big) = \frac{1}{4}. \tag{5.39}$$

This is consistent with the full reflection [196] in class D with reflection symmetry which is the CRT dual of class BDI.

5.3.2 Class DIII

The pin_+ cobordism group in two-dimensional spacetime is given by $\Omega_2^{\mathrm{Pin}_+} = \mathbb{Z}_2$, which is generated by the Klein bottle with periodic boundary condition in the S^1 direction. [123, 196]. The many body $\mathbb{Z}_2$ invariant is constructed in a similar way to Sec. 5.3.1: the topological invariant can be constructed by considering the disjoint intervals (5.19) in the r sector,

$$Z = \mathrm{Tr}_{1,3}\Big[\rho_{I_1 \cup I_3}\big((-1)^{F_2}\big) C_T^{I_1} \rho_{I_1 \cup I_3}^{T_1}\big((-1)^{F_2}\big) [C_T^{I_1}]^\dagger \Big] \tag{5.40}$$

for a given pure state $|\Psi\rangle$.

Numerical calculations

A generating model of non-trivial SPT phases in this symmetry class is given by two copies of the Kitaev Majorana chain Hamiltonian

$$H = -\mu \sum_{i\sigma} f_{i\sigma}^\dagger f_{i\sigma} - t \sum_{i\sigma} \Big[f_{i+1\sigma}^\dagger f_{i\sigma} + \mathrm{H.c.} \Big] + i\Delta \sum_i \Big[f_{i+1\uparrow}^\dagger f_{i\uparrow}^\dagger - f_{i+1\downarrow}^\dagger f_{i\downarrow}^\dagger + \mathrm{H.c.} \Big] \tag{5.41}$$

which describes a superconducting state of spinful fermions, and the TRS is defined as

$$T f_{i\uparrow}^\dagger T^{-1} = -f_{i\downarrow}^\dagger, \qquad T f_{i\downarrow}^\dagger T^{-1} = f_{i\uparrow}^\dagger, \qquad T^2 = (-1)^F, \tag{5.42}$$

and hence, the unitary matrix $\mathscr{U}_T$ associated with T is

$$\mathscr{U}_T = \begin{pmatrix} 0 & 1 \\ -1 & 0 \end{pmatrix} = i\sigma_y \tag{5.43}$$

in the basis of $(\uparrow, \downarrow)$.

For simplicity, we set $t = \Delta$ in the following. The SPT phase of the above model is realized when $|\mu|/t < 2$ and protected by TRS. Figure 5.7 shows the evaluated complex phase and amplitude of disjoint intervals (5.40) in both r and ns sectors, corresponding to periodic and anti-periodic boundary conditions along the time direction for the intermediate interval. In the non-trivial phase and with periodic boundary condition (r sector), we observe that the π phase matches with the $\mathbb{Z}_2$ classification generated by putting on the Klein bottle spacetime manifold. Regarding the amplitude, it reaches 1 deep in the trivial limit, while it is quantized at 1/16 in the non-trivial phase as explained in Sec. 5.3.1 (see also Table 5.4).

Analytical calculations for the fixed-point wave function

Here, we verify the numerical results in the previous section. Let us consider the fixed-point wave function where the correlation length is zero. This state is realized as the ground state of the Hamiltonian (5.41) in the $\mu = 0$ limit, that is

$$H = -\sum_{i\sigma} \left[f_{i\sigma}^\dagger f_{i+1,\sigma} + \text{H.c.} \right] + i \sum_{i\sigma} \left[f_{i\uparrow}^\dagger f_{i+1\uparrow}^\dagger - f_{i\downarrow}^\dagger f_{i+1\downarrow}^\dagger + \text{H.c.} \right]. \tag{5.44}$$

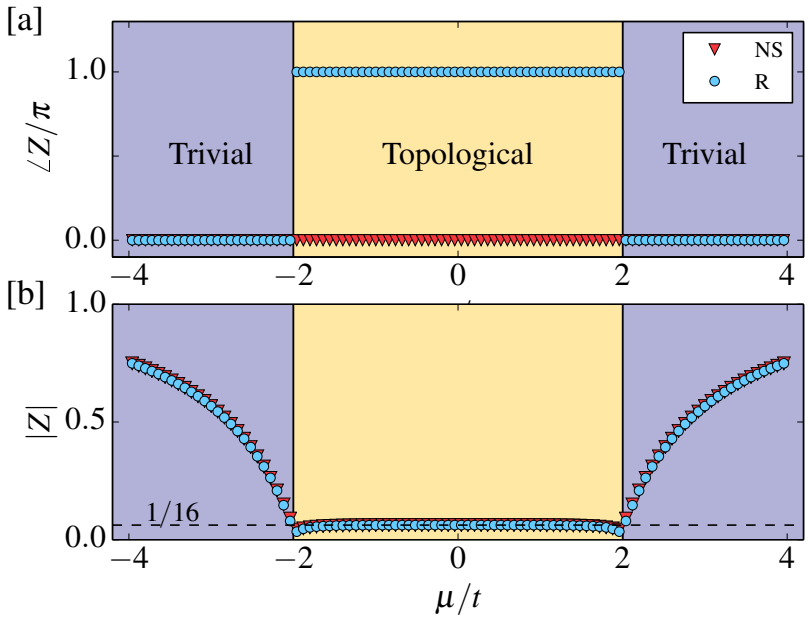

Figure 5.7: [a] Complex phase and [b] amplitude of (5.40) in class DIII. The generating model is given by Eq. (5.41). R and NS refer to periodic and antiperiodic boundary conditions in time direction for the intermediate interval. For each spin, the total number of sites is $N = 80$. Each of the I_1, I_2 and I_3 intervals has 20 sites.

Let $I = I_1 \cup I_2 \cup I_3$ be three adjacent intervals on closed chain S^1. We focus on the 8 Kramers pairs of Majorana fermions at the boundary of three intervals I_1, I_2 and I_3:

$$\cdots c^R_{0,\uparrow} \;\; c^L_{1,\uparrow} \cdots\cdots c^R_{1,\uparrow} \;\; c^L_{2,\uparrow} \cdots\cdots c^R_{2,\uparrow} \;\; c^L_{3,\uparrow} \cdots\cdots c^R_{3,\uparrow} \;\; c^L_{0} \cdots \tag{5.45}$$

$$\cdots c^R_{0,\downarrow} \;\; \underbrace{c^L_{1,\downarrow} \cdots\cdots c^R_{1,\downarrow}}_{I_1} \;\; \underbrace{c^L_{2,\downarrow} \cdots\cdots c^R_{2,\downarrow}}_{I_2} \;\; \underbrace{c^L_{3,\downarrow} \cdots\cdots c^R_{3,\downarrow}}_{I_3} \;\; c^L_{0,\downarrow} \cdots \tag{5.46}$$

We introduce complex fermions inside the intervals as

$$f^\dagger_{i,\sigma} = \frac{c^R_{i,\sigma} + i\, c^L_{i,\sigma}}{2}, \quad (i = 0,1,2,3, \sigma = \uparrow\downarrow). \tag{5.47}$$

The gluing Hamiltonian is

$$H = \frac{i}{2}\sum_{\sigma=\uparrow,\downarrow}\sum_{i=0}^{3} c^R_{i\sigma}c^L_{i+1\sigma} = -\frac{1}{2}\sum_{\sigma=\uparrow,\downarrow}\sum_{i=0}^{3}\left[f^\dagger_{i,\sigma}f_{i+1,\sigma} + f_{i,\sigma}f_{i+1,\sigma} + h.c.\right], \tag{5.48}$$

where $c^L_{4,\sigma} = c^L_{0,\sigma}, f_{4,\sigma} = f_{0,\sigma}$. By a unitary gauge transformation $f_{i,\uparrow} \to e^{-i\pi/4}f_{i,\uparrow}$ and $f_{i,\downarrow} \to e^{i\pi/4}f_{i,\downarrow}$, the pairing part of this Hamiltonian can be brought into the form identical to (5.44). The ground state is given by

$$|\Psi\rangle = \frac{1}{8}\prod_{\sigma=\uparrow,\downarrow}\left[(f^\dagger_{1,\sigma}+f^\dagger_{3,\sigma}) + (1-f^\dagger_{1,\sigma}f^\dagger_{3,\sigma})f^\dagger_{2,\sigma} + (1+f^\dagger_{1,\sigma}f^\dagger_{3,\sigma})f^\dagger_{0,\sigma} + (f^\dagger_{1,\sigma}-f^\dagger_{3,\sigma})f^\dagger_{2,\sigma}f^\dagger_{0,\sigma}\right]|0\rangle\,. \tag{5.49}$$

The reduced density matrix $\rho_{I_1\cup I_3}\left((-1)^{F_2}\right)$ on the disjoint intervals $I_1\cup I_3$ with fermion party twist on I_2 is given by

$$\rho_{I_1\cup I_3}\left((-1)^{F_2}\right) = \mathrm{Tr}_{0,2}\left((-1)^{f^\dagger_2 f_2}|\Psi\rangle\langle\Psi|\right) = \frac{1}{16}(ic^L_{1,\uparrow}c^R_{3,\uparrow})(ic^L_{1,\downarrow}c^R_{3,\downarrow}). \tag{5.50}$$

Noticing that the unitary part of TRS on subsystem I_1 is $C^{I_1}_T = e^{\frac{\pi}{4}(c^R_{1\uparrow}c^R_{1\downarrow} - c^L_{1\uparrow}c^L_{1\downarrow})}$, it holds that

$$\mathrm{Tr}_{I_1\cup I_3}\left[\rho_{I_1\cup I_3}\left((-1)^{F_2}\right)C^{I_1}_T\rho^{T_1}_{I_1\cup I_3}\left((-1)^{F_2}\right)[C^{I_1}_T]^\dagger\right] = -\frac{1}{16}. \tag{5.51}$$

This is consistent with the that is the $\mathbb{Z}_2$ invariant of the partition function on Klein bottle.

5.3.3 Class AIII

Insulators in class AIII are invariant under an anti-unitary PHS, which does not flip $U(1)$ charge of complex fermions, $e^{iQ} \to e^{-i(-Q)} = e^{iQ}$, and are defined on a space manifold with a spin^c structure. In Wick-rotated Euclidean spacetime, the corresponding structure is equivalent to pin^c. In $(1+1)d$ spacetime dimensions, the topological classification is given by $\Omega^{\mathrm{Pin}^c}_2 = \mathbb{Z}_4$ and generated by $\mathbb{R}P^2$. The topological invariant is given in terms of the partition function on $\mathbb{R}P^2$, which can be recast in the operator formalism by using partial particle-hole transformation, in

the way similar to the case of partial time-reversal discussed in Sec. 5.2:

$$Z = \mathrm{Tr}\big[\rho_I U_{CT}^{I_1} \rho_I^{T_1} [U_{CT}^{I_1}]^\dagger\big], \tag{5.52}$$

where I consists of two adjacent interval, $I = I_1 \cup I_2$.

The $U(1)$ holonomy along the $\mathbb{Z}_2$ cycle of $\mathbb{R}P^2$ should be properly chosen to yield the correct formula for the many-body $\mathbb{Z}_4$ invariant. In the current case with $(CT)^2 = 1$, the suitable choice is $\pm i$ holonomy and the $\pm i$ phase rotation is already involved in the definition (5.52).

Similar to the previous cases, the partition function (5.52) can also be expressed in the coherent state basis as follows. We start from a reduced density matrix

$$\rho_I = \int \prod_i d\bar{\alpha}_i d\alpha_i d\bar{\beta}_i d\beta_i e^{-\sum_i (\bar{\alpha}_i \alpha_i + \bar{\beta}_i \beta_i)} \rho_I(\{\bar{\alpha}_i\}, \{\beta_i\}) |\{\alpha_i\}\rangle \langle\{\bar{\beta}_i\}|. \tag{5.53}$$

The partial anti-unitary particle-hole transformed reduced density matrix is given by

$$\begin{aligned} U_{CT}^{I_1} \rho_I^{T_1} [U_{CT}^{I_1}]^\dagger = \int \prod_i d\bar{\gamma}_i d\gamma_i d\bar{\delta}_i d\delta_i e^{-\sum_i (\bar{\gamma}_i \gamma_i + \bar{\delta}_i \delta_i)} \rho_I(\{\bar{\gamma}_i\}, \{\delta_i\}) \\ \times C_f^{I_1} |\{-i\bar{\delta}_j [\mathscr{U}_{CT}]_{ji}\}_{i\in I_1}, \{\gamma_i\}_{i\in I_2}\rangle \langle\{-i[\mathscr{U}_{CT}^\dagger]_{ij}\gamma_j\}_{i\in I_1}, \{\bar{\delta}_i\}_{i\in I_2}| [C_f^{I_1}]^\dagger, \end{aligned} \tag{5.54}$$

where $C_f^{I_1} = (f_1^\dagger + f_1)\cdots(f_{N_1}^\dagger + f_{N_1})$ is the partial particle-hole transformation on $I_1 = \{1, \ldots, N_1\}$. (Here we assumed that ρ_I is Grassmann even.) We need to know the matrix element of the particle-hole transformation. It is sufficient to check it for the coherent state $|\alpha\rangle = e^{-\alpha f^\dagger}|0\rangle$ of a one complex fermion. For $C = f^\dagger + f$, it holds that

$$\langle\alpha|C|-\beta\rangle = \mathrm{Tr}\big[|\beta\rangle\langle\alpha|C^\dagger\big] = \alpha - \beta. \tag{5.55}$$

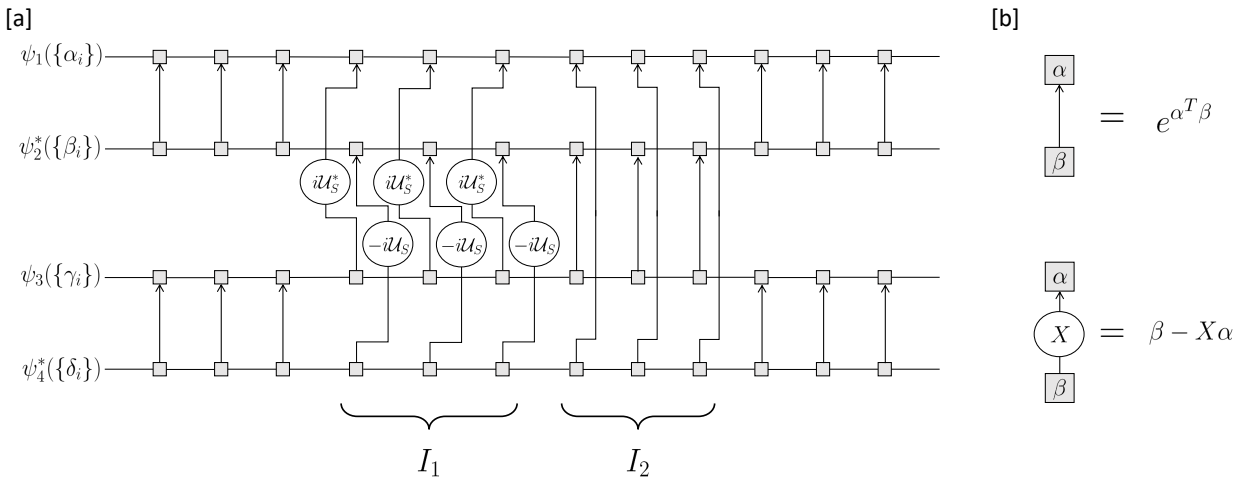

Figure 5.8: [a] Adjacent partial transpose for class AIII chiral symmetry (anti-unitary particle-hole symmetry). [b] Connecting matrices.

This is the delta function of the Grassmann variables. It is natural in the view point of the pin^c structure. If we associate the additional $U(1)$ phase twist, we have

$$\langle\alpha|e^{i\theta f^\dagger f}C|-\beta\rangle = e^{i\theta}\alpha - \beta, \tag{5.56}$$

which is nothing but the coordinate transformation of pin^c structure with $U(1)$ twist. From a straightforward calculation, we obtain the coherent state formula

$$\begin{aligned}
&\mathrm{Tr}\big[\rho_I U_{CT}^{I_1}\rho_I^{\mathsf{T}_1}[U_{CT}^{I_1}]^\dagger\big] \\
&= \int \prod_{i\in I_1\cup I_2}[d\alpha_i d\beta_i d\gamma_i d\delta_i]\prod_{i\in I_1}\big[(\delta_i + [i\mathscr{U}_{CT}]_{ij}\beta_j)(\gamma_i - \alpha_j[i\mathscr{U}_{CT}^\dagger]_{ji})\big]e^{\sum_{i\in I_2}(\alpha_i\delta_i+\beta_i\gamma_i)} \\
&\quad\times\rho_I(\{\alpha_i\};\{\beta_i\})\rho_I(\{\gamma_i\};\{\delta_i\}).
\end{aligned} \tag{5.57}$$

See Fig. 5.8 for a network representation.

Numerical calculations

A canonical model of non-trivial SPT phases in this symmetry class is given by the SSH model,

$$H = -\sum_j [t_2 f_{j+1}^\dagger g_j + t_1 f_j^\dagger g_j + \text{H.c.}], \tag{5.58}$$

where there are two fermion species living on each site f_j and g_j. The anti-unitary PHS S is defined by

$$S f_i^\dagger S^{-1} = f_i, \quad S g_i^\dagger S^{-1} = -g_i, \quad S i S^{-1} = -i. \tag{5.59}$$

This model realizes two topologically distinct phases: Topologically non-trivial phase for $t_2 > t_1$, where the open chain has localized fermion zero-modes at the boundaries, and trivial phase for $t_2 < t_1$ with no boundary mode.

In Fig. 5.9, the complex phase and amplitude of adjacent intervals (5.57) are shown (the blue circles denoted by S), in the non-trivial phase we observe that the $e^{i\pi/2}$ phase which matches the $\mathbb{Z}_4$ classification generated by putting on the $\mathbb{R}P^2$ spacetime manifold. Moreover, the amplitude asymptotes to 1 in the trivial limit, while it is 1/8 in the non-trivial phase consistent with the previous discussion in Sec. 5.3.1 (see also Table 5.4). We also show a reference curve denoted by T, where we do not include the particle-hole transformation (Eq. (5.54) without $C_f^{I_1}$), where the amplitude remains identical to that of S curve while there is no complex phase. This means that we must consider the original symmetry transformation, as defined for the symmetry class, within our partial transformation scheme in order to obtain the complex phase associated with the topological classification.

Analytical calculations for the fixed-point wave function

Here, we show that consistent results can be obtained for the fixed-point wave function and confirm the numerical results in the previous section. This zero-correlation length wave function is

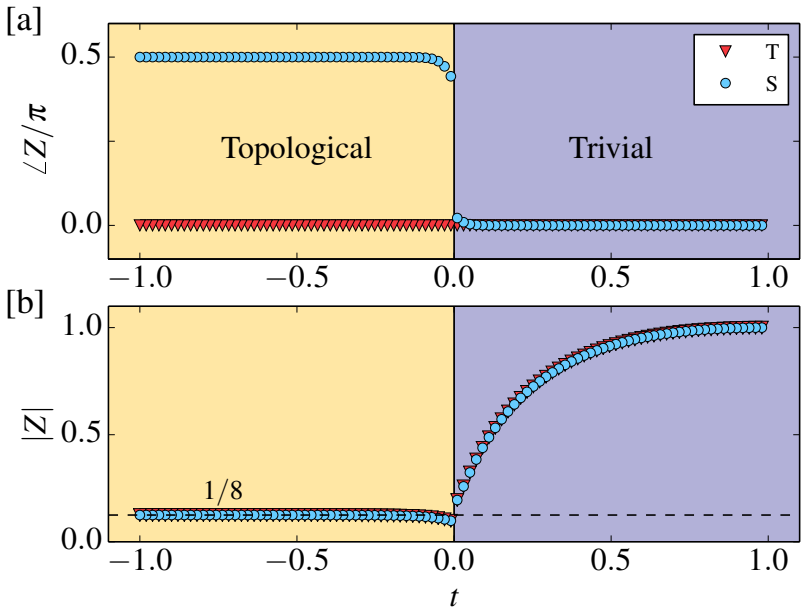

Figure 5.9: [a] Complex phase and [b] amplitude of (5.52) in class AIII, denoted by S. For reference, we also include the partial transformation with no particle-hole transformation (without the C operator in (5.54)), denoted by T. As a model Hamiltonian we use (5.58) with the parameterization $t_2 = (1-t)/2$ and $t_1 = (1+t)/2$. The total number of sites is $N = 80$. Here, I_1, I_2 and I_3 each has 20 sites.

the ground state of the Hamiltonian (5.58) when $t_1 = 0$, which is

$$H = -\sum_{i=1}^{N} g_i^\dagger f_{i+1} + \text{H.c.}. \tag{5.60}$$

It is easy to show that the ground state with N-particle sector is fully occupied state of the "bond" fermions $(g_i^\dagger + f_{i+1}^\dagger)/\sqrt{2}$,

$$|\Psi\rangle = \frac{1}{(\sqrt{2})^N}(g_1^\dagger + f_2^\dagger)(g_2^\dagger + f_3^\dagger)\cdots(g_N^\dagger + f_1^\dagger)|0\rangle\,. \tag{5.61}$$

Let $I = I_1 \cup I_2$ be adjacent intervals on closed chain S^1. According to the cut and glue construction for the reduced density matrix, we focus on the 6 complex fermions at the boundaries of intervals

$$\cdots g_0 \ \underbrace{f_1 \cdots\cdots g_1}_{I_1} \ \underbrace{f_2 \cdots\cdots g_2}_{I_2} \ f_0 \cdots \tag{5.62}$$

The gluing Hamiltonian is

$$H = -(g_0^\dagger f_1 + g_1^\dagger f_2 + g_2^\dagger f_0) + h.c., \tag{5.63}$$

and its ground state is given by

$$|\Psi\rangle = 2^{-3/2}(g_0^\dagger + f_1^\dagger)(g_1^\dagger + f_2^\dagger)(g_2^\dagger + f_0^\dagger)\,|0\rangle\,. \tag{5.64}$$

The reduced density matrix is given by

$$\begin{aligned}
\rho_I &= \mathrm{Tr}_0\,|\Psi\rangle\langle\Psi| \\
&= 2^{-3}\Big[\,|1000\rangle\langle 1000| + |0001\rangle\langle 0001| + |1000\rangle\langle 0001| + |0001\rangle\langle 1000| \\
&\quad + |1100\rangle\langle 1100| + |0101\rangle\langle 0101| - |1100\rangle\langle 0101| - |0101\rangle\langle 1100| \\
&\quad + |1010\rangle\langle 1010| + |0011\rangle\langle 0011| - |1010\rangle\langle 0011| - |0011\rangle\langle 1010| \\
&\quad + |1110\rangle\langle 1110| + |0111\rangle\langle 0111| + |1110\rangle\langle 0111| + |0111\rangle\langle 1110|\,\Big].
\end{aligned} \tag{5.65}$$

Here we defined occupied states in the following order

$$|n_1 n_2 n_3 n_4\rangle := (g_1^\dagger)^{n_1}(f_1^\dagger)^{n_2}(g_2^\dagger)^{n_3}(f_2^\dagger)^{n_4}\,|0\rangle\,. \tag{5.66}$$

The unitary part $U_{CT}^{I_1}$ of the anti-unitary PHS is given by the π phase rotation on the g_1 fermion. From the definition, we obtain

$$\begin{aligned} U_{CT}^{I_1}\rho_I^{T_1}[U_{CT}^{I_1}]^\dagger = 2^{-3}\Big[& |0100\rangle\langle 0100| + |1101\rangle\langle 1101| + i\,|1100\rangle\langle 0101| + i\,|0101\rangle\langle 1100| \\ & + |0000\rangle\langle 0000| + |1001\rangle\langle 1001| - i\,|1000\rangle\langle 0001| - i\,|0001\rangle\langle 1000| \\ & + |0110\rangle\langle 0110| + |1111\rangle\langle 1111| - i\,|1110\rangle\langle 0111| - i\,|0111\rangle\langle 1110| \\ & + |0010\rangle\langle 0010| + |1011\rangle\langle 1011| + i\,|1010\rangle\langle 0011| + i\,|0011\rangle\langle 1010| \Big]. \end{aligned} \tag{5.67}$$

Hence, the non-local order parameter can be computed as

$$\mathrm{Tr}_I\big[\rho_I U_{CT}^{I_1}\rho_I^{T_1}[U_{CT}^{I_1}]^\dagger\big] = -\frac{i}{8}. \tag{5.68}$$

This is precisely the $\mathbb{Z}_4$ invariant.

5.3.4 Class AII

Let us consider one-dimensional systems of complex fermions with spin, where TRS acts on fermion operators as

$$T f_j^\dagger T^{-1} = f_k^\dagger [\mathscr{U}_T]_{kj}, \quad \mathscr{U}_T^{tr} = -\mathscr{U}_T. \tag{5.69}$$

The time-reversal T squares to the fermion number parity. The Wick rotated version of this TRS can be used to introduce a $\mathrm{pin}_+^{\tilde{c}}$ structure in Euclidean quantum field theory. The relevant cobordism group in 2d spacetime is given by $\Omega_2^{\mathrm{Pin}_+^{\tilde{c}}} = \mathbb{Z}$ [80], which is generated by the real projective plane $\mathbb{R}P^2$ with the half monopole flux, $\int_{\mathbb{R}P^2} F/2\pi = 1/2$. The cobordism invariant topological action is given by a theta term

$$Z(X,A) = \exp\left[i\theta \int_X \frac{F}{2\pi} \right], \tag{5.70}$$

where the periodicity of θ is 4π. Because ground states are parametrized by unquantized theta angles, $\Omega_2^{\mathrm{Pin}_+^{\tilde{c}}} = \mathbb{Z}$ does not represent an SPT phase. Nevertheless, from the example treated in this section we will learn how to realize the non-trivial topological sector of $\mathrm{pin}_+^{\tilde{c}}$ connections in the operator formalism.

To have a better understanding of the importance of the non-orientable generating manifold $\mathbb{R}P^2$ and the half monopole flux, it is instructive to recall that the topological response action of one-dimensional TIs is given by the theta term $Z(X,A) = e^{\frac{i\theta}{2\pi}\int_X dA} = e^{i\theta n}$, where X is a closed oriented $(1+1)d$ spacetime manifold, A is the $U(1)$ background gauge field, and $n = \frac{1}{2\pi}\int_X dA$ is the total magnetic flux which is integer-valued $n \in \mathbb{Z}$. It is important to note that this action is invariant under $\theta \to \theta + 2\pi$ and hence the polarization angle θ is defined modulo 2π. When we consider the symmetry class AII which consists of two spin species, the theta angle doubles $\theta = \theta_\uparrow + \theta_\downarrow$. Therefore, the theta must be 4π periodic. However, the 4π periodicity cannot be resolved from measuring the total polarization angle when the system is put an on oriented manifold. The resolution to this is to put the system on $\mathbb{R}P^2$ which admits a half monopole due to the Dirac quantization condition. This means that the partition function of class AII on $\mathbb{R}P^2$ is given by

$$Z(\mathbb{R}P^2, A) = e^{\frac{i\theta}{2\pi}\int_{\mathbb{R}P^2} dA} = e^{i\theta(n+\frac{1}{2})}, \tag{5.71}$$

where the total magnetic flux $\frac{1}{2\pi}\int_{\mathbb{R}P^2} dA \in \mathbb{Z} + 1/2$ is half-integer. From this, one can readily observe that the polarization angle θ is indeed 4π periodic.

Our aim in this section is to construct a many-body invariant (the partition function on $\mathbb{R}P^2$ in the presence of half monopole) to detect this $\theta \in \mathbb{R}/4\pi\mathbb{Z}$ from a given ground state wave function with T symmetry.

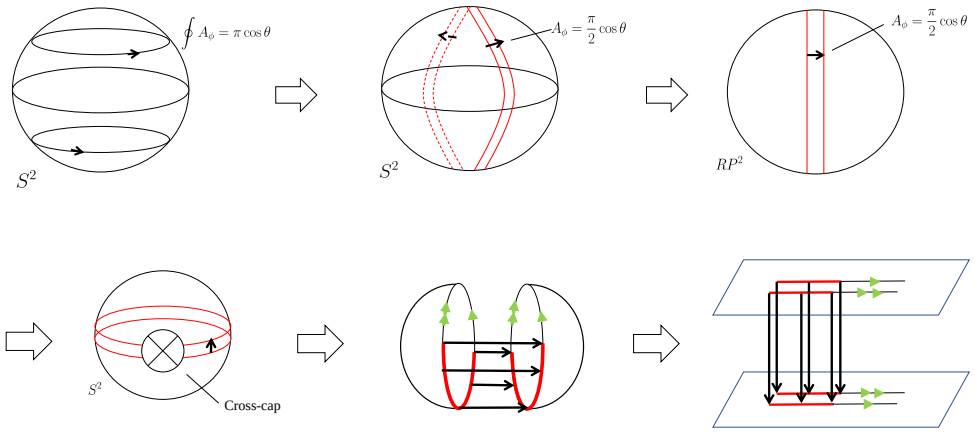

Figure 5.10: Steps to transform a spherical spacetime to the real-projective plane ($\mathbb{R}P^2$) in the presence of a monopole flux.

Two adjacent intervals with the Lieb-Schultz-Mattis twist operator

Our first task is to construct a "tensor-network" description of the the generating manifold ($\mathbb{R}P^2$ with the half monopole flux). Since the projective plane $\mathbb{R}P^2$ can be created from S^2 by applying the antipodal projection, we start from S^2. In the Schwinger gauge, the $\text{pin}_+^{\tilde{c}}$ connection with unit monopole flux on S^2 is given by

$$A_\theta(\theta,\phi) = 0, \quad A_\phi(\theta,\phi) = \frac{1}{2}\cos\theta, \tag{5.72}$$

where we use the spherical coordinate (θ,ϕ) on S^2. Along the circle with the latitude θ, the holonomy is given by $\oint A_\phi d\phi = \pi\cos\theta$. We can deform A such that the contributions to the holonomy "localize" near $\phi = 0$ and $\phi = \pi$ (as shown in the first line of Fig. 5.10), and then take the quotient by the antipodal map $(\theta,\phi) \mapsto (\pi-\theta,\phi+\pi)$. This construction gives $\mathbb{R}P^2$ with the flux line $A_\phi = \frac{\pi}{2}\cos\theta\,\delta(\phi)$, which gives rise to the half monopole charge. The next step is to deform this configuration. Consider a sequence of deformations (with a little care) as shown in the second line of Fig. 5.10. Here, the green arrows are identified with each other. The final configuration can be readily interpreted in the canonical formalism. Hence, we obtain the

following expression in the canonical formalism for the path integral on the generating manifold,

$$Z_{\mathrm{Pin}_+^{\tilde{c}}}\Big(\mathbb{R}P^2, \int_{\mathbb{R}P^2} \frac{F}{2\pi} = \frac{1}{2}\Big) \sim \mathrm{Tr}\Big[\rho_I \prod_{x\in I_1} e^{\frac{\pi i x}{2|I_1|} f_x^\dagger f_x}\, C_T^{I_1} \rho_I^{T_1} [C_T^{I_1}]^\dagger \prod_{x\in I_1} e^{\frac{-\pi i x}{2|I_1|} f_x^\dagger f_x}\Big]. \tag{5.73}$$

Here, $\rho_I = \mathrm{Tr}_{S_x^1 \setminus I_1 \cup I_2}\big(|\psi\rangle\langle\psi|\big)$ is the reduced density matrix of the two adjacent intervals $I_1 \cup I_2$ obtained from a pure state (ground state), $C_T^{I_1} \rho_I^{T_1} [C_T^{I_1}]^\dagger$ is obtained from ρ_I by the partial time-reversal transformation on I_1 associated with T, and finally, the operator $\prod_{x\in I_1} e^{\frac{\pi i x}{2|I_1|} f_x^\dagger f_x}$ is a quarter of the Lieb-Schultz-Mattis twist operator of $U(1)$ charge [137] ($|I_1|$ is the length of the interval I_1).

Numerical calculations

We now explicitly compute the partition function on $\mathbb{R}P^2$ in the presence of half monopole for a microscopic model, following the recipe described in the previous part. Let us consider a pair of SSH chain (5.58) (with arbitrary polarization angle parametrized by ϕ) as the canonical Hamiltonian of the symmetry class AII

$$H = -\frac{t_2}{2} \sum_{j,\sigma} \Big[\psi_{j+1\sigma}^\dagger (\tau_x + i\tau_y)\psi_{j\sigma} + \mathrm{H.c.}\Big] - t_1 \sum_{j,\sigma} \psi_{j\sigma}^\dagger (1 + \cos\phi + i\tau_y \sin\phi)\tau_x \psi_{j\sigma}\,, \tag{5.74}$$

where $\sigma = \uparrow, \downarrow$ are spin labels and we define a two-component fermion operator $\psi_{j,\sigma}^\dagger = (f_j^\dagger, g_j^\dagger)_\sigma$ for each spin species in terms of the notation introduced in (5.58) and τ_i are Pauli matrices in this sublattice basis.

Figure 5.11 shows how the total theta $\theta = \theta_\uparrow + \theta_\downarrow$ varies as a we change ϕ. Here, we compute the complex phase associated with the quantity introduced in (5.73). This way, we effectively obtain $\theta/2$ since we have placed a half monopole inside $\mathbb{R}P^2$ which corresponds to $n = 0$ in (5.71). From the above discussion, we expect $\theta/2$ to be 2π periodic which implies θ to be 4π periodic. This is clearly the case in Fig. 5.11. As a reference, we also show the value of θ using

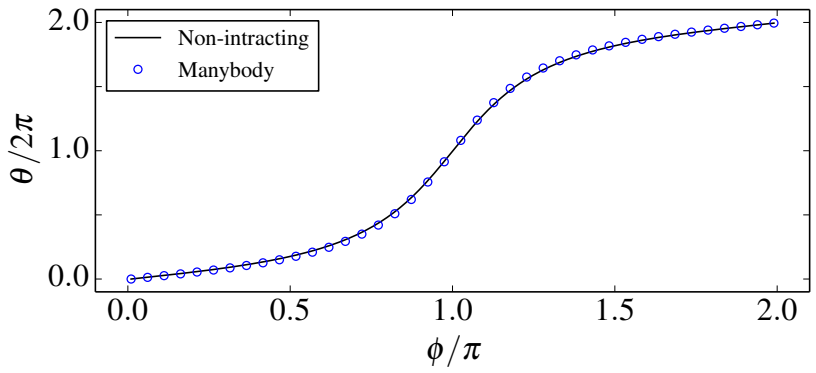

Figure 5.11: The polarization angle as a function of the parameter ϕ in the model Hamiltonian (5.74) for class AII in one dimension. The many-body calculation refers to (5.73) which is equivalent to the partition function on $\mathbb{R}P^2$ in the presence of half-monopole (Eq. (5.71) with $n = 0$). The non-interacting expression (solid curve) is used as a reference based on the formula (5.75). The system size is $N = 80$ and the intervals I_1 and I_2 each contain 20.

the noninteracting formula in terms of the Berry phase

$$\theta = \frac{1}{2\pi} \int_{\mathrm{BZ}} dk \ \mathrm{Tr}\left[a_j\right], \tag{5.75}$$

where $a_j^{\mu\nu} = i \langle u_{\mu\mathbf{k}} | \partial_j | u_{\nu\mathbf{k}} \rangle$ is the Berry connection defined in terms of the Bloch functions of occupied bands $|u_{\nu\mathbf{k}}\rangle$ and $\partial_j = \partial / \partial k_j$. The agreement between the above non-interacting expression and the complex phase of partition function on $\mathbb{R}P^2$ is evident in Fig. 5.11.

5.4 Two-dimensional systems

Continuing from the previous section, we develop the construction of the non-local order parameters for fermionic short-range entangled states protected by anti-unitary symmetry in two and three spatial dimensions. In Sec. 5.4.1, we construct the $\mathbb{Z}_2$ invariant of $(2+1)d$ class DIII TSCs in a way similar to Sec. 5.3.2. Sec. 5.4.2 is devoted to the many-body $\mathbb{Z}_2$ invariant for class AII insulators, which is a many-body counterpart of the Kane-Mele $\mathbb{Z}_2$ invariant. We close this chapter with examples of many-body topological invariants in three spatial dimensions in Sec. 5.5.

The non-local order parameters and symmetry classes discussed in this section are summarized in Table 5.2.

5.4.1 Class DIII

The relevant structures for symmetry class DIII are pin_+ structures. The cobordism group in $(2+1)d$ is given by $\Omega_3^{\text{Pin}_+} = \mathbb{Z}_2$. The generating manifold is the Klein bottle$\times$ S^1, where S^1 is a spatial direction (will be explained shortly), with the periodic boundary condition for both the cycle of the Klein bottle and the S^1 direction. The many-body $\mathbb{Z}_2$ invariant is constructed in a similar way to Sec. 5.3.1. In order to construct the relevant spacetime manifold to detect the topological invariant, we first note that TRS changes the sign of the pairing terms in the y-direction. Therefore, in analogy to class DIII in $(1+1)d$, we partition the system in this direction. The remaining x-direction is left untouched and this way we realize the Klein bottle $\times S^1$ as the spacetime manifold of the quantity,

$$Z = \text{Tr}_{R_1 \cup R_3}\Big[\rho_{R_1\cup R_3}\big((-1)^{F_2}\big) C_T^{R_1} [\rho_{R_1\cup R_3}\big((-1)^{F_2}\big)]^{\mathsf{T}_1} [C_T^{R_1}]^\dagger\Big], \tag{5.76}$$

where $R_{1,3} = I_{1,3} \times S^1_y$, and the reduced density matrix is found by

$$\rho_{R_1\cup R_3}\big((-1)^{F_2}\big) = \text{Tr}_{\overline{R_1\cup R_3}}\Big[e^{i\pi\sum_{\mathbf{r}\in R_2} n(\mathbf{r})} |GS\rangle\langle GS|\Big], \tag{5.77}$$

and $|GS\rangle$ is the ground state of the Hamiltonian (5.78). A schematic diagram of this partitioning is shown in Fig. 5.12[a].

Numerical calculations

A generating model of non-trivial SPT phases in this symmetry class is given by the following $(p_x + i\,p_y)_\uparrow \times (p_x - i\,p_y)_\downarrow$ Hamiltonian [171]

$$H = -\mu \sum_{i\sigma} f^\dagger_{i\sigma} f_{i\sigma} - \frac{t}{2} \sum_{\langle ij\rangle\sigma} \Big[f^\dagger_{i\sigma} f_{j\sigma} + \text{H.c.} \Big] + \frac{\Delta}{2} \sum_i \Big[f^\dagger_{i\uparrow} f^\dagger_{i+\hat{x}\uparrow} + f^\dagger_{i\downarrow} f^\dagger_{i+\hat{x}\downarrow} + \text{H.c.} \Big] + i\frac{\Delta}{2} \sum_i \Big[f^\dagger_{i\uparrow} f^\dagger_{i+\hat{y}\uparrow} - f^\dagger_{i\downarrow} f^\dagger_{i+\hat{y}\downarrow} + \text{H.c.} \Big], \tag{5.78}$$

which describes a superconducting state of spinful fermions. TRS acts on the fermion operators as

$$T f^\dagger_{i\uparrow} T^{-1} = -f^\dagger_{i\downarrow}, \quad T f^\dagger_{i\downarrow} T^{-1} = f^\dagger_{i\uparrow}, \quad T^2 = (-1)^F, \tag{5.79}$$

and hence, the unitary matrix is $\mathscr{U}_T = i\sigma_y$ in the $(\uparrow,\downarrow)$ basis.

As shown in Fig. 5.12[b], the complex phase of the quantity (5.76) is π in the non-trivial phase which consistently reproduces the $\mathbb{Z}_2$ classification of class DIII in $(2+1)d$. The amplitude in the topological phase shows an area law behavior, $\sim e^{-\alpha L_x}$ where α depends on microscopic details. As usual, the amplitude reaches 1 deep in the trivial phase regardless of the dimensionality.

A simple way to explain the $\mathbb{Z}_2$ phase observed above is by going to momentum space along the compactified direction (which is the x-direction in our model (5.78), also shown in Fig. 5.12[a]). This way, one can view the model Hamiltonian (5.78) as a set of decoupled $(1+1)d$ models in the symmetry class DIII. For each k_x, the Hamiltonian reads

$$H_{k_x} = (-\mu - t\cos k_x) \sum_{y\sigma} f^\dagger_{k_x,y\sigma} f_{k_x,y\sigma} - \frac{t}{2} \sum_{y\sigma} \Big[f^\dagger_{k_x,y\sigma} f_{k_x,y+1\sigma} + \text{H.c.} \Big] + i\Delta \sin k_x \sum_{y\sigma} \Big[f^\dagger_{k_x,y\sigma} f^\dagger_{-k_x,y\sigma} + \text{H.c.} \Big] + i\frac{\Delta}{2} \sum_y \Big[f^\dagger_{k_x,y\uparrow} f^\dagger_{-k_x,y+1\uparrow} - f^\dagger_{k_x,y\downarrow} f^\dagger_{-k_x,y+1\downarrow} + \text{H.c.} \Big] \tag{5.80}$$

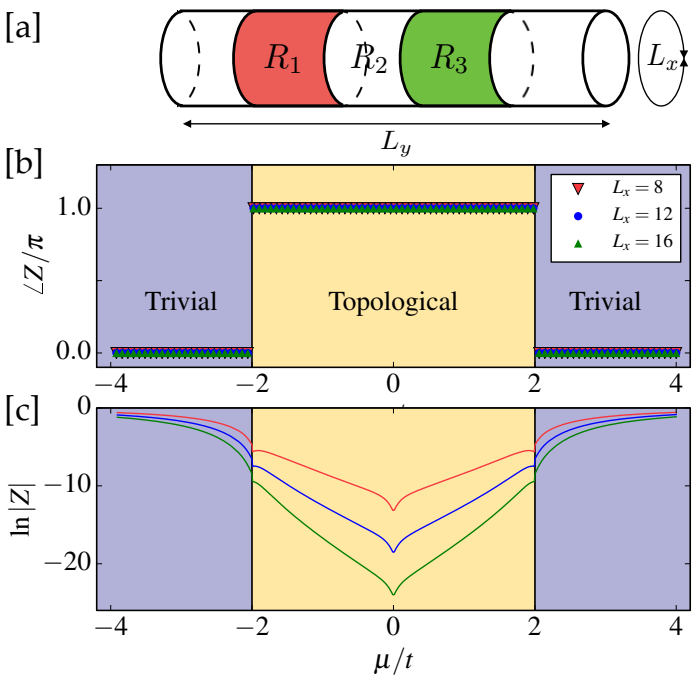

Figure 5.12: [a] Schematic of spatial partitioning for class DIII in $(2+1)d$. [b] Complex phase and [c] amplitude of the many-body invariant (5.76) for the model Hamiltonian (5.78). We set $L_y = 40$, and R_1, R_2 and R_3 each has 10 sites in the y-direction.

where $f_{k_x,y\sigma} = \frac{1}{\sqrt{L_x}} \sum_x f_{x,y\sigma} e^{-ik_x x}$. The overall value of (5.76) is given by the product of all k_x modes each evaluated by (5.40). For $k_x \neq 0, \pi$ the density matrix is a combination of both k_x and $-k_x$ modes and the resulting quantity (5.40) is a complete square; thus, the associated complex phase vanishes. However, at the time-reversal invariant points $k_x = 0, \pi$ the Hamiltonian (5.80) is very similar to (5.41). When $-2t < \mu < 0$, the $k_x = 0$ mode is a $(1+1)d$ class DIII in the topological phase and gives the π phase, while $k_x = \pi$ is in the trivial phase and does not have a complex phase. Hence, the overall phase which is the sum of all corresponding phases for k_x modes becomes π. A similar argument can also be applied to the regime $0 < \mu < 2t$ where the $k_x = \pi$ mode is described by the non-trivial phase of the $(1+1)d$ class DIII and $k_x = 0$ is in the trivial phase.

5.4.2 Class AII

Symmetry class AII is characterized by TRS which squares to -1. It acts on the fermionic creation/annihilation operators as

$$T f_j^\dagger T^{-1} = f_k^\dagger [\mathscr{U}_T]_{kj}, \quad \mathscr{U}_T^{tr} = -\mathscr{U}_T. \tag{5.81}$$

The Wick rotated version of this TRS corresponds to a $\text{pin}_+^{\tilde{c}}$ structure in the Euclidean quantum field theory. The $\text{pin}_+^{\tilde{c}}$ cobordism group in $(2+1)d$ is given by $\Omega_2^{\text{Pin}_+^{\tilde{c}}} = \mathbb{Z}_2$, which implies the existence of $\mathbb{Z}_2$ SPT phases, i.e, the celebrated time-reversal symmetric topological insulators. [115, 147, 175] The generating manifold is the Klein bottle$\times S^1$, where S^1 is a spatial direction (similar to class DIII), with a magnetic flux piercing through the two-dimensional subspace consisting of the cycle of the Klein bottle and S^1.

Many-body $\mathbb{Z}_2$ invariant

The construction of the many-body topological invariant for class AII topological insulators in $(2+1)d$ is analogous to the case of class A+CR (because of CRT (CPT) theorem). In the case of class A+CR, the relevant spacetime manifold is the Klein bottle$\times S_y^1$ where the cycle of the Klein bottle is S_x^1 (see Fig. 5.13[a]). The magnetic flux is inserted in the $S_x^1 \times S_y^1$ subspace. Similarly, for class AII TIs in $(2+1)d$, the relevant generating spacetime is the Klein bottle$\times S_y^1$ where the cycle of the Klein bottle is along the time direction S_t^1 (recall Fig. 5.3[b]). This spacetime manifold can be realized, in the operator formalism, by using the partial transpose on the disjoint intervals (Fig. 5.14[a]). Furthermore, in analogy to the CR-symmetric case, we need to insert a unit magnetic flux through the $S_t^1 \times S_y^1$ sub-manifold, which can be realized by turning on the temporal component of the gauge field $A_t(t,y) = \frac{2\pi y}{L_y}\delta(t-t_0)$. Putting together, we can write the desired many-body topological invariant as the phase of

$$Z = \text{Tr}_{R_1 \cup R_3}\Big[\rho^+_{R_1\cup R_3} C_T^{I_1} [\rho^-_{R_1\cup R_3}]^{\text{T}_1} [C_T^{I_1}]^\dagger\Big], \tag{5.82}$$

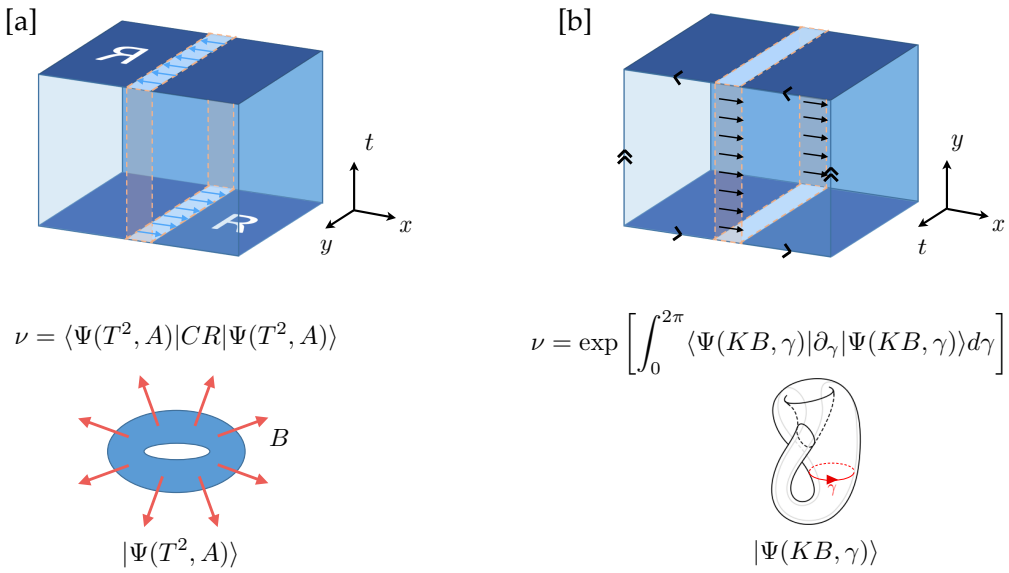

Figure 5.13: Two methods of computing the topological invariant ν of class A+CR in $(2+1)d$. Top panels show the spacetime manifold and the small arrows represent the background gauge field $A=(A_t,A_x,A_y)$. Lower panels show the spatial manifold and the background gauge fields, which are non-flat (unit magnetic flux) and flat (twisted boundary condition) in [a] and [b], respectively. [a] ν is defined as the expectation value of the CR operator where the spatial manifold is torus and the system is subjected to one unit of background magnetic flux $A=(0,2\pi y/L_y,0)$. [b] ν is computed in terms of Berry phase as the twisted boundary condition $\gamma=2\pi t/L_t$, i.e., $A=(0,2\pi t/L_t,0)$, along the cycle of (spatial) Klein bottle is swept from 0 to 2π. The Klein bottle is obtained through twisting by the CR symmetry along the y-direction of the original torus.

where the two-dimensional spatial manifold is partitioned as in (Fig. 5.14[a]) with $R_{1,2,3}=I_{1,2,3}\times S^1_y$ where $I_{1,2,3}$ is an interval in the x-direction, and we introduce the reduced density matrix on $R_1\cup R_3$ with the intermediate magnetic flux on R_2 by

$$\rho^{\pm}_{R_1\cup R_3}=\mathrm{Tr}_{\overline{R_1\cup R_3}}\left[e^{\pm\sum_{\mathbf{r}\in R_2}\frac{2\pi i y}{L_y}n(\mathbf{r})}|GS\rangle\langle GS|\right]. \tag{5.83}$$

Note that the effect of temporal gauge field is incorporated as a phase twist in the above expression. A schematic diagram of the spatial partitioning is shown in Fig. 5.14[a].

The $\mathbb{Z}_2$ many-body topological invariant (5.82) can be tested for a specific microscopic model. A generating model of non-trivial SPT phases in class AII is the celebrated quantum spin Hall effect, which consists of two copies of Chern insulator with Chern numbers $ch_\uparrow=-ch_\downarrow=$

1, [115]

$$H = \frac{1}{2}\sum_{\substack{\mathbf{r}\\ s=1,2}}\Big[\psi^\dagger(\mathbf{r}+\hat{x}_s)(i\Delta\Gamma_s - t\Gamma_3)\psi(\mathbf{r}) + \text{H.c.}\Big] + m\sum_i \psi^\dagger(\mathbf{r})\Gamma_3\psi(\mathbf{r}) \tag{5.84}$$

where $\psi(\mathbf{r}) = (\psi_{a\uparrow}(\mathbf{r}), \psi_{b\uparrow}(\mathbf{r}), \psi_{a\downarrow}(\mathbf{r}), \psi_{b\downarrow}(\mathbf{r}))^T$ is a four-component fermion operator in spin $(\uparrow,\downarrow)$ and orbit (a,b) bases and the hopping amplitudes are given by $\Gamma_s = (\sigma_z\tau_x, \sigma_0\tau_y, \sigma_0\tau_z)$. The σ and τ are Pauli matrices which act on the spin and orbital degrees of freedom respectively and the 0 subscript denotes the identity matrix. TRS is defined by $T = i\sigma_y K$. It is worth noting that the above Hamiltonian commutes with σ_z and hence the overall $SU(2)$ spin rotation symmetry is reduced to $U(1)$ rotation symmetry around the z-axis. The Hamiltonian in the momentum space can be written as $H = \sum_{\mathbf{k}} \psi^\dagger(\mathbf{k})h(\mathbf{k})\psi(\mathbf{k})$, where

$$h(\mathbf{k}) = \sum_{s=1,2}\Big[t\Gamma_s \sin k_s - r\Gamma_3\cos k_s\Big] + m\Gamma_3. \tag{5.85}$$

The $\mathbb{Z}_2$ classification from the complex phase of the quantity (5.82) is obvious in Fig. 5.14[b]. Moreover, the amplitude in the non-trivial phase assumes an area law behavior, $\sim e^{-\alpha L_x}$, where α depends on microscopic details similar to class DIII, and the amplitude approaches 1 deep in the trivial phase.

5.5 Three-dimensional systems

There are SPT phases in $(3+1)d$, which are protected by orientation-reversing symmetry, and the generating manifold of the relevant cobordism group is the $4d$ real projective space, $\mathbb{R}P^4$. For example, $(3+1)d$ TSCs with inversion/reflection symmetry, which are the CPT dual of class DIII time-reversal symmetric TSCs, are classified by the Pin^+ cobordism group, $\Omega_4^{\text{Pin}^+}(pt) = \mathbb{Z}_{16}$. The abelian group $\mathbb{Z}_{16}$ is generated by $\mathbb{R}P^4$ [118, 123]. In this section, we aim at directly computing the many-body topological invariant associated with $\mathbb{R}P^4$.

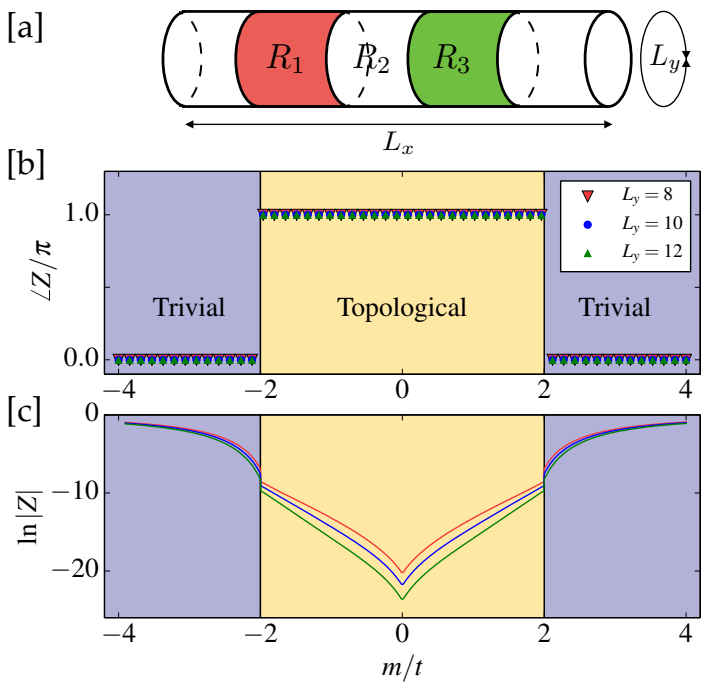

Figure 5.14: [a] Schematic of spatial partitioning for class AII in (2+1)d. [b] Complex phase and [c] amplitude of the many-body topological invariant (5.82) for the model Hamiltonian (5.84). We set $L_y = 32$, and I_1, I_2 and I_3 each has 8 sites in the y-direction.

However, at the time of writing this dissertation, it is not clear to us how to use the partial transpose to construct $\mathbb{R}P^4$. Hence, we describe how to realize $\mathbb{R}P^4$ in a CPT dual theory by using the partial inversion. We should note that $\mathbb{R}P^4$ is not a mapping torus, and hence we need to employ a partial symmetry operation similar to partial reflection (see Fig. 5.2(b)). Topologically, $\mathbb{R}P^4$ is realized by inserting a cross-cap in S^4. The path-integral on $\mathbb{R}P^4$ is expected to be simulated by considering an expectation value of the partial inversion operator I_D defined for a subregion D, which is a three-ball of the total system (Fig. 5.15).

Taking three-dimensional TSCs and TIs as an example, we demonstrate below that the expectation value of the partial inversion correctly reproduces the known topological classification. We evaluate the expectation value of partial inversion both numerically and analytically. For our analytical calculations, we again make use of the cut and glue construction [169]. We assume that the reduced density matrix for the 3-ball D, obtained by taking the partial trace $\mathrm{Tr}_{\bar{D}}$ for the complimentary region $\bar{D} = T^3 \backslash D$ of the pure state $|GS\rangle\langle GS|$, is given approximately by the

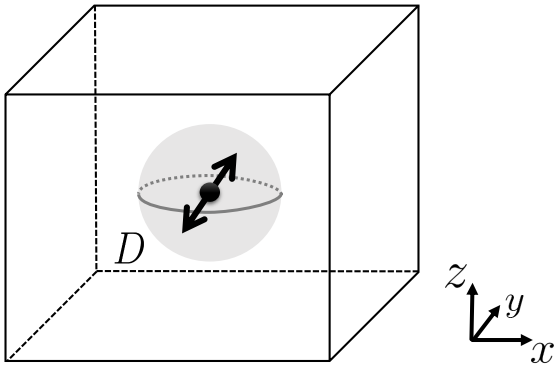

Figure 5.15: Partial inversion on a ground state on 3d space torus T^3. The partial inversion transformation is performed only on inside of the 3-ball D (the shadow region).

canonical thermal density matrix of a gapless theory (CFT) realized on the boundary $S^2 = \partial D$. The fictitious temperature is determined by the correlation length ξ of the bulk. Namely,

$$\rho_D = \mathrm{Tr}_{T^3 \setminus D}\big[\, |GS\rangle \langle GS| \,\big] \sim \frac{e^{-\frac{\xi}{v} H_{S^2}}}{\mathrm{Tr}\big[e^{-\frac{\xi}{v} H_{S^2}}\big]}, \tag{5.86}$$

where v is a velocity of gapless theory on S^2. The gapless theory is defined on the spacetime manifold $S^2(R) \times S^1(\xi/v)$ where R is the radius of the 3-ball D. We assume, for simplicity, that the Hamiltonian H_{S^2} is rotation symmetric, and exclude the possibility of surface topological order [219]. The expectation value of the partial inversion is given in terms of the gapless surface theory as the expectation value of an antipodal map I_{S^2} on S^2:

$$\langle GS|I_D|GS\rangle \sim \frac{\mathrm{Tr}\big[I_{S^2} e^{-\frac{\xi}{v} H_{S^2}}\big]}{\mathrm{Tr}\big[e^{-\frac{\xi}{v} H_{S^2}}\big]}, \qquad I_{S^2} : (\theta, \phi) \mapsto (\pi - \theta, \phi + \pi), \tag{5.87}$$

where (θ, ϕ) is the polar coordinates of S^2. We are interested in the behavior of (5.87) for sufficiently large R, $R \gg \xi$.

In this section, we deal with two examples of free theories: class D superconductors with inversion symmetry and class A insulators with inversion symmetry. It turns out that the surface CFT calculations of partial inversions indeed provide $\mathbb{Z}_{16}$ and $\mathbb{Z}_8$ topological invariants [80, 118,

145, 148, 222, 245]. We also show numerical calculations for lattice models, in which the results are consistent with the calculation of the surface CFTs.

5.5.1 Class DIII

Let us consider $(3+1)d$ TSCs protected by inversion symmetry I with $I^2=(-1)^F$. The topological classification is given by the Pin^+ cobordism group, $\Omega_4^{\mathrm{Pin}^+}(pt)=\mathbb{Z}_{16}$. Notice that the π rotation C_π of the real fermions leads to an additional $\pm i$ phase factor, which implies that the inversion transformation $I=C_\pi R$ with $I^2=(-1)^F$ in 3-space dimensions is equivalent to the reflection transformation with $R^2=1$, that is, the Pin^+ structure. The generating manifold is $\mathbb{R}P^4$. [118, 123, 245] A convenient model Hamiltonian, which describes the ^{3}He-B phase, is given by

$$H=\sum_{\mathbf{k}}\Psi^\dagger(\mathbf{k})\Big[\Big(\frac{k^2}{2m}-\mu\Big)\tau_z+\Delta\tau_x\boldsymbol{\sigma}\cdot\mathbf{k}\Big]\Psi(\mathbf{k}),\quad \Psi(\mathbf{k})=(\psi_\uparrow(\mathbf{k}),\psi_\downarrow(\mathbf{k}),\psi_\downarrow^\dagger(-\mathbf{k}),-\psi_\uparrow^\dagger(-\mathbf{k}))^T. \tag{5.88}$$

The model is invariant under inversion defined by

$$I\psi_\sigma^\dagger(\boldsymbol{x})I^{-1}=i\psi_\sigma^\dagger(-\boldsymbol{x}),\quad (\sigma=\uparrow,\downarrow). \tag{5.89}$$

To compute the expectation value of partial inversion using the cut and glue construction, we first look for the effective surface theory on the boundary of the 3-ball. [111] We consider the Hamiltonian (5.88) on the open 3-ball with radius R. We introduce a polar coordinate $(x,y,z)=(r\sin\theta\cos\phi, r\sin\theta\sin\phi, r\cos\theta)$. Instead of specifying a boundary condition, we consider the following Jackiw-Rebbi type domain wall one-particle Hamiltonian Instead of specifying a boundary condition, we consider the following Jackiw-Rebbi type domain wall

one-particle Hamiltonian

$$\mathscr{H} = -i\Delta\tau_x(\sigma_x\partial_x + \sigma_y\partial_y + \sigma_z\partial_z) + \mu(r)\tau_z. \tag{5.90}$$

with $\mu(r) < 0$ for $r < R$ and $\mu(r) > 0$ for $r > R$. Here, we give a brief description of how the calculation is done and refer the interested reader to Ref. [196] for details.

From a straightforward calculation, we obtain the explicit form of the complex fermion operators $\gamma^\dagger(\theta,\phi)$ creating gapless surface excitations

$$\begin{aligned}
\gamma^\dagger(\theta,\phi) &\sim \Big[-e^{-i\frac{\phi}{2}} \sin\frac{\theta}{2}\{i\psi_\uparrow^\dagger(r,\theta,\phi) + \psi_\downarrow(r,\theta,\phi)\} + e^{i\frac{\phi}{2}} \cos\frac{\theta}{2}\{i\psi_\downarrow^\dagger(r,\theta,\phi) - \psi_\uparrow(r,\theta,\phi)\}\Big] e^{-\int^r \frac{\mu(r')}{\Delta} dr'}, \\
\gamma(\theta,\phi) &\sim \Big[-e^{-i\frac{\phi}{2}} \cos\frac{\theta}{2}\{\psi_\uparrow^\dagger(r,\theta,\phi) + i\psi_\downarrow(r,\theta,\phi)\} - e^{i\frac{\phi}{2}} \sin\frac{\theta}{2}\{\psi_\downarrow^\dagger(r,\theta,\phi) - i\psi_\uparrow(r,\theta,\phi)\}\Big] e^{-\int^r \frac{\mu(r')}{\Delta} dr'}.
\end{aligned} \tag{5.91}$$

Notice that the anti-periodic boundary condition in the ϕ direction, $\gamma^\dagger(\theta,\phi+2\pi) = -\gamma^\dagger(\theta,\phi)$, is satisfied. In terms of these fermion operators, the effective surface BdG Hamiltonian is given by

$$\begin{aligned}
H_{S^2} &= \int \sin\theta d\theta d\phi \big(\gamma^\dagger(\theta,\phi), -\gamma(\theta,\phi)\big) \mathscr{H} \begin{pmatrix} \gamma(\theta,\phi) \\ -\gamma^\dagger(\theta,\phi) \end{pmatrix}, \\
\mathscr{H} &= \frac{\Delta}{R} \begin{pmatrix} 0 & -i\partial_\theta - \frac{1}{\sin\theta}\partial_\phi - \frac{i\cot\theta}{2} \\ -i\partial_\theta + \frac{1}{\sin\theta}\partial_\phi - \frac{i\cot\theta}{2} & 0 \end{pmatrix}.
\end{aligned} \tag{5.92}$$

To compute the partial inversion on the surface theory, we first derive the antipodal transformation I_{S^2} on the Bogoliubov operators. As explained around (5.87), the expectation value of the partial inversion is given by that of the antipodal map within the surface theory and can be evaluated in the same way as in CFTs [40].

The final expression for the partial inversion is given by

$$\langle GS|I_D|GS\rangle = |\langle GS|I_D|GS\rangle| e^{i\theta_{\text{top}}}, \quad \theta_{\text{top}} = -\frac{\pi}{8}, \tag{5.93}$$

$$|\langle GS|I_D|GS\rangle| \sim \exp\Big[\frac{1}{12}\ln(2) - \frac{21}{16}\zeta(3)\Big(\frac{R}{\xi}\Big)^2\Big]. \tag{5.94}$$

The topological $U(1)$ phase $e^{-\frac{\pi i}{8}}$ is indeed consistent with the cobordism classification $\Omega_4^{\text{Pin}^+}(pt) = \mathbb{Z}_{16}$. Also, observe that in addition to the topological $U(1)$ phase, a topological amplitude $e^{\frac{1}{12}\ln(2)}$ appears.

Numerical results for lattice systems

In this part, we provide a direct numerical evidence for the partial inversion of the three-dimensional lattice models. A generating model in class D is given by the BdG Hamiltonian

$$\hat{H} = \frac{1}{2}\sum_{\mathbf{k}} \Psi^\dagger(\mathbf{k}) h(\mathbf{k}) \Psi(\mathbf{k}), \tag{5.95}$$

on a cubic lattice, where

$$h(\mathbf{k}) = \Big[-t(\cos k_x + \cos k_y + \cos k_z) - \mu\Big]\tau_z + \Delta\Big[\sin k_x \tau_x \sigma_x + \sin k_y \tau_x \sigma_y + \sin k_z \tau_x \sigma_z\Big].$$

in which the τ and σ matrices act on particle-hole and spin subspaces, respectively. As mentioned earlier, the above Hamiltonian also describes the ^{3}He-B phase. The inversion symmetry in this model is defined as in Eq. (5.89). This model exhibits three different topological phases depending on the chemical μ potential as follows:

1. $|\mu| < t$: Top. II. This phase supports an even number of 2d gapless Majorana surface states. It is topologically equivalent to a stack of 2d TSCs in the same symmetry class.

2. $t < |\mu| < 3t$: Top. I. This phase hosts a 2d gapless Majorana surface states.

3. $|\mu| > 3t$: Trivial. No topological surface states.

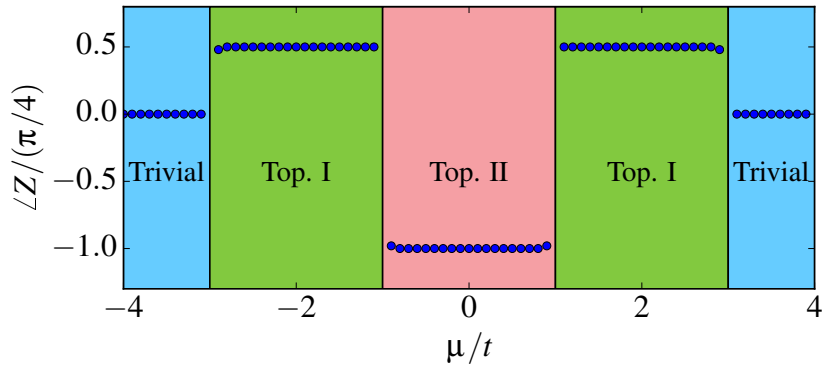

Figure 5.16: Complex phase of the partial inversion $\angle Z = \mathrm{Im}\ln\langle GS|I_D|GS\rangle$ computed for 3d inversion symmetric topological superconductor (class D). Top. I (II) corresponds to the phase with odd (even) number of gapless Majorana surface states. Here, we set $t = \Delta$. The size of total system and subsystem are $N = 12^3$ and $N_{\mathrm{part}} = 6^3$, respectively.

Figure 5.16 shows the calculated complex phases $\angle Z = \mathrm{Im}\ln\langle GS|I_D|GS\rangle$ of the partial inversion for various values of μ. This quantity is computed in a similar fashion to the two-dimensional case that is to calculate the inner product $Z = \langle GS|I_D|GS\rangle$ after rearranging the lattice sites in the subsystem (to get $I_D|GS\rangle$). Remarkably, the partial inversion gives the correct $\mathbb{Z}_{16}$ and $\mathbb{Z}_8$ phases in the topological phases characterized by odd and even number of gapless Majorana surface modes, respectively. We should note that the latter case is topologically equivalent to stacking two dimensional reflection symmetric class D SPT layers which obey a $\mathbb{Z}_8$ classification.

5.5.2 Class AIII

Similar to the previous case, we now consider CPT dual of $(3+1)d$ insulators in class AIII, i.e., TIs protected by inversion symmetry which is The topological classification is given by the Pin^c cobordism [84]

$$\Omega_4^{\mathrm{Pin}^c}(pt) = \mathbb{Z}_8 \times \mathbb{Z}_2. \tag{5.96}$$

The latter direct summand $\mathbb{Z}_2$ arises from bosonic SPT phases corresponding to one of $\mathbb{Z}_2$ of the non-orientable cobordism group $\Omega_4^O(pt) = \mathbb{Z}_2 \times \mathbb{Z}_2$. [224] Our focus here is on the former direct

summand $\mathbb{Z}_8$. This part is generated by $\mathbb{R}P^4$, and the following four-orbital free fermion model

$$H = \sum_{\boldsymbol{k}} \psi^\dagger(\boldsymbol{k}) \mathscr{H}(\boldsymbol{k}) \psi(\boldsymbol{k}), \quad \psi(\boldsymbol{k}) = \{\psi_{\tau,\sigma}\}_{\tau,\sigma=1,2},$$
$$\mathscr{H}(\boldsymbol{k}) = (\frac{k^2}{2m} - \mu)\tau_z + \Delta \tau_x \boldsymbol{k} \cdot \boldsymbol{\sigma}, \quad (m, \mu, \Delta > 0), \tag{5.97}$$

which is equivalent to the two copies of the $(3+1)d$ superconductor (5.88). The inversion symmetry is defined by

$$I \psi^\dagger(\boldsymbol{x}) I^{-1} = \psi^\dagger(-\boldsymbol{x}) \tau_z. \tag{5.98}$$

In addition to the inversion symmetry, there is the $U(1)$ charge conservation symmetry,

$$U_b \psi^\dagger(\boldsymbol{x}) U_b^{-1} = e^{-2\pi i b} \psi^\dagger(\boldsymbol{x}). \tag{5.99}$$

As in the case of $(3+1)d$ TSCs protected by inversion, the expectation value of the partial inversion is a candidate of the $\mathbb{Z}_8$ SPT invariant. The $U(1)$ phase in the expectation value of the partial inversion is simply twice that of the $(3+1)d$ superconductors. On the other hand, in the TI system, there is an additional charge $U(1)$ symmetry, which can be combined with the partial inversion to introduce $I_D U_{b,D}$, where I_D and $U_{b,D}$ is the partial inversion and partial $U(1)$ transformation for the 3-ball D. The expectation value of the combined partial inversion with partial $U(1)$ charge transformation can be written in the form $\langle GS | U_b I | GS \rangle = |\langle GS | U_b I | GS \rangle| e^{i\theta_{\text{top}}}$, where the complex phase and amplitude are found to be

$$\theta_{\text{top}} = \begin{cases} \frac{\pi}{4} & (0 < b < \frac{1}{2}) \\ -\frac{\pi}{4} & (-\frac{1}{2} < b < 0) \end{cases}, \tag{5.100}$$

$$|\langle GS|U_b I|GS\rangle| = \exp\Big[-\Big(3\zeta(3)+\frac{1}{4}\{\mathrm{Li}_3(e^{4\pi i b})+\mathrm{Li}_3(e^{-4\pi i b})\}\Big)\Big(\frac{R}{\xi}\Big)^2-\frac{1}{6}\ln\Big|\frac{\sin(2\pi b)}{2}\Big| + \frac{3+\cos(4\pi b)}{480\sin^2(2\pi b)}\Big(\frac{\xi}{R}\Big)^2+\frac{125+68\cos(4\pi b)-\cos(8\pi b)}{96768\sin^4(2\pi b)}\Big(\frac{\xi}{R}\Big)^4+\cdots\Big], \tag{5.101}$$

for $e^{-2\pi i b}\neq\pm 1$. Notice that the result of the $U(1)$ phase part $e^{i\theta_{\mathrm{top}}}$ is exact, which is independent of the scale ξ/R. The quantized scale-independent $U(1)$ phase (5.100) is somewhat unexpected from the viewpoint of Pin^c structure. In the Pin^c structure on $\mathbb{R}P^4$, the holonomy associated to the $\mathbb{Z}_2$ nontrivial loop threading the cross-cap is quantized to $\pm i$. However, (5.100) means that even if the holonomy is not properly chosen to be $e^{-2\pi i b}=\pm i$, the $U(1)$ phase of the partial inversion is well quantized. This agrees with the numerical calculation (see Fig. 5.18), where the plateau structure of the $U(1)$ phase becomes sharper as one increases the sizes of the subsystem. As b approaches the "phase transition" points $e^{-2\pi i b}=\pm 1$, the higher-order terms proportional to $(\xi/\sin(2\pi b)R)^{2\ell}$ in (5.101) contribute to the amplitude.

Numerical results for lattice systems

In this part, we study the standard Wilson-Dirac Hamiltonian on a cubic lattice as a simple model of the three-dimensional inversion-symmetric TI [168, 237]

$$H=\frac{1}{2}\sum_{\substack{\mathbf{x}\\ s=1,2,3}}\Big[\psi^\dagger_{\mathbf{x}+\mathbf{e}_s}(it\alpha_s-r\beta)\psi_{\mathbf{x}}+h.c.\Big]+m\sum_{\mathbf{x}}\psi^\dagger_{\mathbf{x}}\beta\psi_{\mathbf{x}} \tag{5.102}$$

where the Dirac matrices are given by

$$\alpha_s=\tau_1\otimes\sigma_s=\begin{pmatrix}0 & \sigma_s\\ \sigma_s & 0\end{pmatrix},\quad \beta=\tau_3\otimes 1=\begin{pmatrix}\mathbb{I} & 0\\ 0 & -\mathbb{I}\end{pmatrix}.$$

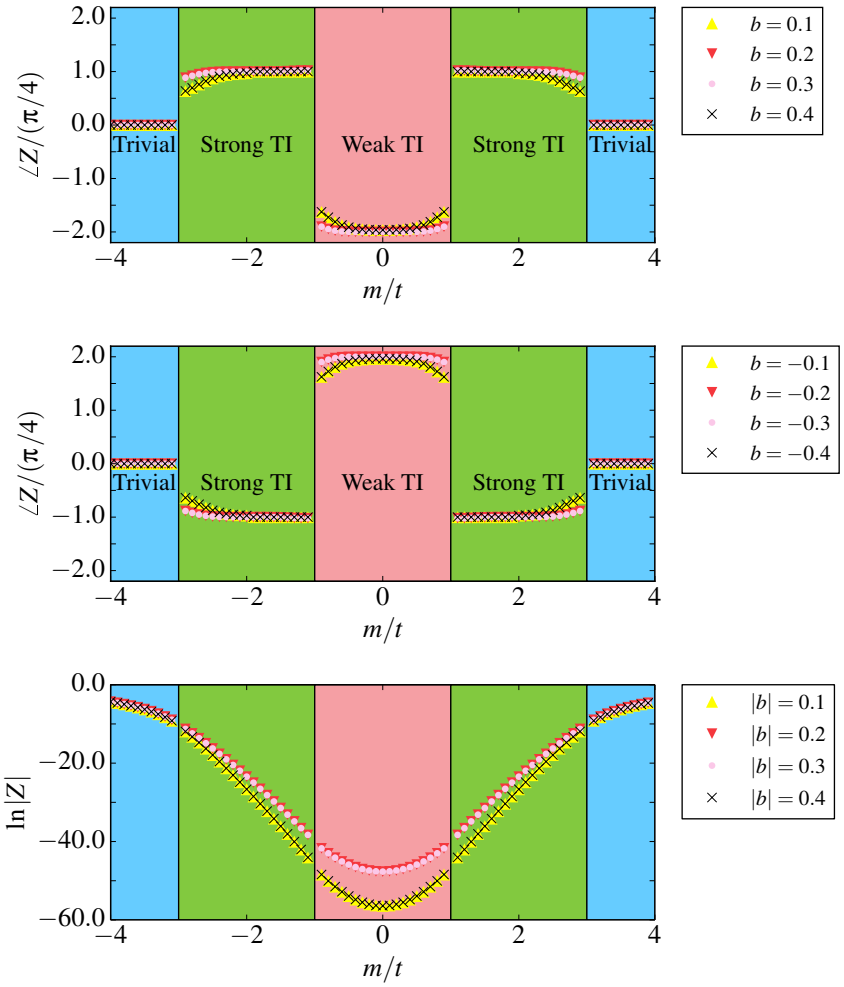

Figure 5.17: The phase ($\angle Z$) and modulus ($|Z|$) of the expectation value of the partial inversion, $Z = \langle GS|I_D|GS\rangle$, computed for the 3d inversion symmetric topological insulator (class A) as a function of the mass parameter m for various values of the $U(1)$ phase transformation b defined in Eq. (5.99). Strong (weak) TI refers to the phase with odd (even) number of Dirac surface states. Here, we set $t = r$. The size of total system and subsystem are $N = 12^3$ and $N_{\text{part}} = 6^3$, respectively.

In this convention the σ and τ matrices act on the spin and orbital degrees of freedom respectively. Transforming to reciprocal space, the Bloch Hamiltonian reads

$$h(\mathbf{k}) = \sum_{s=1,2,3} \Big[t\alpha_s \sin k_s - r\beta \cos k_s \Big] + m\beta.$$

This model can exhibit a non-trivial 3d TI phase protected by the inversion symmetry which is defined by Eq. (5.98). In fact, as the mass parameter m is varied, the Hamiltonian shows the following phases:

1. $|m| < r$: weak TI with an even number of Dirac cones on each boundary surface.

2. $r < |m| < 3r$: strong TI with a single Dirac cone on each boundary surface.

3. $|m| > 3r$: trivial phase equivalent to the atomic limit.

As shown in Fig. 5.17, we compute the complex phase $\angle Z = \mathrm{Im} \ln \langle GS|U_b I|GS\rangle$ of the partial inversion for various values of the $U(1)$ phase $e^{i2\pi b}$ for $t = r$. The calculation procedure is a follows: In order to get $U_b I\,|GS\rangle$ we relocate the lattice points inside the subsystem according to the inversion symmetry operator I and multiply the states by the $U(1)$ phase given by U_b and finally the inner product $Z = \langle GS|\,U_b I\,|GS\rangle$ is computed. In particular, we observe that as b changes from negative values to positive values the complex phase transitions from $-\pi/4$ to $\pi/4$ (see Fig. 5.18). It is worth noting that as the subsystem is made larger, the transition becomes sharper and sharper indicating that this change will turn into a discontinuity in the thermodynamic limit. All these observations conform with our analytical results.

5.6 Summary and future directions

In this chapter, we developed an approach to detect interacting fermionic SPT phases, focusing on those protected by orientation reversing symmetries. To this end, we used the fermionic partial transpose and showed how its combination with the unitary part of the anti-unitary symmetry

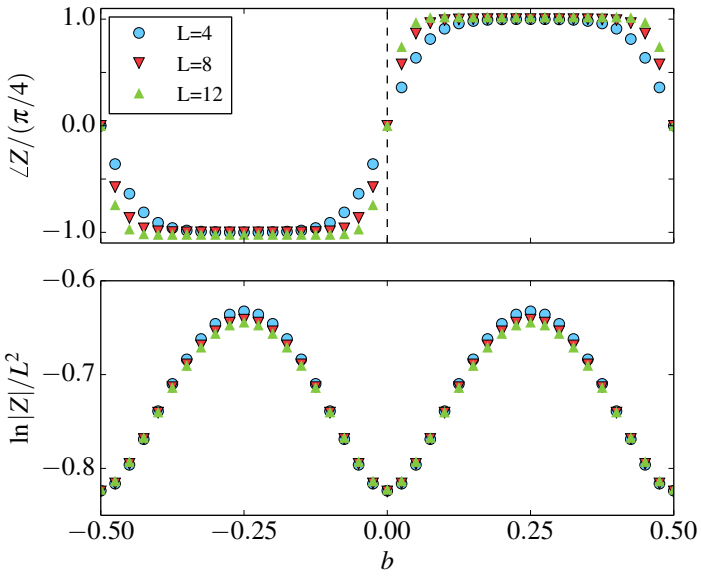

Figure 5.18: The phase ($\angle Z$) and modulus ($|Z|$) of the expectation value of the partial inversion, $Z = \langle GS|I_D|GS\rangle$, computed for the 3d inversion symmetric topological insulator as a function of the $U(1)$ phase twist b defined in Eq. (5.99). Here, we set $t = r$ and $m = 2$. The sizes of the whole system and the subsystem are $N = 16^3$ and $N_{\text{part}} = L^3$, respectively.

can be used to simulate the path-integral on non-orientable spacetime manifold. The only inputs for the many-body topological invariants are the ground state wave function and the symmetry operators in question. In this sense, our many-body topological invariants may be regarded as *order parameters*. We should also note that although partial transpose is a basis dependent operation, the final expression for SPT invariant is basis independent (see Appendix A for more details).

It should be re-empathized that our definition of the fermionic partial transpose (2.13) is different from that of Ref. [69]. The resulting spacetime manifold after taking the fermionic partial transpose is a non-orientable spacetime manifold with a single spin structure — this very characteristic enables us to compute the partition function on the generating manifold corresponding to the many-body topological invariant.

Let us close this chapter by a number of interesting future directions.

• While we use various non-interacting fermionic models to benchmark our many-body invariants, we emphasize that our SPT invariants are applicable to interacting models and can be

used in numerical simulations, such as quantum Monte Carlo or density matrix renormalization group. In addition, throughout this chapter, we consider Bardeen-Cooper-Schrieffer (BCS) mean-field wave functions which do not preserve the particle number. One important question is whether the partial transpose works for particle number conserving systems or not [47, 77, 131, 154, 155]. As a first step in this direction, we examine the partial transpose for projected-BCS wave functions, obtained by projecting the ground state of the mean-field Hamiltonian (5.23) to the space of fixed number of particles. Using variational Monte Carlo, we find that the phase of Z remains quantized as in the mean-field wave function [190]. The other related issue which has still remained open is the explicit proof of quantization of our proposed SPT invariants. There have been some progress in this direction. For example in 1d systems, one can use the matrix product state representation to rigorously prove the quantization [31].

• It would be interesting to apply our formalism to finite-temperature states. However, one needs to be cautious here, as there is a recent claim that SPT phases are unstable at any finite temperature [173]. Historically, Ulmann phases [215] was introduced as a generalization of Berry phases to probe the topology of density matrices [30, 87, 106, 138, 220, 221]. This approach usually involves adiabatic processes in some parameter space, which differs from our approach in terms of non-local order parameters. Our constructions of many-body topological invariants are straightforwardly generalized to a density matrix as well as a pure state, thus, it can be applied to finite temperature canonical ensembles. See also recent studies [14, 15] which discuss the mixed state charge polarization as a finite-temperature topological invariant. Further, the many-body topological invariants for the thermal pure states [200, 201] is worth studying.

• In this chapter, we were mostly concerned with the behaviors of the phase and modulus of the partition functions deep inside gapped SPT phases. It would also be interesting to study their behaviors at or near criticalities which are in proximity to SPT phases. As we cross a critical point between two distinct SPT phases, the modulus becomes zero in the thermodynamic limit, and the $U(1)$ phase jumps at the criticality. More generally, the phase and modulus should depend on (the ratios between) the (sub-)system size, the distance to the critical point, etc., and a natural

question is whether there is a scaling relation similar to usual order parameters. Plus, strictly at a critical point or within a critical phase, the modulus may show an interesting scaling behavior. For instance in $(1+1)d$ systems, the modulus at the criticality admits a logarithmic behavior in the subsystem size, $\log(Z) = -(\dots)\log L + \dots$, as opposed to the *area law* in the in gapped phases $\log(Z) = \text{const}$, similar to the behavior of the entanglement entropy and other entanglement measures. Universal data of criticalities (such as central charge) may be extracted from this scaling. For instance, the scaling of the entanglement negativity at $(1+1)d$ critical points described by conformal field theory shows a similar behavior (see Chapter 4). For a recent study of the partition function (free energy) of $(1+1)d$ lattice systems on a spacetime Klein bottle, see Ref. [208, 210].

• As we discussed in the last section, class DIII superconductors in $(3+1)d$ are classified by $\mathbb{Z}_{16}$ and the generating manifold is the 4-dimensional real projective space ($\mathbb{R}P^4$) [74, 118]. Following the spirit of non-local order parameters discussed in this chapter, the corresponding many-body topological invariant should be constructed only by using the symmetry operator of the problem, i.e., TRS. However, we have not succeeded so far in figuring out the construction of the many-body $\mathbb{Z}_{16}$ invariant in this manner. As we have shown here, the partial transpose combined with the TRS simulates some non-orientable spacetime manifolds, the Klein bottle and real projective plane and its product with other space, where the partial transpose essentially behaves as a reflection in a spacetime manifold. However, it seems rather a challenging problem to find a way to simulate the $\mathbb{R}P^4$ only by using TRS.

• In this dissertation, we did not study class C, CI and CII TIs/TSCs. The relativistic pin structures are $SU(2)$-analogs of spin^c and pin^c structures: Instead of the $U(1)$ charge symmetry, the $SU(2)$ color symmetry is assumed for Majorana fermions, and the Spin(n) 2π spin rotation is identified with the $SU(2)$ 2π color rotation. Class C, CI and CII naturally appear in fermionic systems with $SU(2)$ spin rotation symmetry, for example, superconductors with $SU(2)$ spin rotation symmetry. It would be interesting to explore the many-body topological invariant for class C, CI, and CII.

Chapter 6

Conclusions and Outlook

"The ideal is to reach proofs by comprehension rather than by computation."

— Bernhard Riemann

QUANTUM information theory has stimulated significant developments in the study of quantum many-body systems. Entanglement entropies, as a measure of quantum entanglement in pure states, play a crucial role in many of these advancements such as characterization of gapped and critical states and construction of variational states collectively known as tensor network states. A natural generalization of entanglement entropies is a set of entanglement measures for mixed states. Besides academic interests, mixed states are ubiquitous in condensed matter systems, for example, in an open system interacting with its environment or in tripartite systems. Furthermore, having efficient computational frameworks to measure entanglement between two parts of a many-body system could be crucial for identifying useful resources to implement quantum processes.

The entanglement negativity associated with the spectrum of partially transposed density matrix is known as a good measure of quantum entanglement for mixed states of many-body systems such as spin chains, critical theories, and topological order. Surprisingly, the extension

of the partial transpose (and so the negativity) to fermionic systems remained intractable even at the non-interacting level.

As we showed in this dissertation this could be due to the lack of a consistent definition. We proposed to use the partial time-reversal transformation as an intrinsically fermionic approach to computing the entanglement in mixed states of fermions. One way to see why this is intrinsically fermionic is by noting that the entanglement measure associated with partial time-reversal captures the Majorana dimers as a unit of entanglement whereas regular (bosonic) entanglement measures quantify entanglement in units of Bell pairs. This entanglement measure has opened several avenues for research including concepts in fermionic quantum computing (Chapter 3), the study of Fermi liquids and quantum statistical mechanics (Chapter 4).

Studying fermionic Hilbert spaces has taught us that global symmetries could furnish additional structures to the spectrum of density matrices. An interesting direction is to seek the possibility of extracting new information from these structures. To name a few examples of the Hilbert spaces with super-selection sectors, we may consider gauge theories and anyons, the quasiparticles with fractional statistics realized in 2d topologically ordered phases, which are building blocks of a topological quantum computer.

Moreover, global symmetries may impose constraints on the form of reduced density matrices and modify the separability condition. It is well-known that deciding whether a mixed state is separable is a computationally intractable (NP-hard) problem. The PPT criterion (i.e., zero entanglement negativity) was proposed as an easily computable diagnosis of separable states. However, PPT is only a necessary condition for separability, and there exists a large set of entangled PPT states. In contrast, in fermionic systems with global fermion-number parity symmetry, our results in Chapter 3 suggest that PPT may be a necessary and sufficient condition for separability. Because of these modifications, it is worth studying the relation between PPT criterion and separability in the presence of global symmetries.

As mentioned, quantum entanglement has garnered substantial interest in the condensed matter and high energy physics communities. Here, we introduced a new scheme to compute mixed-

state entanglement. It is yet to be understood what this framework has to offer in the context of holographic theories, thermal states of matter, and non-equilibrium dynamics.

As we have seen in Chapter 5, partial transpose can further be used to define and compute bulk topological invariants for TIs and TSCs protected anti-unitary symmetries. The common theme in all symmetry classes is that our proposed quantities effectively simulate the partition function on suitable non-orientable spacetime manifolds such as the Klein bottle or real-projective plane ($\mathbb{R}P^2$). In principle, this idea could be extended to interacting topological phases with long-range entanglements, such as fractional quantum Hall states or spin liquids in the presence of symmetries the so-called symmetry enriched topological order. Furthermore, our formalism may provide a useful tool to study the recently discovered topological phases in periodically driven systems (Floquet topological phases) and time-crystals.

Throughout this dissertation, we focused on the theoretical aspects of entanglement and topological invariants. Our proposed invariants may be viewed as a *topological* response to external perturbations (in our case non-orientable manifolds). As we saw, such invariant quantities provide a framework to classify topological phases. More importantly, they may be related to the physical response coefficients which can be measured experimentally, or used to distinguish topological phases in numerical simulations. For example, the many-body Chern number appears as the Hall conductance. It is yet to be understood how the partial transpose can be measured experimentally. The generic form $\mathrm{Tr}(\rho\rho^{T_A})$ indicates its similarity to the second REE $\mathrm{Tr}\rho^2$ which was shown to be measurable in a cold atomic setup [1, 57, 94, 112, 121, 149, 161]. On the other hand, there are some recent proposals for measuring the spectrum of ρ^{T_A} in terms of particle-number difference fluctuations between the two subsystems A and B [52, 86].

The realization of topological phases on non-orientable manifolds may seem a bit far reaching from an experimental point of view. However, recent experiments on synthetic materials such as photonic crystals or circuits offer unique opportunities for such exotic realizations. For instance, Ref. [151] reports putting a topological capacitor-inductor network on a Möbius strip. We hope to see further progress in this direction.

Appendix A

Invariance under local unitarites

In this appendix, we show that a generic SPT invariant for a time-reversal symmetric system in the form of $\mathrm{Tr}(\rho U_1 \rho^{T_1} U_1^\dagger)$, where TRS operator is $T = U\mathscr{K}$, is invariant under local basis transformations. The key in this proof is to note that upon a local basis transformation the unitary part of the TRS operator $U = \prod_j U_j$ is also transformed.

We define a basis transformation from an old basis $|\Psi\rangle$ to a new basis $|\Phi\rangle$ by

$$|\Psi\rangle := V|\Phi\rangle \tag{A.1}$$

where V is a unitary transformation $VV^\dagger = V^\dagger V = \mathbb{I}$ and in the case of fermions preserves the fermion-number parity.

The action of an operator O in the old basis is

$$|\Psi_o\rangle = O|\Psi\rangle\,. \tag{A.2}$$

It is easy to find how the operator acts in the new basis,

$$|\Psi_o\rangle = OV|\Phi\rangle \tag{A.3}$$

$$\Rightarrow V|\Phi_o\rangle = OV|\Phi\rangle \tag{A.4}$$

which implies

$$|\Phi_o\rangle = V^\dagger O V |\Phi\rangle . \tag{A.5}$$

and the operator in the new basis $|\Phi\rangle$ act as

$$O \to \tilde{O} = V^\dagger O V. \tag{A.6}$$

For an anti-unitary operator

$$T = U\mathscr{K} \tag{A.7}$$

which has a unitary part U and a complex conjugation $\mathscr{K}$, the action of operator is defined by

$$|\Psi_T\rangle = T |\Psi\rangle . \tag{A.8}$$

Now, in the new basis we have

$$V |\Phi_T\rangle = T V |\Phi\rangle \tag{A.9}$$

$$\Rightarrow V |\Phi_T\rangle = U V^* \mathscr{K} |\Phi\rangle \tag{A.10}$$

which gives the transformation rule for the unitary part of T,

$$U \to \tilde{U} = V^\dagger U V^*. \tag{A.11}$$

With the above relations, let us now check whether or not the SPT order parameter

$$Z = \mathrm{tr}[\rho(U_1 \otimes \mathbb{I}_2)\rho^{T_1}(U_1^\dagger \otimes \mathbb{I}_2)] \tag{A.12}$$

is invariant under the local basis transformation. Recall that ρ is the density matrix of a composite subsystem $A_1 \cup A_2$. Note that the anti-unitary transformation involves $T = U_1 \otimes U_2 \mathscr{K}$. We want to check the invariance of (A.12) under the local many-body basis transformations

$$\rho \to \tilde{\rho} = (V_1^\dagger \otimes V_2^\dagger)\rho(V_1 \otimes V_2). \tag{A.13}$$

From the definition of the partial transpose, we write

$$\tilde{\rho}^{T_1} = [(V_1^\dagger \otimes V_2^\dagger)\rho(V_1 \otimes V_2)]^{T_1} \tag{A.14}$$

$$= (V_1^T \otimes V_2^\dagger)\rho^{T_1}(V_1^* \otimes V_2), \tag{A.15}$$

which holds for any fermion-number parity preserving local unitary transformations [189]. From the previous section, the unitary part of T within subsystem is transformed as

$$U_1 \to \tilde{U}_1 = V_1^\dagger U_1 V_1^*. \tag{A.16}$$

Hence, we may write

$$\tilde{Z} = \mathrm{tr}[\tilde{\rho} \cdot (\tilde{U}_1 \otimes \mathbb{I}_2) \cdot \tilde{\rho}^{T_1} \cdot (\tilde{U}_1^\dagger \otimes \mathbb{I}_2)] \tag{A.17}$$

$$= \mathrm{tr}\left[(V_1^\dagger \otimes V_2^\dagger)\rho(V_1 \otimes V_2) \cdot (V_1^\dagger U_1 V_1^* \otimes \mathbb{I}_2) \cdot (V_1^T \otimes V_2^\dagger)\rho^{T_1}(V_1^* \otimes V_2) \cdot (V_1^T U_1^\dagger V_1 \otimes \mathbb{I}_2)\right] \tag{A.18}$$

$$= \mathrm{tr}\left[(V_1^\dagger \otimes V_2^\dagger)\rho \cdot (V_1 V_1^\dagger U_1 V_1^* V_1^T \otimes V_2 V_2^\dagger) \cdot \rho^{T_1} \cdot (V_1^* V_1^T U_1^\dagger V_1 \otimes V_2)\right] \tag{A.19}$$

$$= \mathrm{tr}\left[(V_1 V_1^\dagger \otimes V_2 V_2^\dagger)\rho \cdot (U_1 \otimes \mathbb{I}_2) \cdot \rho^{T_1} \cdot (U_1^\dagger \otimes \mathbb{I}_2)\right] \tag{A.20}$$

$$= \mathrm{tr}\left[\rho \cdot (U_1 \otimes \mathbb{I}_2) \cdot \rho^{T_1} \cdot (U_1^\dagger \otimes \mathbb{I}_2)\right] = Z \tag{A.21}$$

which shows the invariance of the SPT order parameter.

References

[1] Dmitry A. Abanin and Eugene Demler. Measuring entanglement entropy of a generic many-body system with a quantum switch. *Phys. Rev. Lett.*, 109:020504, Jul 2012.

[2] A. Acín, A. AndriaNov, L. Costa, E. Jané, J. I. Latorre, and R. Tarrach. Generalized schmidt decomposition and classification of three-quantum-bit states. *Phys. Rev. Lett.*, 85:1560–1563, Aug 2000.

[3] A. Acín, D. Bruß, M. Lewenstein, and A. Sanpera. Classification of mixed three-qubit states. *Phys. Rev. Lett.*, 87:040401, Jul 2001.

[4] Vincenzo Alba. Entanglement negativity and conformal field theory: a monte carlo study. *J. Stat. Mech.: Theory Exp.*, 2013(05):P05013, 2013.

[5] Vincenzo Alba, Pasquale Calabrese, and Erik Tonni. Entanglement spectrum degeneracy and the cardy formula in 1+1 dimensional conformal field theories. *J. Phys. A: Math. Theor.*, 51(2):024001, 2018.

[6] Alexander Altland and Martin R Zirnbauer. Nonstandard symmetry classes in mesoscopic normal-superconducting hybrid structures. *Physical Review B*, 55(2):1142, 1997.

[7] Luigi Amico, Rosario Fazio, Andreas Osterloh, and Vlatko Vedral. Entanglement in many-body systems. *Rev. Mod. Phys.*, 80:517–576, May 2008.

[8] Janet Anders. Thermal state entanglement in harmonic lattices. *Phys. Rev. A*, 77:062102, Jun 2008.

[9] Janet Anders and Andreas Winter. Entanglement and separability of quantum harmonic oscillator systems at finite temperature. *Quantum Info. Comput.*, 8:0245–0262, Mar 2008.

[10] Guillaume Aubrun, Stanislaw J. Szarek, and Deping Ye. Entanglement thresholds for random induced states. *Communications on Pure and Applied Mathematics*, 67(1):129–171, 2014.

[11] K. Audenaert, J. Eisert, M. B. Plenio, and R. F. Werner. Entanglement properties of the harmonic chain. *Phys. Rev. A*, 66:042327, Oct 2002.

[12] JoSeph E. Avron and Ruedi Seiler. Quantization of the hall conductance for general, multiparticle schrödinger hamiltonians. *Phys. Rev. Lett.*, 54:259–262, Jan 1985.

[13] Mari-Carmen Bañuls, J. Ignacio Cirac, and Michael M. Wolf. Entanglement in fermionic systems. *Phys. Rev. A*, 76:022311, Aug 2007.

[14] Charles-Edouard Bardyn. A recipe for topological observables of density matrices. *arXiv:1711.09735*, 2017.

[15] Charles-Edouard Bardyn, Lukas Wawer, Alexander Altland, Michael Fleischhauer, and Sebastian Diehl. Probing the topology of density matrices. *Phys. Rev. X*, 8:011035, Feb 2018.

[16] Maissam Barkeshli, Parsa Bonderson, Meng Cheng, and Zhenghan Wang. Symmetry, Defects, and GAuging of Topological Phases. *arXiv:1410.4540*, 2014.

[17] T. Barthel, M.-C. Chung, and U. Schollwöck. Entanglement scaling in critical two-dimensional fermionic and bosonic systems. *Phys. Rev. A*, 74:022329, Aug 2006.

[18] Estelle L. Basor. A localization theorem for toeplitz determinants. *Indiana Math. J.*, 28:975, 1979.

[19] Abolfazl Bayat, Sougato Bose, and Pasquale Sodano. Entanglement routers using macroscopic singlets. *Phys. Rev. Lett.*, 105:187204, Oct 2010.

[20] Abolfazl Bayat, Sougato Bose, Pasquale Sodano, and Henrik Johannesson. Entanglement probe of two-impurity kondo physics in a spin chain. *Phys. Rev. Lett.*, 109:066403, Aug 2012.

[21] Abolfazl Bayat, Pasquale Sodano, and Sougato Bose. Negativity as the entanglement measure to probe the kondo regime in the spin-chain kondo model. *Phys. Rev. B*, 81:064429, Feb 2010.

[22] Y. Ben-Aryeh and A. Mann. Explicit constructions of all separable two-qubits density matrices and related problems for three-qubits systems. *International Journal of Quantum Information*, 13(08):1550061, 2015.

[23] F. Benatti, R. Floreanini, and U. Marzolino. Entanglement in fermion systems and quantum metrology. *Phys. Rev. A*, 89:032326, Mar 2014.

[24] G. Benfatto and G. Gallavotti. Perturbation theory of the fermi surface in a quantum liquid. a general quasiparticle formalism and one-dimensional systems. *Journal of Statistical Physics*, 59(3):541–664, May 1990.

[25] Lakshya Bhardwaj, Davide Gaiotto, and Anton Kapustin. State sum constructions of spin-TFTs and string net constructions of fermionic phases of matter. *arXiv:1605.01640*, 2016.

[26] Olivier Blondeau-Fournier, Olalla A Castro-Alvaredo, and Benjamin Doyon. Universal scaling of the logarithmic negativity in massive quantum field theory. *J. Phys. A: Math. Theor.*, 49(12):125401, 2016.

[27] Jan Borchmann, Aaron Farrell, Shunji Matsuura, and T. Pereg-Barnea. Entanglement spectrum as a probe for the topology of a spin-orbit-coupled superconductor. *Phys. Rev. B*, 90:235150, Dec 2014.

[28] Sergey B. Bravyi and Alexei Yu. Kitaev. Fermionic quantum computation. *Annals of Physics*, 298(1):210 – 226, 2002.

[29] DagMar Bruß. Characterizing entanglement. *Journal of Mathematical Physics*, 43(9):4237–4251, 2002.

[30] Jan Carl Budich and Sebastian Diehl. Topology of density matrices. *Phys. Rev. B*, 91:165140, Apr 2015.

[31] Nick Bultinck, Dominic J. Williamson, Jutho Haegeman, and Frank Verstraete. Fermionic matrix product states and one-dimensional topological phases. *Phys. Rev. B*, 95:075108, Feb 2017.

[32] Pasquale Calabrese and John Cardy. Entanglement entropy and quantum field theory. *J. Stat. Mech.: Theory Exp.*, 2004(06):P06002, 2004.

[33] Pasquale Calabrese and John Cardy. Entanglement entropy and conformal field theory. *J. Phys. A: Math. Theor.*, 42(50):504005, 2009.

[34] Pasquale Calabrese, John Cardy, and Benjamin Doyon. Entanglement entropy in extended quantum systems. *J. Phys. A: Math. Theor.*, 42(50):500301, 2009.

[35] Pasquale Calabrese, John Cardy, and Erik Tonni. Entanglement negativity in quantum field theory. *Phys. Rev. Lett.*, 109:130502, Sep 2012.

[36] Pasquale Calabrese, John Cardy, and Erik Tonni. Entanglement negativity in extended systems: a field theoretical approach. *J. Stat. Mech.: Theory Exp.*, 2013(02):P02008, 2013.

[37] Pasquale Calabrese, John Cardy, and Erik Tonni. Finite temperature entanglement negativity in conformal field theory. *J. Phys. A: Math. Theor.*, 48(1):015006, 2015.

[38] Pasquale Calabrese and Fabian H L Essler. Universal corrections to scaling for block entanglement in spin-1/2 xx chains. *Journal of Statistical Mechanics: Theory and Experiment*, 2010(08):P08029, 2010.

[39] Pasquale Calabrese, Luca Tagliacozzo, and Erik Tonni. Entanglement negativity in the critical ising chain. *J. Stat. Mech.: Theory Exp.*, 2013(05):P05002, 2013.

[40] John L. Cardy. Operator content and modular properties of higher-dimensional conformal field theories. *Nuclear Physics B*, 366(3):403–419, Dec 1991.

[41] H Casini, C D Fosco, and M Huerta. Entanglement and alpha entropies for a massive dirac field in two dimensions. *Journal of Statistical Mechanics: Theory and Experiment*, 2005(07):P07007, 2005.

[42] C. CastelNovo. Negativity and topological order in the toric code. *Phys. Rev. A*, 88:042319, Oct 2013.

[43] Daniel Cavalcanti, Alessandro Ferraro, Artur García-Saez, and Antonio Acín. Distillable entanglement and area laws in spin and harmonic-oscillator systems. *Phys. Rev. A*, 78:012335, Jul 2008.

[44] Po-Yao Chang and Xueda Wen. Entanglement negativity in free-fermion systems: An overlap matrix approach. *Phys. Rev. B*, 93:195140, May 2016.

[45] Xie Chen, Zheng-Cheng Gu, Zheng-Xin Liu, and Xiao-Gang Wen. Symmetry protected topological orders and the group cohomology of their symmetry group. *Physical Review B*, 87(15):155114, Apr 2013.

[46] Xie Chen, Zheng-Cheng Gu, and Xiao-Gang Wen. Classification of gapped symmetric phases in one-dimensional spin systems. *Physical Review B*, 83(3):035107, Jan 2011.

[47] Meng Cheng and Hong-Hao Tu. Majorana edge states in interacting two-chain ladders of fermions. *Phys. Rev. B*, 84:094503, Sep 2011.

[48] Yu-Ju Chiu, Xie Chen, and Isaac L. Chuang. Fermionic measurement-based quantum computation. *Phys. Rev. A*, 87:012305, Jan 2013.

[49] Gil Young Cho, Chang-Tse Hsieh, Takahiro Morimoto, and Shinsei Ryu. Topological phases protected by reflection symmetry and cross-cap states. *Phys. Rev. B*, 91:195142, May 2015.

[50] Gil Young Cho and Joel E. Moore. Topological BF field theory description of topological insulators. *Annals of Physics*, 326(6):1515–1535, Jun 2011.

[51] Chia-Min Chung, Vincenzo Alba, Lars Bonnes, Pochung Chen, and Andreas M. Läuchli. Entanglement negativity via the replica trick: A quantum monte carlo approach. *Phys. Rev. B*, 90:064401, Aug 2014.

[52] Eyal Cornfeld, Moshe Goldstein, and Eran Sela. Imbalance entanglement: Symmetry decomposition of negativity. *Phys. Rev. A*, 98:032302, Sep 2018.

[53] Andrea Coser, Erik Tonni, and Pasquale Calabrese. Entanglement negativity after a global quantum quench. *J. Stat. Mech.: Theory Exp.*, 2014(12):P12017, 2014.

[54] Andrea Coser, Erik Tonni, and Pasquale Calabrese. Partial transpose of two disjoint blocks in xy spin chains. *J. Stat. Mech.: Theory Exp.*, 2015(8):P08005, 2015.

[55] Andrea Coser, Erik Tonni, and Pasquale Calabrese. Spin structures and entanglement of two disjoint intervals in conformal field theories. *J. Stat. Mech.: Theory Exp.*, 2016(5):053109, 2016.

[56] Andrea Coser, Erik Tonni, and Pasquale Calabrese. Towards the entanglement negativity of two disjoint intervals for a one dimensional free fermion. *J. Stat. Mech.: Theory Exp.*, 2016(3):033116, 2016.

[57] A. J. Daley, H. Pichler, J. SchachenMayer, and P. Zoller. Measuring entanglement growth in quench dynamics of bosons in an optical lattice. *Phys. Rev. Lett.*, 109:020505, Jul 2012.

[58] P. Di Francesco, P. Mathieu, and D. Senechal. *Conformal Field Theory*. Springer, New York, USA, 1997.

[59] Robbert Dijkgraaf and Edward Witten. Topological gAuge theories and group cohomology. *Communications in Mathematical Physics*, 129(2):393–429, Apr 1990.

[60] Letian Ding, Noah Bray-Ali, Rong Yu, and Stephan Haas. Subarea law of entanglement in nodal fermionic systems. *Phys. Rev. Lett.*, 100:215701, May 2008.

[61] W. Dür and J. I. Cirac. Classification of multiqubit mixed states: Separability and distillability properties. *Phys. Rev. A*, 61:042314, Mar 2000.

[62] W. Dür, J. I. Cirac, and R. Tarrach. Separability and distillability of multiparticle quantum systems. *Phys. Rev. Lett.*, 83:3562–3565, Oct 1999.

[63] W. Dür, G. Vidal, and J. I. Cirac. Three qubits can be entangled in two inequivalent ways. *Phys. Rev. A*, 62:062314, Nov 2000.

[64] Maxim Dzero, Jing Xia, Victor Galitski, and Piers Coleman. Topological kondo insulators. *Annual Review of Condensed Matter Physics*, 7(1):249–280, 2016.

[65] J. Eisert, M. Cramer, and M. B. Plenio. *Colloquium* : Area laws for the entanglement entropy. *Rev. Mod. Phys.*, 82:277–306, Feb 2010.

[66] Jens Eisert. *Entanglement in Quantum Information Theory*. PhD thesis, University of Potsdam, Germany, 2001.

[67] Jens Eisert and Martin B. Plenio. A comparison of entanglement measures. *Journal of Modern Optics*, 46(1):145–154, 1999.

[68] Viktor Eisler and Zoltán Zimborás. Entanglement negativity in the harmonic chain out of equilibrium. *New Journal of Physics*, 16(12):123020, 2014.

[69] Viktor Eisler and Zoltán Zimborás. On the partial transpose of fermionic Gaussian states. *New Journal of Physics*, 17(5):53048, 2015.

[70] Viktor Eisler and Zoltán Zimborás. Entanglement negativity in two-dimensional free lattice models. *Phys. Rev. B*, 93:115148, Mar 2016.

[71] Christopher Eltschka and Jens Siewert. Entanglement of three-qubit greenberger-horne-zeilinger–symmetric states. *Phys. Rev. Lett.*, 108:020502, Jan 2012.

[72] Andrew M. Essin and Michael Hermele. Classifying fractionalization: Symmetry classification of gapped $\mathbb{Z}_2$ spin liquids in two dimensions. *Phys. Rev. B*, 87:104406, Mar 2013.

[73] Alessandro Ferraro, Daniel Cavalcanti, Artur García-Saez, and Antonio Acín. Thermal bound entanglement in macroscopic systems and area law. *Phys. Rev. Lett.*, 100:080502, Feb 2008.

[74] Lukasz Fidkowski, Xie Chen, and Ashvin Vishwanath. Non-abelian topological order on the surface of a 3d topological superconductor from an exactly solved model. *Phys. Rev. X*, 3:041016, Nov 2013.

[75] Lukasz Fidkowski and Alexei Kitaev. Effects of interactions on the topological classification of free fermion systems. *Phys. Rev. B*, 81:134509, Apr 2010.

[76] Lukasz Fidkowski and Alexei Kitaev. Topological phases of fermions in one dimension. *Phys. Rev. B*, 83:075103, Feb 2011.

[77] Lukasz Fidkowski, Roman M. Lutchyn, Chetan Nayak, and Matthew P. A. Fisher. Majorana zero modes in one-dimensional quantum wires without long-ranged superconducting order. *Phys. Rev. B*, 84:195436, Nov 2011.

[78] Fabio Franchini and Alexander G AbaNov. Asymptotics of toeplitz determinants and the emptiness formation probability for the xy spin chain. *Journal of Physics A: Mathematical and General*, 38(23):5069, 2005.

[79] Daniel S. Freed. Short-range entanglement and invertible field theories. *arXiv:1406.7278*, Jun 2014.

[80] Daniel S. Freed and Michael J. Hopkins. Reflection positivity and invertible topological phases. *arXiv:1604.06527*, 2016.

[81] Daniel S. Freed and Gregory W. Moore. Twisted Equivariant Matter. *Annales Henri Poincaré*, 14(8):1927–2023, Dec 2013.

[82] Liang Fu, C. L. Kane, and E. J. Mele. Topological insulators in three dimensions. *Phys. Rev. Lett.*, 98:106803, Mar 2007.

[83] G. Giedke, B. Kraus, M. Lewenstein, and J. I. Cirac. Entanglement criteria for all bipartite gaussian states. *Phys. Rev. Lett.*, 87:167904, Oct 2001.

[84] P Gilkey. *The Geometry of Spherical Space Form Groups*. World Scientific, 1989.

[85] Dimitri Gioev and Israel Klich. Entanglement entropy of fermions in any dimension and the widom conjecture. *Phys. Rev. Lett.*, 96:100503, Mar 2006.

[86] Johnnie Gray, Leonardo Banchi, Abolfazl Bayat, and Sougato Bose. Machine-learning-assisted many-body entanglement measurement. *Phys. Rev. Lett.*, 121:150503, Oct 2018.

[87] F. Grusdt. Topological order of mixed states in correlated quantum many-body systems. *Phys. Rev. B*, 95:075106, Feb 2017.

[88] Zheng-Cheng Gu and Michael Levin. Effect of interactions on two-dimensional fermionic symmetry-protected topological phases with Z_2 symmetry. *Phys. Rev. B*, 89:201113, May 2014.

[89] Zheng-Cheng Gu and Xiao-Gang Wen. Symmetry-protected topological orders for interacting fermions: Fermionic topological nonlinear σ models and a special group supercohomology theory. *Physical Review B*, 90(11):115141, Sep 2014.

[90] Leonid Gurvits. Classical deterministic complexity of edmonds' problem and quantum entanglement. In *Proceedings of the Thirty-fifth Annual ACM Symposium on Theory of Computing*, STOC '03, pages 10–19, New York, NY, USA, 2003. ACM.

[91] Jutho Haegeman, David Pérez-García, Ignacio Cirac, and Norbert Schuch. Order parameter for symmetry-protected phases in one dimension. *Phys. Rev. Lett.*, 109:050402, Jul 2012.

[92] M. Z. Hasan and C. L. Kane. Colloquium: Topological insulators. *Reviews of Modern Physics*, 82(4):3045–3067, Nov 2010.

[93] M B Hastings. An area law for one-dimensional quantum systems. *Journal of Statistical Mechanics: Theory and Experiment*, 2007(08):P08024, 2007.

[94] Philipp Hauke, Markus Heyl, Luca Tagliacozzo, and Peter Zoller. Measuring multipartite entanglement through dynamic susceptibilities. *Nature Physics*, 12:778 EP, Mar 2016.

[95] Robert Helling, Hajo Leschke, and Wolfgang Spitzer. A special case of a conjecture by widom with implications to fermionic entanglement entropy. *International Mathematics Research Notices*, 2011(7):1451–1482, 2011.

[96] Christopher P. Herzog and Tatsuma Nishioka. Entanglement entropy of a massive fermion on a torus. *Journal of High Energy Physics*, 2013(3):77, 2013.

[97] Christopher P Herzog and Yihong Wang. Estimation for entanglement negativity of free fermions. *J. Stat. Mech.: Theory Exp.*, 2016(7):073102, 2016.

[98] Christoph Holzhey, Finn Larsen, and Frank Wilczek. Geometric and renormalized entropy in conformal field theory. *Nuclear Physics B*, 424(3):443 – 467, 1994.

[99] Marianne Hoogeveen and Benjamin Doyon. Entanglement negativity and entropy in non-equilibrium conformal field theory. *Nuclear Physics B*, 898:78 – 112, 2015.

[100] Michał HoroDecki, Paweł HoroDecki, and Ryszard HoroDecki. Separability of mixed states: necessary and sufficient conditions. *Physics Letters A*, 223(1):1 – 8, 1996.

[101] Michał HoroDecki, Paweł HoroDecki, and Ryszard HoroDecki. Mixed-state entanglement and distillation: Is there a "bound" entanglement in nature? *Phys. Rev. Lett.*, 80:5239–5242, Jun 1998.

[102] Pawel HoroDecki. Separability criterion and inseparable mixed states with positive partial transposition. *Physics Letters A*, 232(5):333 – 339, 1997.

[103] Chang-Tse Hsieh, Gil Young Cho, and Shinsei Ryu. Global anomalies on the surface of fermionic symmetry-protected topological phases in (3+1) dimensions. *Phys. Rev. B*, 93:075135, Feb 2016.

[104] Chang-Tse Hsieh, Olabode Mayodele Sule, Gil Young Cho, Shinsei Ryu, and Robert G. Leigh. Symmetry-protected topological phases, generalized laughlin argument, and orientifolds. *Phys. Rev. B*, 90:165134, Oct 2014.

[105] Ching-Yu Huang and Tzu-Chieh Wei. Detecting and identifying two-dimensional symmetry-protected topological, symmetry-breaking, and intrinsic topological phases with modular matrices via tensor-network methods. *Physical Review B*, 93(15):155163, Apr 2016.

[106] Zhoushen Huang and Daniel P. Arovas. Topological indices for open and thermal systems via uhlmann's phase. *Phys. Rev. Lett.*, 113:076407, Aug 2014.

[107] Ling-Yan Hung and Xiao-Gang Wen. Quantized topological terms in weak-coupling gAuge theories with a global symmetry and their connection to symmetry-enriched topological phases. *Physical Review B*, 87(16):165107, Apr 2013.

[108] Ling-Yan Hung and Xiao-Gang Wen. Universal symmetry-protected topological invariants for symmetry-protected topological states. *Physical Review B*, 89(7):075121, 2014.

[109] Karol Życzkowski. Volume of the set of separable states. ii. *Phys. Rev. A*, 60:3496–3507, Nov 1999.

[110] Karol Życzkowski, Paweł HoroDecki, Anna Sanpera, and Maciej Lewenstein. Volume of the set of separable states. *Phys. Rev. A*, 58:883–892, Aug 1998.

[111] Ken-Ichiro Imura, Yukinori Yoshimura, Yositake Takane, and Takahiro Fukui. Spherical topological insulator. *Physical Review B*, 86(23):235119, 2012.

[112] Rajibul Islam, Ruichao Ma, Philipp M. Preiss, M. Eric Tai, Alexander Lukin, Matthew Rispoli, and Markus Greiner. Measuring entanglement entropy in a quantum many-body system. *Nature*, 528:77 EP, Dec 2015.

[113] H. Isobe and L. Fu. Theory of interacting topological crystalline insulators. *Phys. Rev. B*, 92(8):081304, August 2015.

[114] B.-Q. Jin and V. E. Korepin. Quantum spin chain, toeplitz determinants and the fisher—hartwig conjecture. *Journal of Statistical Physics*, 116(1):79–95, 2004.

[115] C. L. Kane and E. J. Mele. Z_2 topological order and the quantum spin hall effect. *Phys. Rev. Lett.*, 95:146802, Sep 2005.

[116] Anton Kapustin. Bosonic topological insulators and paramagnets: a view from cobordisms. *arXiv:1404.6659*, Apr 2014.

[117] Anton Kapustin. Symmetry protected topological phases, anomalies, and cobordisms: Beyond group cohomology. *arXiv:1403.1467*, 2014.

[118] Anton Kapustin, Ryan Thorngren, Alex Turzillo, and Zitao Wang. Fermionic symmetry protected topological phases and cobordisms. *J. High Energy Phys.*, 2015(12):1–21, 2015.

[119] Anton Kapustin and Alex Turzillo. Equivariant topological quantum field theory and symmetry protected topological phases. *arXiv:1504.01830*, Apr 2015.

[120] Anton Kapustin, Alex Turzillo, and Minyoung You. Spin topological field theory and fermionic matrix product states. *arXiv:1610.10075*, 2016.

[121] Adam M. Kaufman, M. Eric Tai, Alexander Lukin, Matthew Rispoli, Robert Schittko, Philipp M. Preiss, and Markus Greiner. Quantum thermalization through entanglement in an isolated many-body system. *Science*, 353(6301):794–800, 2016.

[122] R. D. King-Smith and David Vanderbilt. Theory of polarization of crystalline solids. *Phys. Rev. B*, 47:1651–1654, Jan 1993.

[123] R. Kirby and L. Taylor. Pin Structures on Low dimensional Manifolds. *Geometry of low-dimensional manifolds*, 2:177–242, 1990.

[124] A Yu Kitaev. Unpaired majorana fermions in quantum wires. *Physics-Uspekhi*, 44(10S):131, 2001.

[125] Alexei Kitaev. Anyons in an exactly solved model and beyond. *Annals of Physics*, 321(1):2–111, Jan 2006.

[126] Alexei Kitaev. Periodic table for topological insulators and superconductors. In *AIP Conference Proceedings*, volume 1134, pages 22–30. AIP, Jan 2009.

[127] Alexei Kitaev and John Preskill. Topological entanglement entropy. *Phys. Rev. Lett.*, 96:110404, Mar 2006.

[128] A.Yu. Kitaev. Fault-tolerant quantum computation by anyons. *Annals of Physics*, 303(1):2–30, Jan 2003.

[129] Liang Kong and Xiao-Gang Wen. Braided fusion categories, gravitational anomalies, and the mathematical framework for topological orders in any dimensions. *arXiv:1405.5858*, 2014.

[130] Markus König, Steffen Wiedmann, Christoph Brüne, Andreas Roth, Hartmut Buhmann, Laurens W. Molenkamp, Xiao-Liang Qi, and Shou-Cheng Zhang. Quantum spin hall insulator state in hgte quantum wells. *Science*, 318(5851):766–770, 2007.

[131] Christina V. Kraus, Marcello Dalmonte, Mikhail A. BaraNov, Andreas M. Läuchli, and P. Zoller. Majorana edge states in atomic wires coupled by pair hopping. *Phys. Rev. Lett.*, 111:173004, Oct 2013.

[132] Yirun Arthur Lee and Guifre Vidal. Entanglement negativity and topological order. *Phys. Rev. A*, 88:042318, Oct 2013.

[133] Michael Levin and Zheng-Cheng Gu. Braiding statistics approach to symmetry-protected topological phases. *Physical Review B*, 86(11):115109, Sep 2012.

[134] Michael Levin and Xiao-Gang Wen. Detecting topological order in a ground state wave function. *Phys. Rev. Lett.*, 96:110405, Mar 2006.

[135] Michael A. Levin and Xiao-Gang Wen. String-net condensation: A physical mechanism for topological phases. *Physical Review B*, 71(4):045110, Jan 2005.

[136] Weifei Li, Letian Ding, Rong Yu, Tommaso Roscilde, and Stephan Haas. Scaling behavior of entanglement in two- and three-dimensional free-fermion systems. *Phys. Rev. B*, 74:073103, Aug 2006.

[137] Elliott Lieb, Theodore Schultz, and Daniel Mattis. Two soluble models of an antiferromagnetic chain. *Annals of Physics*, 16(3):407 – 466, 1961.

[138] D. Linzner, L. Wawer, F. Grusdt, and M. Fleischhauer. Reservoir-induced thouless pumping and symmetry-protected topological order in open quantum chains. *Phys. Rev. B*, 94:201105, Nov 2016.

[139] Yuan-Ming Lu and Ashvin Vishwanath. Theory and classification of interacting integer topological phases in two dimensions: A Chern-Simons approach. *Physical Review B*, 86(12):125119, Sep 2012.

[140] Yuan-Ming Lu and Ashvin Vishwanath. Classification and properties of symmetry-enriched topological phases: Chern-Simons approach with applications to $\mathbb{Z}_2$ spin liquids. *Physical Review B*, 93(15):155121, Apr 2016.

[141] S. Marcovitch, A. Retzker, M. B. Plenio, and B. Reznik. Critical and noncritical long-range entanglement in klein-gordon fields. *Phys. Rev. A*, 80:012325, Jul 2009.

[142] Glen Bigan Mbeng, Vincenzo Alba, and Pasquale Calabrese. Negativity spectrum in 1d gapped phases of matter. *J. Phys. A: Math. Theor.*, 50(19):194001, 2017.

[143] Andrej Mesaros and Ying Ran. Classification of symmetry enriched topological phases with exactly solvable models. *Physical Review B*, 87(15):155115, Apr 2013.

[144] M. A. Metlitski, L. Fidkowski, X. Chen, and A. Vishwanath. Interaction effects on 3D topological superconductors: surface topological order from vortex condensation, the 16 fold way and fermionic Kramers doublets. *arXiv:14063032*, June 2014.

[145] Max A. Metlitski. S-duality of u(1) gauge theory with $\theta = \pi$ on non-orientable manifolds: Applications to topological insulators and superconductors. *arXiv:1510.05663*, 2015.

[146] Gregory Moore and Nicholas Read. Nonabelions in the fractional quantum hall effect. *Nuclear Physics B*, 360(2-3):362–396, Aug 1991.

[147] J. E. Moore and L. Balents. Topological invariants of time-reversal-invariant band structures. *Phys. Rev. B*, 75:121306, Mar 2007.

[148] Takahiro Morimoto, Akira Furusaki, and Christopher Mudry. Breakdown of the topological classification $\mathbb{Z}$ for gapped phases of noninteracting fermions by quartic interactions. *Physical Review B*, 92(12):125104, Sep 2015.

[149] C. Moura Alves and D. Jaksch. Multipartite entanglement detection in bosons. *Phys. Rev. Lett.*, 93:110501, Sep 2004.

[150] V. Mourik, K. Zuo, S. M. Frolov, S. R. Plissard, E. P. A. M. Bakkers, and L. P. Kouwenhoven. Signatures of majorana fermions in hybrid superconductor-semiconductor nanowire devices. *Science*, 336(6084):1003–1007, 2012.

[151] Jia Ningyuan, Clai Owens, Ariel Sommer, David Schuster, and Jonathan Simon. Time- and site-resolved dynamics in a topological circuit. *Phys. Rev. X*, 5:021031, Jun 2015.

[152] Qian Niu, D. J. Thouless, and Yong-Shi Wu. Quantized hall conductance as a topological invariant. *Phys. Rev. B*, 31:3372–3377, Mar 1985.

[153] Cristiano De Nobili, Andrea Coser, and Erik Tonni. Entanglement entropy and negativity of disjoint intervals in cft: some numerical extrapolations. *J. Stat. Mech.: Theory Exp.*, 2015(6):P06021, 2015.

[154] Gerardo Ortiz and Emilio Cobanera. What is a particle-conserving topological superfluid? the fate of majorana modes beyond mean-field theory. *Ann Phys. (Amsterdam)*, 372:357 – 374, 2016.

[155] Gerardo Ortiz, Jorge Dukelsky, Emilio Cobanera, Carlos Esebbag, and Carlo Beenakker. Many-body characterization of particle-conserving topological superfluids. *Phys. Rev. Lett.*, 113:267002, Dec 2014.

[156] Yong-Cheng Ou and Heng Fan. Monogamy inequality in terms of negativity for three-qubit states. *Phys. Rev. A*, 75:062308, Jun 2007.

[157] A.A. Ovchinnikov. Fisher-hartwig conjecture and the correlators in xy spin chain. *Physics Letters A*, 366(4):357 – 362, 2007.

[158] YeJe Park, Jeongmin Shim, S.-S. B. Lee, and H.-S. Sim. Nonlocal entanglement of 1d thermal states induced by fermion exchange statistics. *Phys. Rev. Lett.*, 119:210501, Nov 2017.

[159] Asher Peres. Separability criterion for density matrices. *Phys. Rev. Lett.*, 77:1413–1415, Aug 1996.

[160] Ingo Peschel and Viktor Eisler. Reduced density matrices and entanglement entropy in free lattice models. *J. Phys. A: Math. Theor.*, 42(50):504003, 2009.

[161] Hannes Pichler, Guanyu Zhu, Alireza Seif, Peter Zoller, and Mohammad Hafezi. Measurement protocol for the entanglement spectrum of cold atoms. *Phys. Rev. X*, 6:041033, Nov 2016.

[162] M. B. Plenio. Logarithmic negativity: A full entanglement monotone that is not convex. *Phys. Rev. Lett.*, 95:090503, Aug 2005.

[163] JoSeph Polchinski. Effective field theory and the fermi surface. *arXiv:hep-th/9210046*, Oct 1992.

[164] Frank Pollmann and Ari M Turner. Detection of symmetry-protected topological phases in one dimension. *Physical Review B*, 86(12):125441, Sep 2012.

[165] Frank Pollmann, Ari M. Turner, Erez Berg, and Masaki Oshikawa. Entanglement spectrum of a topological phase in one dimension. *Physical Review B*, 81(6):064439, Feb 2010.

[166] Mark de Wild Propitius. *Topological interactions in broken gAuge theories*. PhD thesis, University of Amsterdam, Nov 1995.

[167] X.-L. Qi. A new class of (2+1)-d topological superconductor with Z8 topological classification. *New J. Phys.*, 15:065002, 2013.

[168] Xiao-Liang Qi, Taylor L. Hughes, and Shou-Cheng Zhang. Topological field theory of time-reversal invariant insulators. *Physical Review B*, 78(19):195424, Nov 2008.

[169] Xiao-Liang Qi, Hosho Katsura, and Andreas W. W. Ludwig. General Relationship between the Entanglement Spectrum and the Edge State Spectrum of Topological Quantum States. *Physical Review Letters*, 108(19):196402, May 2012.

[170] Xiao-Liang Qi and Shou-Cheng Zhang. Topological insulators and superconductors. *Reviews of Modern Physics*, 83(4):1057–1110, Oct 2011.

[171] N. Read and Dmitry Green. Paired states of fermions in two dimensions with breaking of parity and time-reversal symmetries and the fractional quantum hall effect. *Phys. Rev. B*, 61:10267–10297, Apr 2000.

[172] Raffaele Resta. Quantum-Mechanical Position Operator in Extended Systems. *Physical Review Letters*, 80(9):1800–1803, Mar 1998.

[173] Sam Roberts, Beni Yoshida, Aleksander Kubica, and Stephen D. Bartlett. Symmetry-protected topological order at nonzero temperature. *Phys. Rev. A*, 96:022306, Aug 2017.

[174] Rahul Roy. Topological phases and the quantum spin hall effect in three dimensions. *Phys. Rev. B*, 79:195322, May 2009.

[175] Rahul Roy. Z_2 classification of quantum spin hall systems: An approach using time-reversal invariance. *Phys. Rev. B*, 79:195321, May 2009.

[176] Paola Ruggiero, Vincenzo Alba, and Pasquale Calabrese. Entanglement negativity in random spin chains. *Phys. Rev. B*, 94:035152, Jul 2016.

[177] Paola Ruggiero, Vincenzo Alba, and Pasquale Calabrese. Negativity spectrum of one-dimensional conformal field theories. *Phys. Rev. B*, 94:195121, Nov 2016.

[178] Shinsei Ryu, Andreas P Schnyder, Akira Furusaki, and Andreas W W Ludwig. Topological insulators and superconductors: tenfold way and dimensional hierarchy. *New Journal of Physics*, 12(6):065010, Jun 2010.

[179] Shinsei Ryu and Shou-Cheng Zhang. Interacting topological phases and modular invariance. *Phys. Rev. B*, 85:245132, Jun 2012.

[180] C. Sabín and G. García-Alcaine. A classification of entanglement in three-qubit systems. *The European Physical Journal D*, 48(3):435–442, Jul 2008.

[181] Raul A. Santos, V. Korepin, and Sougato Bose. Negativity for two blocks in the one-dimensional spin-1 affleck-kennedy-lieb-tasaki model. *Phys. Rev. A*, 84:062307, Dec 2011.

[182] Andreas Schnyder, Shinsei Ryu, Akira Furusaki, and Andreas Ludwig. Classification of topological insulators and superconductors in three spatial dimensions. *Physical Review B*, 78(19):195125, Nov 2008.

[183] Andreas P. Schnyder, Shinsei Ryu, Akira Furusaki, and Andreas W. W. Ludwig. Classification of topological insulators and superconductors. *AIP Conference Proceedings*, 1134(1):10–21, 2009.

[184] Norbert Schuch, David Pérez-García, and Ignacio Cirac. Classifying quantum phases using matrix product states and projected entangled pair states. *Physical Review B*, 84(16):165139, Oct 2011.

[185] Nathan Seiberg and Edward Witten. Gapped boundary phases of topological insulators via weak coupling. *Progress of Theoretical and Experimental Physics*, 2016(12):12C101, 2016.

[186] Alessio Serafini, Gerardo Adesso, and Fabrizio Illuminati. Unitarily localizable entanglement of gaussian states. *Phys. Rev. A*, 71:032349, Mar 2005.

[187] R. Shankar. Renormalization-group approach to interacting fermions. *Rev. Mod. Phys.*, 66:129–192, Jan 1994.

[188] Hassan Shapourian and Shinsei Ryu. Finite-temperature entanglement negativity of free fermions. *arXiv:1807.09808*, Jul 2018.

[189] Hassan Shapourian and Shinsei Ryu. Entanglement negativity of fermions: Monotonicity, separability criterion, and classification of few-mode states. *Phys. Rev. A*, 99:022310, Feb 2019.

[190] Hassan Shapourian, Ken Shiozaki, and Shinsei Ryu. Many-body topological invariants for fermionic symmetry-protected topological phases. *Phys. Rev. Lett.*, 118:216402, May 2017.

[191] Hassan Shapourian, Ken Shiozaki, and Shinsei Ryu. Partial time-reversal transformation and entanglement negativity in fermionic systems. *Phys. Rev. B*, 95:165101, Apr 2017.

[192] Nicholas E. Sherman, Trithep Devakul, Matthew B. Hastings, and Rajiv R. P. Singh. Nonzero-temperature entanglement negativity of quantum spin models: Area law, linked cluster expansions, and sudden death. *Phys. Rev. E*, 93:022128, Feb 2016.

[193] Ken Shiozaki and Shinsei Ryu. Matrix product states and equivariant topological field theories for bosonic symmetry-protected topological phases in (1+1) dimensions. *Journal of High Energy Physics*, 2017(4):100, 2017.

[194] Ken Shiozaki, Masatoshi Sato, and Kiyonori Gomi. Topology of nonsymmorphic crystalline insulators and superconductors. *Physical Review B*, 93(19):195413, May 2016.

[195] Ken Shiozaki, Hassan Shapourian, Kiyonori Gomi, and Shinsei Ryu. Many-body topological invariants for fermionic short-range entangled topological phases protected by antiunitary symmetries. *Phys. Rev. B*, 98:035151, Jul 2018.

[196] Ken Shiozaki, Hassan Shapourian, and Shinsei Ryu. Many-body topological invariants in fermionic symmetry-protected topological phases: Cases of point group symmetries. *Phys. Rev. B*, 95:205139, May 2017.

[197] R. Simon. Peres-horodecki separability criterion for continuous variable systems. *Phys. Rev. Lett.*, 84:2726–2729, Mar 2000.

[198] Allan I Solomon and Choon-Lin Ho. Condition for tripartite entanglement. *Journal of Physics: Conference Series*, 343(1):012114, 2012.

[199] Robert E Stong. *Notes on cobordism theory*. Princeton University Press, 2015.

[200] S. Sugiura and A. Shimizu. Thermal Pure Quantum States at Finite Temperature. *Physical Review Letters*, 108(24):240401, June 2012.

[201] S. Sugiura and A. Shimizu. Canonical Thermal Pure Quantum State. *Physical Review Letters*, 111(1):010401, July 2013.

[202] Olabode Mayodele Sule, Xiao Chen, and Shinsei Ryu. Symmetry-protected topological phases and orbifolds: Generalized LAughlin's argument. *Physical Review B*, 88(7):075125, Aug 2013.

[203] Brian Swingle. Entanglement entropy and the fermi surface. *Phys. Rev. Lett.*, 105:050502, Jul 2010.

[204] Brian Swingle. Highly entangled quantum systems in 3+1 dimensions. *arXiv:1003.2434*, Mar 2010.

[205] Brian Swingle. Conformal field theory approach to fermi liquids and other highly entangled states. *Phys. Rev. B*, 86:035116, Jul 2012.

[206] Brian Swingle. Rényi entropy, mutual information, and fluctuation properties of fermi liquids. *Phys. Rev. B*, 86:045109, Jul 2012.

[207] Brian Swingle and T. Senthil. Universal crossovers between entanglement entropy and thermal entropy. *Phys. Rev. B*, 87:045123, Jan 2013.

[208] Wei Tang, Lei Chen, Wei Li, X. C. Xie, Hong-Hao Tu, and Lei Wang. Universal boundary entropies in conformal field theory: A quantum monte carlo study. *Phys. Rev. B*, 96:115136, Sep 2017.

[209] Jeffrey C Y Teo, Taylor L. Hughes, and Eduardo Fradkin. Theory of twist liquids: GAuging an anyonic symmetry. *Annals of Physics*, 360:349–445, 2015.

[210] Hong-Hao Tu. Universal entropy of conformal critical points on a klein bottle. *arXiv:1707.05812*, 2017.

[211] V. G. Turaev and O. Y. Viro. State sum invariants of 3-manifolds and quantum 6j-symbols. *Topology*, 31(4):865–902, 1992.

[212] Vladimir G. Turaev. Homotopy field theory in dimension 3 and crossed group-categories. *arXiv:math/0005291*, 2000.

[213] Vladimir G Turaev. *Homotopy quantum field theory*, volume 10. European Mathematical Society, 2010.

[214] Ari M. Turner, Frank Pollmann, and Erez Berg. Topological phases of one-dimensional fermions: An entanglement point of view. *Phys. Rev. B*, 83:075102, Feb 2011.

[215] Armin Uhlmann. Parallel transport and "quantum holonomy" along density operators. *Reports on Mathematical Physics*, 24(2):229 – 240, 1986.

[216] V. Vedral, M. B. Plenio, M. A. Rippin, and P. L. Knight. Quantifying entanglement. *Phys. Rev. Lett.*, 78:2275–2279, Mar 1997.

[217] G. Vidal, J. I. Latorre, E. Rico, and A. Kitaev. Entanglement in quantum critical phenomena. *Phys. Rev. Lett.*, 90:227902, Jun 2003.

[218] G. Vidal and R. F. Werner. Computable measure of entanglement. *Phys. Rev. A*, 65:032314, Feb 2002.

[219] Ashvin Vishwanath and T. Senthil. Physics of Three-Dimensional Bosonic Topological Insulators: Surface-Deconfined Criticality and Quantized Magnetoelectric Effect. *Physical Review X*, 3(1):011016, Feb 2013.

[220] O. Viyuela, A. Rivas, and M. A. Martin-Delgado. Two-dimensional density-matrix topological fermionic phases: Topological uhlmann numbers. *Phys. Rev. Lett.*, 113:076408, Aug 2014.

[221] O. Viyuela, A. Rivas, and M. A. Martin-Delgado. Uhlmann phase as a topological measure for one-dimensional fermion systems. *Phys. Rev. Lett.*, 112:130401, Apr 2014.

[222] Chong Wang, Andrew C Potter, and T Senthil. Classification of interacting electronic topological insulators in three dimensions. *Science (New York, N.Y.)*, 343(6171):629–31, 2014.

[223] Chong Wang, Andrew C. Potter, and T. Senthil. Classification of interacting electronic topological insulators in three dimensions. *Science*, 343(6171):629–631, 2014.

[224] Chong Wang and T Senthil. Interacting fermionic topological insulators/superconductors in three dimensions. *Physical Review B*, 89(19):195124, May 2014.

[225] X. G. Wen and Q. Niu. Ground-state degeneracy of the fractional quantum Hall states in the presence of a random potential and on high-genus Riemann surfaces. *Physical Review B*, 41(13):9377–9396, May 1990.

[226] Xiao-Gang Wen. Quantum orders and symmetric spin liquids. *Physical Review B*, 65(16):165113, Apr 2002.

[227] Xiao-Gang Wen. *Quantum field theory of many-body systems: from the origin of sound to an origin of light and electrons*. Oxford University Press on Demand, 2004.

[228] Xiao-Gang Wen. Symmetry-protected topological invariants of symmetry-protected topological phases of interacting bosons and fermions. *Physical Review B*, 89(3):035147, 2014.

[229] Xueda Wen, Po-Yao Chang, and Shinsei Ryu. Entanglement negativity after a local quantum quench in conformal field theories. *Phys. Rev. B*, 92:075109, Aug 2015.

[230] Xueda Wen, Po-Yao Chang, and Shinsei Ryu. Topological entanglement negativity in chern-simons theories. *Journal of High Energy Physics*, 2016(9):12, 2016.

[231] Xueda Wen, Shunji Matsuura, and Shinsei Ryu. Edge theory approach to topological entanglement entropy, mutual information, and entanglement negativity in chern-simons theories. *Phys. Rev. B*, 93:245140, Jun 2016.

[232] R. F. Werner and M. M. Wolf. Bound entangled gaussian states. *Phys. Rev. Lett.*, 86:3658–3661, Apr 2001.

[233] H. Wichterich, J. Molina-Vilaplana, and S. Bose. Scaling of entanglement between separated blocks in spin chains at criticality. *Phys. Rev. A*, 80:010304, Jul 2009.

[234] Hannu Wichterich, Julien Vidal, and Sougato Bose. Universality of the negativity in the lipkin-meshkov-glick model. *Phys. Rev. A*, 81:032311, Mar 2010.

[235] G. C. Wick, A. S. Wightman, and E. P. Wigner. The intrinsic parity of elementary particles. *Phys. Rev.*, 88:101–105, Oct 1952.

[236] E. Wigner. On the quantum correction for thermodynamic equilibrium. *Phys. Rev.*, 40:749–759, Jun 1932.

[237] Kenneth G. Wilson. Confinement of quarks. *Phys. Rev. D*, 10:2445–2459, Oct 1974.

[238] William Witczak-Krempa, Gang Chen, Yong Baek Kim, and Leon Balents. Correlated quantum phenomena in the strong spin-orbit regime. *Annual Review of Condensed Matter Physics*, 5(1):57–82, 2014.

[239] Edward Witten. Quantum field theory and the Jones polynomial. *Communications in Mathematical Physics*, 121(3):351–399, Sep 1989.

[240] Edward Witten. Fermion path integrals and topological phases. *Rev. Mod. Phys.*, 88:035001, Jul 2016.

[241] Michael M. Wolf. Violation of the entropic area law for fermions. *Phys. Rev. Lett.*, 96:010404, Jan 2006.

[242] Y. Xia, D. Qian, D. Hsieh, L. Wray, A. Pal, H. Lin, A. Bansil, D. Grauer, Y. S. Hor, R. J. Cava, and M. Z. Hasan. Observation of a large-gap topological-insulator class with a single dirac cone on the surface. *Nature Physics*, 5:398 EP, 2009.

[243] Cao Xin and Shang Yun. Fermionic one-way quantum computation. *Chinese Physics Letters*, 31(11):110302, 2014.

[244] Hong Yao and Shinsei Ryu. Interaction effect on topological classification of superconductors in two dimensions. *Phys. Rev. B*, 88:064507, Aug 2013.

[245] Yi-Zhuang You and Cenke Xu. Symmetry-protected topological states of interacting fermions and bosons. *Physical Review B*, 90(24):245120, Dec 2014.

[246] Michael P. Zaletel. Detecting two-dimensional symmetry-protected topological order in a ground-state wave function. *Physical Review B*, 90(23):235113, Dec 2014.

[247] Zoltán Zimborás, Robert Zeier, Michael Keyl, and Thomas Schulte-Herbrüggen. A dynamic systems approach to fermions and their relation to spins. *EPJ Quantum Technology*, 1(1):11, Sep 2014.